Investigations of the Photorefractive Effect in Potassium Tantalum Niobate

Thesis by

Victor Leyva

In Partial Fulfillment of the Requirements
for the Degree of
Doctor of Philosophy

California Institute of Technology
Pasadena, California
1991
(Submitted May 20, 1991)

Acknowledgements

I will always recall with fondness the diverse and highly talented group of individuals I have encountered during my graduate studies. First and foremost I would like to thank Dr. Amnon Yariv for the opportunity he opened to me and for his guidance. I have benefitted greatly from my work with Dr. Aharon Agranat. His assistance is appreciated.

Of the many students of the Quantum Electronics group, I would especially like to acknowledge those involved in the photorefractive field with whom I have had many productive discussions and collaborations. These include Norman Kwong, George Rakuljic, Yasuo Tomita, Koichi Sayano, and Rudy Hoffmeister.

The group owes much to the excellent technical support of Jana Mercado, Ali Ghaffari, Desmond Armstrong, and Kevin Cooper. I thank each of them for their assistance. In addition, the mechanical design and machine shop support of Larry Begay, Guy Duremberg, and Tony Stark is gratefully acknowledged.

Abstract

This thesis describes results of investigations of the photorefractive effect in potassium tantalum niobate ($KTa_{1-x}Nb_x O_3$) crystals. A band transport model is used to describe the photorefractive effect. The coupled mode equations are then introduced and used to solve self-consistently for the interaction of the light and space charge fields in a photorefractive material. The design and construction of a high temperature crystal growth system is discussed. The growth of photorefractive KTN crystals doped with a variety of transition metal dopants using the top seeded solution growth method is described. Two applications in the areas of volume holography are described which take advantage of the unique ferroelectric properties of KTN. The first makes use of the quadratic electrooptic effect in paraelectric KTN to control the magnitude of a diffracted wave with an externally applied field. Full amplitude modulation at speeds much faster than the grating formation time is demonstrated. The second application described is a procedure used to fix a holographic diffraction grating in KTN. It invovles the writing of a photorefractive grating in the paraelectric phase of KTN and cooling the sample under an applied field through successive phase transitions into the rhombohedral phase.

Materials investigations of the photorefractive effect are described. Investigations focused on the optimization of the photorefractive properties of KTN by the control of the concentration and the valence state of the photorefractive donor ions both during and after the growth stage. Absorption, photoconductivity, and electron microprobe measurements are used to identify the photorefractive species and to determine all relevant parameters which enter into the band transport model in a KTN:Cu,V sample after a series of thermal oxidation and reduction treatments. Holographic diffraction measurements are compared with those expected from theory. The oxidation and reduction process is modelled. Approaches to optimize the photorefractive sensitivity are discussed. The photorefractive properties of Fe and Ti doped KTN samples are investigated. Absorption and photoconductivity measurements indicate that the double dopant combination of Fe and Ti leads to an increased Fe^{2+} and total Fe concentrations as compared to single doped samples. A corresponding increase in photorefractive sensitivity is measured. The dependence of the photorefractive properties of Fe and Ti doped KTN on electric field, grating period, and temperature is characterized.

TABLE OF CONTENTS

CHAPTER ONE

INTRODUCTION TO THE PHOTOREFRACTIVE EFFECT

1.1 Introduction

The photorefractive effect refers to certain light induced changes in the index of refraction in an electrooptic material. The effect leads to the generation of large optical nonlinearities at relatively low light power levels. The photorefractive effect arises due to a redistribution of electronic charge in a material which is correlated with a light intensity pattern. The resultant electric space charge field modifies the index of refraction through the electrooptic effect. An ever increasing number of novel devices and applications which make use of the photorefractive effect have been demonstrated in the areas of optical phase conjugation, optical computing, and optical data storage.

The photorefractive effect was first observed during second harmonic generation experiments in $LiNbO_3$ by Ashkin in 1966 and by Chen in $KTa_{1-x}Nb_xO_3$ (KTN) in 1967.[1,2] Because the photoinduced index change was detrimental to harmonic generation experiments the term "optical damage" was originally used to describe it. The usefulness of this effect was first realized by Chen who used this "damage" to store thick holographic phase gratings in $LiNbO_3$.[3] A large effort in developing photorefractive materials ensued due to the tremendous holographic data storage potential of these materials. In principle, storage densities of the order of 10^{12} bits/cm^3 can be achieved in a volume holographic storage medium.[4,5] Due to the parallel readout of information in the form of two dimensional images, very fast access of information is possible. In addition, a photorefractive storage medium offers "read/write" and "read only" data storage capability.

During this period a great deal of progress was made in the development of photorefractive materials for use as a volume holographic storage medium. The photoexcitation, charge transport, and index change mechanisms responsible for the photorefractive effect were investigated. In $LiNbO_3$, multivalent transition metal impurities were identified as the species responsible for the photorefractive effect.[6,7] Charge transport was determined to occur through the drift, diffusion, and the photovoltaic effect.[8-11] Results of these efforts led to the development of several techniques to enhance the photorefractive properties of a material. Intentional doping of crystals with transition metals led to significantly increased photorefractive sensitivity.[7] Similiar improvements were achieved by thermal heat treatments which modified the valence state of the photorefractive species.[12]

Fixing techniques, used to create holographic gratings which are not erased under illumination or during long term storage, were also developed. Gratings were fixed in $LiNbO_3$ and $LiTaO_3$ by heating a sample, in which a photorefractive grating was written, to a temperature which allows ionic defects to become mobile.[13] The ionic defects create a compensating space charge field which cancels the photorefractive grating. The sample is then cooled to room temperature and illuminated, erasing the electronic grating and leaving the fixed ionic charge distribution. Fixing procedures were also demonstrated in $Sr_xBa_{1-x}Nb_2O_6$ (SBN) which create locally switched ferroelectric domains which are correlated with a photorefractive grating.[14,15] Early efforts at data storage in photorefractive materials culminated in the storage by Saeblar of 500 fixed holographic gratings in a $LiNbO_3$ sample.[16]

Despite these advances, for a variety of reasons, the potential of photorefractives as a holographic data storage medium was not realized. Chief among them was material limitations. No one material combined all of the desired properties of a large index change, high sensitivity, and the capability to fix gratings. Approaches which increased the magnitude of the index change in a sample came only at the expense of increased response time and decreased sensitivity.[17] Fixing procedures and the storage of multiple holograms in a single volume significantly reduces the diffraction efficiency of each hologram. In addition competing technologies such as magnetic storage media advanced rapidly. These technologies are compatible with existing electronic systems and did not require the development of supporting technologies such as spatial light modulators or compact visible light sources.

A resurgence of interest in photorefractives occured with the emergence of the field of phase conjugate optics.[18] Optical phase conjugation is used to generate a wave which has the same wavefronts as another input wave, but is reversed in direction. It was first observed in stimulated Brillouin backscattering experiments by Zel'dovich in 1972.[19] The backscattered light was observed to regain the original wavefront after retraversing any phase distortion introduced into the beam path. Nonlinear optical processes including stimulated backscattering and three and four wave mixing can generate a phase conjugate wave. In 1978, Yariv pointed out that the wave mixing techniques were analogous to real time volume holography.[20] Soon thereafter, Huignard demonstrated phase conjugation using four wave mixing in photorefractive BSO.[21] Photorefractive materials are an attractive medium for real time applications due to a strong response at low cw power levels. The distortion correction capability of optical phase conjugation was used to demonstrate a variety of applications such as one way image transmission through a distorting medium and intracavity laser distortion correction.[22,23] Four wave mixing in photorefractive crystals has been used to perform the operations of optical correlation, convolution, subtraction, and edge enhancement of images.[24-26] The photorefractive effect is a nonlocal one, the maxima of the intensity and index patterns are spatially shifted from one another. This results in an exchange of power between incident waves. Beam coupling gains up to 4000 have been measured in $BaTiO_3$.[27] Photorefractive wave coupling has been used to construct devices such as coherent optical amplifiers, self-pumped phase conjugate mirrors, optical limiters, and photorefractive oscillators and resonators.[28-30] Recently, photorefractive materials have found roles in the implementation of optical neural networks and associative memories as a reconfigurable storage medium for the optical interconnection between "neurons."[31,32] Also, the nonlinear gain provided by photorefractive coupling has been used to perform the optical thresholding operation.[33]

As with previous efforts at data storage, the applications which relied on the dynamic photorefractive effect have not progressed past the laboratory demonstration stage primarily due to severe material limitations. Materials which produce large nonlinearities have slow response for many applications. The response is even slower in the longer wavelength regions in which compact light sources exist. Availability is also a severe problem. Few facilities are equipped to or have the necessary experience to grow nonlinear optical crystals. Until recently there existed only one commercial supplier of $BaTiO_3$, the most widely used photorefractive material. Many promising photorefractive materials have not been fully investigated due to a lack of samples.[34]

1.2 Photorefractive materials

The photorefractive effect requires an electrooptic material with a partially filled, photoionizable, mid-gap impurity level. Materials in which the photorefractive effect has been observed include ferroelectric oxides, cubic oxides (sillenites), and compound semiconductors. Each of these classes of materials have distinct photorefractive properties which determines their suitability for various applications. Properties which are of interest include the magnitude of the refractive index change, the spatial phase shift between the intensity and index pattern, the time and spectral response of the material, and the photorefractive sensitivity defined as the index change per absorbed unit of energy.

1.2.1 Ferroelectric oxides

The photorefractive effect has been observed in ferroelectric oxides of the perovskite ($BaTiO_3$, $KNbO_3$, $KTa_{1-x}Nb_xO_3$), tungsten bronze($Sr_xBa_{1-x}Nb_20_6$(SBN), $Ba_{1-x}Sr_x K_{1-y}Na_yNb_5O_{15}$(BSKNN)), and ilmenite ($LiNbO_3$, $LiTaO_3$) structures.[35,36]

These materials are cubic at high temperatures and become ferroelectric on cooling through a phase transition. The ferroelectric properties are strongly temperature dependent and vary with composition. As a result, these are the most difficult of photorefractive materials to grow and to prepare with good optical quality. Ferroelectric oxides have bandgaps over 3eV and are tranparent throughout the visible and near uv. The photorefractive response, however, drops off sharply at longer wavelengths.

The photorefractive properties of the ferroelectric oxides $BaTiO_3$, SBN, and $LiNbO_3$ have been characterized extensively over a wide range of experimental conditions. Despite structural differences, they share common photorefractive properties. They have large electrooptic coefficients which produce large refractive index changes. They suffer from slow response partly due to low carrier mobilities. Of the three classes of photorefractive materials, the ferroelectric oxides have the lowest reported sensitivities. However, most as-grown samples are far from attaining their limiting sensitivities.

These materials offer the greatest ability to modify the photorefractive properties both during and after growth. Properties can be modified by the type and amount of transition metal dopant added to the flux. After growth, properties can be modified by thermal reduction or oxidation treatments. These treatments create oxygen vacancies which result in changes in the valence state of the dopant ions. For long term data storage applications the ferroelectric oxides are the only class of materials in which it has been possible to create fixed gratings which are not erased under illumination.

$KTa_{1-x}Nb_xO_3$ (KTN) was one of the first materials in which the photorefractive effect was observed.[2] It exhibits a large quadratic electrooptic effect near the ferroelectric phase transition. An early sample was found to possess a high photorefractive sensitivity through two photon absorption.[37] Recently, a new photorefractive mechanism, the dielectric photorefractive effect was observed in KTN.[38] Refractive index changes are the result of valence changes to impurity ions which induce changes in the Curie temperature. Very little work in KTN has been reported primarily due to a lack of samples. It was considered a difficult material to grow optical quality samples free of striations.

1.2.2 Sillenites

The sillenites are non centrosymmetric cubic oxides of point group symmetry $\bar{4}3m$. They show no birefringence without an applied field and are strongly optically active. The sillenites which include $Bi_{12}SiO_{20}$(BSO), $Bi_{12}GeO_{20}$ (BGO), and $Bi_{12}TiO_{20}$(BTO) have the highest reported sensitivities of photorefractive materials.[35,36] Sensitivities in BSO comparable to that of silver halide photographic film have been reported.[39] These large values are the result of high mobilities which assist in the formation of a space charge field by allowing carriers to be transported long distances before being retrapped. Intrinsic defect centers are responsible for the photorefractive effect in the sillenites which prevents the modification of properties by the addition of dopants or by thermal heat treatments. Even so, a variety of approaches have been developed to enhance their photorefractive properties. Techniques to enhance the two-beam coupling coefficients include the use of moving gratings and the application of an ac field.[40,41] For storage applications, thermal procedures have been used to create an assymetry between writing and readout response times.[42] No fixing procedure has been found for long term storage applications.

1.2.3 Compound semiconductors

Compound semiconductors in which the photorefractive effect has been observed include GaAs, GaAs:Cr, InP:Fe, CdTe, and CdS.[35,36] Both intrinsic defect centers, such as EL2 in GaAs, and transition metal impurities have been identified as the photorefractive species. Due to their small bandgap, some compound semiconductors exhibit response in the infrared spectral region. While the magnitude of the photorefractive index change in these materials is generally small, their fast response leads to large sensitivities. This is the result of large carrier mobilities, ($\mu_e = 8500 cm^2/Vs$ in GaAs), which allows for carriers to be transported distances comparable to a grating period.

Several approaches have been used to enhance the photrefractive properties of these materials. The application of ac electric fields have increased beam coupling gain.[43] By operating near the band edge, the photorefractive effect has produced large index and absorption gratings through the Franz-Keldish effect.[44] Other novel demonstrations include a photorefractive effect arising to charge transport in a quantum well.[45]

1.3 Outline of the thesis

The photorefractive effect shows great promise in a number of applications, but until material limitations are overcome the full potential will not be realized. The aim of this thesis was to investigate the photorefractive effect in $KTa_{1-x}Nb_xO_3$ in order to develop approaches for optimizing the photorefractive properties. The results are applicable to any ferroelectric oxide material. A comprehensive approach was used which involved the areas of crystal growth, materials studies, and applications development.

In Chapter 2 a band transport model of the photorefractive effect is introduced. Solutions for the space charge field and response time are presented for the cases of both one and two carrier charge transport. The coupled mode equations are then used to solve self consistently for the interacting space charge and light fields in a photorefractive medium.

As part of this effort a high temperature crystal growth system was designed and constructed in order to grow photorefractive KTN. Chapter 3 describes the system and the top seeded solution crystal growth method. A summary of the KTN crystals which were grown is given followed by a discussion of the structural and ferroelectric properties of these crystals.

Chapter 4 describes two applications of the photorefractive effect which take advantage of the ferroelectric properties of KTN. In the paraelectric phase of KTN the quadratic electrooptic effect is utilized to express the photorefractive space charge distribution as a refractive index change. The result is a diffraction grating whose magnitude is proportional to and can be controlled by an externally applied field. Full amplitude modulation of the diffraction efficiency is possible at speeds limited by the dielectric response, which is orders of magnitude faster than the photorefractive space charge creation time. Modulation at 20 khz is demonstrated. Also described is a procedure used to fix photorefractive diffraction gratings in KTN. Fixing efficiencies as high as 10% are reported. Possible mechanisms responsible for the effect are discussed.

Chapter 5 describes an investigation of the microscopic parameters which govern the photorefractive effect in KTN:Cu,V. A series of thermal oxidation and reduction treatments are performed on the sample. After each treatment, absorption, photoconductivity, and photorefractive measurements are made. Results allow the determination of all relevant parameters which enter into the Kukhtarev band transport model of the photorefractive effect.[43] These includes values for the concentration of the filled and ionized donor level, the ratio of the mobility to electron recombination rate, and the electron photoexcitation cross section. The dependence of holographic diffraction and response measurements on trap concentration are compared with theory. Results indicate a substantially smaller index change compared to theory and suggest that not all donor ions participate in the photorefractive effect. The oxidation/reduction heat treatment process is modelled and relevant parameters are determined. Results indicate the temperature and partial pressure of oxygen needed to produce a desired photerefractive property. Also discussed are approaches to optimize the photorefactive sensitivity in the sample.

In Chapter 6 the photorefractive properties of Fe and Ti doped KTN are investigated. The photorefractive properties of three KTN samples are studied: an Fe doped sample, a Ti doped sample, and a double doped Fe and Ti sample. Absorption and phtoconductivity measurements indicate that double doping Ti results in an increased Fe^{2+} concentration and total Fe concentration which leads to an order of magnitude increase in photorefractive sensitivity as compared to single doping. The dependence of the photorefractive index change, response time and sensitivity on temperature, grating period and applied field are characterized for all three samples.

References

1. A. Ashkin, G.D. Boyd, J.M. Dziedzic, R.G. Smith, A.A. Ballman, H.J. Levinstein, K. Nassau, "Optically-induced refractive index inhomegeneities in $LiNbO_3$ and $LiTaO_3$," Appl. Phys. Lett. **9**, 72 (1966).
2. F.S. Chen, "A laser-induced inhomogeneity of refractive indices in KTN," J. Appl. Phys. **38**, 3418 (1967).
3. F.S. Chen, J.T. LaMacchia, D.B. Fraser, "Holographic storage in lithium niobate," Appl. Phys. Lett. **13**, 223 (1968).
4. P.J. van Heerden, "Theory of optical information storage in solids," Appl. Opt. **2**, 393 (1963).
5. T. Jannson, "Structural information in volume holography," Opt. Appl. **IX**, 169 (1979).
6. G.E. Peterson, A.M. Glass, T.J. Negran, "Control of the susceptibility of lithium niobate to laser-induced refractive index changes," Appl. Phys. Lett. **19**, 130 (1971).
7. W. Phillips, J.J. Amodei, D.L. Staebler, "Optical and holographic properties of transition metal doped lithium niobate," RCA Rev. **33**, 94 (1972).
8. M.G. Clark, F.J. DiSalvo, A.M. Glass, G.E. Peterson, "Electronic structure and optical index damage of iron-doped lithium niobate," J. Chem. Phys. **59**, 6209 (1973).
9. J.B. Thaxter, "Electrical control of holographic storage in Strontium-Barium Niobate," Appl. Phys. Lett. **15**, 210 (1969).

10. J.J. Amodei, "Analysis of transport processes during holographic recording in insulators," RCA Review. **32**, 185 (1971).

11. A.M. Glass, D. von der Linde, D.H. Auston, T.J. Negran, "Excited state polarization, bulk photovoltaic effect and the photorefractive effect in electrically polarized media," J. Elect. Matls. **4**, 915 (1975).

12. W. Phillips and D.L. Staebler, "Control of the Fe^{2+} concentration in iron-doped lithium niobate," J. Elect. Matl. **3**, 601 (1974).

13. J. Amodei, D. Staebler, "Holographic pattern fixing in electro-optic crystals," Appl. Phys. Lett. **18**, 540(1971).

14. F. Micheron, G. Bismuth, "Field and time thresholds for the electrical fixation of holograms recorded in $Sr_{0.75}Ba_{0.25}Nb_2O_6$ crystals," Appl. Phys. Lett.**22**,71 (1973).

15. F. Micheron, J. Trotier, Ferroelect., "Photoinduced phase transitions in $(Sr,Ba)Nb_2O_6$ crystals and applications," **8**, 441 (1974).

16. D.L. Staebler, W.J. Burke, W. Phillips, J.J. Amodei, "Multiple storage and erasure of fixed holograms in Fe-doped $LiNbO_3$," Appl. Phys. Lett. **26**, 182 (1975).

17. D.L. Staebler, W. Phillips, "Fe-doped $LiNbO_3$ for read-write applications," Appl. Opt. **13**, 788 (1974).

18. R.A. Fisher (ed.),"Optical phase conjugation," Academic Press, Orlando (1983).

19. B. Ya. Zel'dovich, V.I. Popovichev, V.V. Ragul'skii, F.S. Faizullov, "Connection between the wavefronts of the reflected and exciting light in stimulated

Mandel'shtam-Brillouin scattering," Sov. Phys. JETP **15**, 109 (1972).

20. A. Yariv, "Phase conjugate optics and real-time holography," IEEE J. Quant. Elect. QE 14, 650 (1978).
21. J.P. Huignard, J.P. Herriau, P. Aubourg, E. Spitz, "Phase conjugate wavefront generation via real time holography in $Bi_{12}SiO_{20}$ crystals," Opt. Lett. **4**, 21 (1979).
22. K. Sayano, Y. Tomita, A. Yariv, "One way image transmission through distorting media using orthogonally polarized beams and phase conjugation," unpublished.
23. M. Cronin-Golomb, B. Fisher, J. Nilsen, J.O. White, A. Yariv, Appl. Phys. Lett. **41**, 219 (1982).
24. J. O. White, A. Yariv, "Real time image processing via four-wave mixing in a photorefractive medium," Appl. Phys. Lett. **37**, 5 (1980).
25. S.K. Kwong, G. A. Rakuljic, V. Leyva, A. Yariv, "Real-time image processing using a self-pumped phase conjugate mirror," Proc. SPIE **613**, 36 (1986).
26. J.P. Huignard, J.P. Herriau, "Real-time coherent object edge reconstruction with $Bi_{12}SiO_{20}$," Appl. Opt. **17**, 2671 (1978).
27. F. Laeri, T. Tschudi, J. Albers, "Coherent cw image amplifier and oscillator using two-wave interaction in a $BaTiO_3$ crystal," Opt. Comm. **47**, 387 (1983).
28. M. Cronin-Golomb, B. Fisher, J. White, A. Yariv, "Theory and applications of four-wave mixing in photorefractive media," IEEE J. Quantum Elect. QE-20, 12 (1984).

29. M. Cronin-Golomb, A. Yariv, "Optical limiters using photorefractive nonlinearities," J. Appl. Phys. **57**, 4906 (1985).

30. J.O. White, M. Cronin-Golomb, B. Fisher, A. Yariv, "Coherent oscillation by self induced gratings in the photorefractive crystal $BaTiO_3$," Appl. Phys. Lett. **40**, 450 (1982).

31. B.H. Soffer, G.J. Dunning, Y. Owechko, E. Marom, " Associative holographic memory with feedback using phase-conjugate mirrors," Opt. Lett. **11**, 118 (1986).

32. A. Yariv, S.K. Kwong, K. Kyuma, "Demonstration of an all-optical associative holographic memory," Appl. Phys. Lett. **48**, 1114 (1986).

33. K. Sayano, G. A. Rakuljic, A. Yariv, "Thresholding semilinear phase conjugate mirror," Opt. Lett. **13**, 143 (1988).

34. D. H. Auston, et al., "Research on nonlinear optical materials: an assessment," Appl. Opt. **26**, 211 (1987).

35. P. Gunther, J.P. Huignard, (eds.), "Photorefractive materials and their applications I.," Springer-Verlag, Berlin (1987).

36. G.C. Valley, M.B. Klein, R.A. Mullen, D. Rytz, B. Wechsler, "Photorefractive materials," Ann. Rev. Mater. Sci. **18**, 165 (1988).

37. D. von der Linde, A. M. Glass, K.F. Rodgers, "High-sensitivity optical recording in KTN by two-photon absorption," Appl. Phys. Lett. **26**, 22 (1975).

38. A. Agranat, Y. Yacoby, "Photorefractive effect produced by photoinduced metastable changes in the dielectric constant," Phys. Rev. B **27**, 5712 (1983).

39. P. Gunther, "Photorefractive Materials," Phys. Reports **93**, 199 (1982).

40. J.P. Huignard, A. Marrakchi, "Coherent signal beam amplification in two-wave mixing experiments with photorefractive $Bi_{12}SiO_{20}$ crystals," Opt. Comm. **38**, 249 (1981).

41. S.I. Stepanov, M.P. Petrov, "Efficient unstationary holographic recording in photorefractive crystals under an external alternating electric field," Opt. Comm. **53**, 292 (1985).

42. J.P. Herriau, J.P. Huignard, "Hologram fixing process at room temperature in photorefractive $Bi_{12}SiO_{20}$ crystals," Appl. Phys. Lett. **49**, 1140 (1986).

43. N.V. Kukhtarev, V.B. Markov, S.G. Odulov, M.S. Soskin, and V.L. Vinetski, "Holographic storage in electrooptic crystals. I. Steady state," Ferroelect. **22**, 949 (1979).

CHAPTER TWO

THE PHOTOREFRACTIVE EFFECT

2.1 Introduction

The photorefractive effect produces changes in the refractive index as a result of a light induced redistribution of electric charge. In a photorefractive material free carriers are preferentially generated in regions of high light intensity, undergo transport, and are preferentially retrapped in regions of low light intensity (Fig. 2-1). The result is a space charge field correlated with the light intensity pattern which modifies the index of refraction through the electrooptic effect. Light waves are able to interact in a photorefractive medium by mutually scattering from the grating which they create. Due to the interaction the phase of each wave is modified and one wave can gain intensity at the expense of another. In this chapter we present a band transport model of the photorefractive effect which includes both electron and hole conductivity and then solve for the dependence of the space charge field on material parameters. The coupled mode equations are then introduced to solve self-consistently for the interaction of the light waves with the space charge field in a photorefractive medium.

The photorefractive effect was first observed by Ashkin in $LiNbO_3$.[1] It was shortly thereafter observed in KTN by Chen who proposed that the refractive index change was a result of the drift of photoexcited carriers of unknown origin to regions of low light intensity.[2] Retrapped carriers created a space charge field which

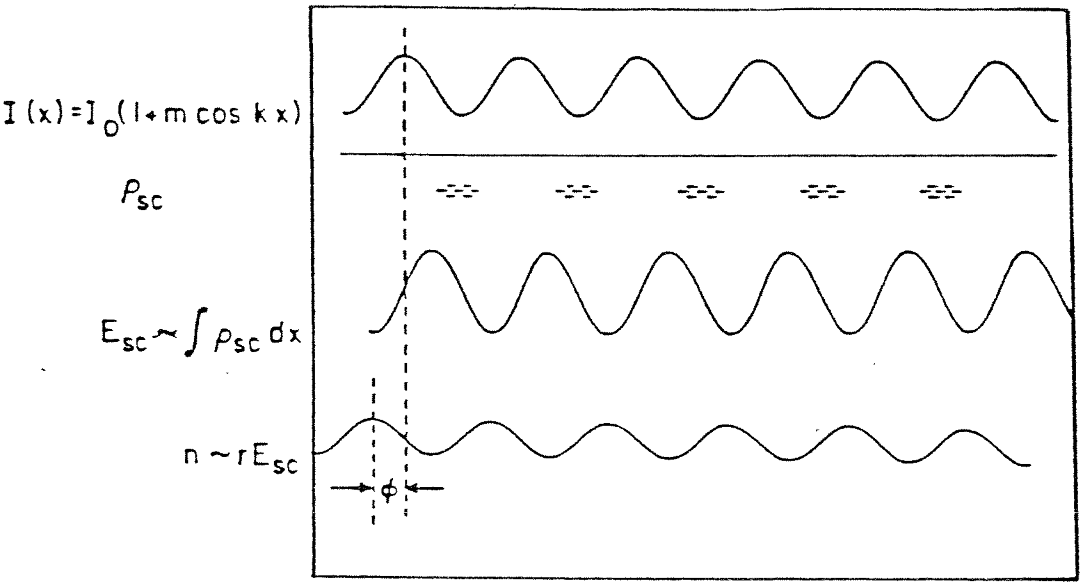

Fig. 2-1 The photorefractive effect. A light intensity pattern creates an electronic charge distribution which modifies the refractive index through the electrooptic effect. In general the refractive index pattern is spatially shifted with respect to the light intensity pattern.

modified the refractive index through the electrooptic effect. Early investigations of the photorefractive effect focused on identifying the photoexcitation and trapping centers responsible for the photorefractive effect and in identifying the mechanisms by which carriers underwent transport. A number of analytic techniques including absorption spectroscopy, electron paramagnetic resonance(epr), and mossbauer spectroscopy identified multivalent transition metal impurities as the photorefractive species in samples of $LiNbO_3$ and $LiTaO_3$.[3-7] Charge transport was found to occur through drift, diffusion, and the photovoltaic effect.[8-11]

The diffraction of light by a thick phase hologram was first modelled by Kogelnik using the coupled mode equations.[12] This approach was extended by others to describe the dynamic wave coupling which occurs in a photorefractive material.[13-15] While these dynamic models could explain the observed beam coupling and the time evolution of the index grating, the dependence of the index of refraction on intensity was assumed rather than obtained self-consistently. Kukhtarev introduced a band transport model of the photorefractive effect and solved for the dependence of the index change on intensity and on material parameters.[16] The solution was then introduced into the coupled mode equations to self-consistently solve for the light and space charge fields in a photorefractive medium. This model has been widely used to describe the photorefractive effect in a number of materials and under a variety of experimental conditions. Extensions have been made to include the effect of multiple carriers,[17,18] multiple species,[19] moving gratings,[20] and time varying applied fields.[21]

The hopping model of the photorefractive effect was introduced by Feinberg.[22] Charge carriers are assumed to "hop" between sites with a probability proportional to light intensity. Analytical solutions are difficult to arrive at, though the two models do agree in limiting regimes.[23] The band transport model will be described in this chapter and used throughout this thesis to describe all photorefractive measurements.

2.2. Band Transport Model of the Photorefractive Effect

The band transport model of the photorefractive effect for the case of two carrier transport from a single photorefractive species is illustrated in Fig. 2-2. The total concentration of the donor species is given by N_D. A fraction of these are positvely ionized with concentration N_D^+. In order to preserve overall charge neutrality there exists a compensating acceptor level of concentration $N_A = N_D^+$. This level is non photoactive. The light induced charge redistribution in such a material occurs as follows. Both free electrons and holes are generated from transitions involving the donor level. Electrons can be photo or thermally excited from filled donor centers into the conduction band. Similiarly a mobile hole can be created in the valence band by photo or thermal excitation of an electron from the valence band into an empty donor site. The free carriers thus excited then undergo transport through drift, diffusion, and the photovoltaic effect. The electrons (holes) recombine at an empty (filled) donor site. A space charge field is formed as a result of the charge seperation and modifies the refractive index through the electrooptic effect. The process is described by rate and current equations for both holes and electrons,

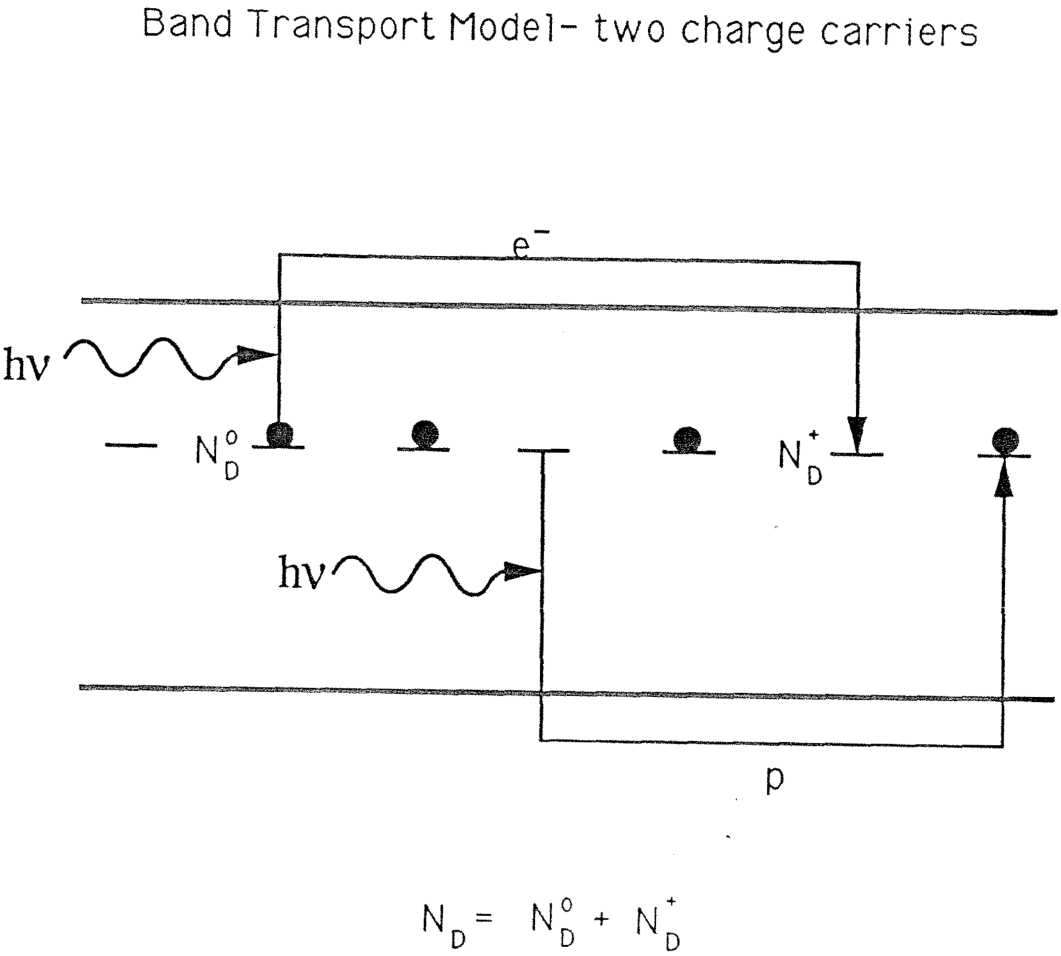

Fig. 2-2 Band transport model of the photorefractive effect for the case of a single species, N_D, with both electron and hole conductivity. Electrons (holes) are photoexcited from an N_D^0 (N_D^-) ion, undergo transport, and are retrapped at an N_D^- (N_D^0) site.

an equation of continuity, and Poisson's equation.

The rate equation for electrons and holes are:

$$\frac{\partial n_e}{\partial t} - \nabla \cdot \frac{j_e}{e} = (s_e \frac{I}{h\nu} + \beta_e)(N_D - N_D^+) - \gamma_e n_e N_D^+ \tag{2.1}$$

$$\frac{\partial p_h}{\partial t} - \nabla \cdot \frac{j_h}{e} = (s_h \frac{I}{h\nu} + \beta_h) N_D^+ - \gamma_h p_h (N_D - N_D^+) \tag{2.2}$$

The current equations for electrons and holes are:

$$j_e = e\mu_e n_e E + k_B T \mu_e \nabla n_e + \kappa_e s_e (N_D - N_D^+) I \tag{2.3}$$

$$j_h = e\mu_h p_h E + k_B T \mu_h \nabla p_h + \kappa_h s_h N_D^+ I \tag{2.4}$$

The continuity equation is:

$$\frac{\partial}{\partial t}(n_e - N_D^+ - p_h) = \nabla \cdot \frac{j_e}{e} + \nabla \cdot \frac{j_h}{e} \tag{2.5}$$

The Poisson equation is:

$$\nabla \cdot E = -(\frac{e}{\epsilon \epsilon_o})(n_e + N_A - N_D^+ - p_h) \tag{2.6}$$

where

n_e = free electron density

p_h= free hole density

e= electronic charge

I= light intenstiy

h= Plank's constant

E= electric field (applied plus space charge)

ϵ= dielectric constant

ν = frequency of the optical wave

$s_e(s_h)$= electron (hole) photoexcitation cross section

$\beta_e(\beta_h)$= electron (hole) thermal generation rate

$\gamma_e(\gamma_h)$= electron (hole) recombination rate

$j_e(j_h)$= electron (hole) current density

$\mu_e(\mu_h)$= electron (hole) mobility

$\kappa_e(\kappa_h)$= electron (hole) photovoltaic coefficient

The solution of the above set of nonlinearly coupled equations for the case of a sinusoidal intensity pattern given by

$$I = I_o(1 + me^{iKx} + c.c.) \tag{2.7}$$

proceeds as follows.[24] Equations (2.3), (2.4), and (2.6) are used to directly eliminate for j_e, j_h, and N_D^+. The remaining equations are linearized as follows:

$$n_e = n_{e,0} + n_{e,1}e^{iKx+i\delta\omega t} + c.c. \tag{2.8}$$

$$p_h = p_{h,0} + p_{h,1}e^{iKx+i\delta\omega t} + c.c. \tag{2.9}$$

$$E = E_0 + E_{sc} e^{iKx+i\delta\omega t} + c.c. \tag{2.10}$$

Two approximations are made. The first is that the response is linear in intensity modulation, which requires that $m = I_1/I_0 << 1$. This allows for the neglect of higher order terms in the above expansions. Solutions for large intensity modulation are discussed elsewhere.[25] The other requirement is that both $p_{h.0} - n_{e.0} << (N_D - N_A, N_A)$. This is valid under typical experimental conditions using continuous wave (c.w.) illumination. Neglecting second order quantities results in a set of three linear equations in three unknowns (E_{sc}, $n_{e.1}$, $p_{h.1}$). The response time, $\tau^{-1} = \delta\omega$ is found from the requirement that for the existence of unique solutions the determinant of the set of equations must vanish. Solutions will be given for two limiting cases.

2.2.1 Single Species Solutions

In this section the solutions for the case of single carrier electron charge transport with no photovoltaic field are given.[16,24] We take $p_h = j_h = s_h = \gamma_h = \beta_h = \kappa_e = \kappa_h = 0$. The magnitude of the space charge field is given by:

$$E_{sc} = \frac{m}{(1+\frac{\beta_e}{s_e I/h\nu})} E_q \frac{(E_o^2 + E_D^2)^{1/2}}{((E_q + E_D)^2 + E_o^2)^{1/2}} \tag{2.11}$$

where the characteristic fields are given by

E_o= applied field

$E_D = k_B T K/e$ (diffusion field)

$E_q = eN_D^+(1 - N_D^+/N_D)/\epsilon_o\epsilon K$ (limiting space charge field)

The limiting space charge field, E_q is that which occurs if all of the available charge were to be seperated by one grating period. The space charge field is always smaller than E_q and is usually limited to a value determined by the smaller of E_D or E_q. The field can be enhanced to values approaching the limiting field by the application of an external field which assists in the separation of charge.

The spatial phase shift between the intensity pattern and space charge field is given by

$$\Psi = tan^{-1}\left(\frac{E_D(E_D + E_q) + E_0^2}{E_0 E_q}\right) \tag{2.12}$$

Without an applied field charge transport is through diffusion and the space charge grating is shifted $\pi/2$ from the intensity grating.

The response time, τ_e, is complex valued and is given by

$$Re[\tau_e^{-1}] = \tau_{die}^{-1}\frac{(1 + \tau_{Re}\tau_{die}/(\tau_{De}\tau_{Ie}))(1 + \tau_{Re}/\tau_{De}) + (\tau_{Re}/\tau_{Ee})^2(\tau_{die}/\tau_{Ie})}{(1 + \tau_{Re}/\tau_{De})^2 + (\tau_{Re}/\tau_{Ee})^2} \tag{2.13}$$

$$Im[\tau_e^{-1}] = \tau_{die}^{-1}\frac{(\tau_{Re}/\tau_{Ee})(\tau_{die}/\tau_{Ie} - 1)}{(1 + \tau_{Re}/\tau_{De})^2 + (\tau_{Re}/\tau_{Ee})^2} \tag{2.14}$$

where

$$\tau_{die} = \frac{\epsilon_o\epsilon}{e\mu_e n_d}\text{(dielectric relaxation time)} \tag{2.15}$$

$$\tau_{Ee} = \frac{1}{K\mu_e E_o}\text{(drift time)} \tag{2.16}$$

$$\tau_{De} = \frac{e}{\mu_e k_B T K^2}\text{(diffusion time)} \tag{2.17}$$

$$\tau_{Re} = \frac{1}{\gamma_{Re} N_D^+} (\text{recombination time}) \tag{2.18}$$

$$\tau_{Ie} = \frac{1}{s_e I / h\nu + \gamma_{Re} n_d} \tag{2.19}$$

and

$$n_d = \frac{s_e I (N_D - N_D^+)}{h\nu \gamma_{Re} N_D^+} \tag{2.20}$$

is the free electron density.

The response time becomes imaginary with the application of an external field which leads to oscillations during the writing or erasing of a diffraction grating. The response time strongly depends on the electron transport length and the grating period. In the limit of large grating periods or small transport lengths the response time approaches that of a uniform charge distribution given by the dielectric relaxation time. In this limit the response time increases with grating period due to the requirement that an electron must undergo an increasing number of photoexcitation and retrapping steps before charge can be separated by a grating period. For small grating periods the response time approaches τ_{Ie}, the inverse of the photoproduction and recombination rates.

2.2.2 Two Species Solutions

The solution for space charge field for the case of both hole and electron conductivity with no applied or photvoltaic fields is given by[17,24]

$$E_{sc} = -imE_D \frac{(1 - (\sigma_h/\sigma_e) + (E_D/E_q)((\tau_{Ih}/\tau_{dih}) - (\tau_{Ie}/\tau_{dih})))}{(1 + (E_D/E_q))(1 + (\sigma_h/\sigma_e) + (E_D/E_q)((\tau_{Ih}/\tau_{dih}) + (\tau_{Ie}/\tau_{dih})))} \tag{2.21}$$

where σ_e and σ_h are the electron and hole conductivities and τ_{dih} and τ_{Ih} are given by replacing the electron parameters by the corresponding hole parameters in (2.15,19). Note that no grating can form if the electron and hole conductivities are equal.

The response time is given by

$$\tau = \tau_{die}\frac{(1+(\tau_{Re}/\tau_{De}))(1+(\tau_{Rh}/\tau_{Dh}))}{(1+(E_D/E_q))(1+(\sigma_h/\sigma_e)+(E_D/E_q)((\tau_{Ih}/\tau_{dih})+(\tau_{Ie}/\tau_{dih})))} \tag{2.22}$$

2.2.3 Photorefractive index change

The photorefractive space charge field modifies the refractive index of a material through the electrooptic effect. Changes to refractive index are described by changes to the index index ellipsoid given by

$$\Delta(\frac{1}{n_{ij}^2}) = r_{ijk}E_k + p_{ijkl}E_kE_l + ... \tag{2.23}$$

where E_k is the kth component of the electric field, and r_{ijk} and p_{ijkl} are the linear and quadratic electrooptic coefficients.

In a material with a linear electrooptic effect and in which higher order electrooptic terms can be neglected the index change, Δn, created by the photorefractive space charge field, E_{sc}, is given by

$$\Delta n = -(\frac{n_o^3}{2})r_{eff}E_{sc} \tag{2.24}$$

where n_o is the index of refraction of the material with no applied field and r_{eff} is the effective linear electrooptic coefficient.

For materials with inversion symmetry, such as paraelectric KTN, the linear electrooptic effect vanishes and the lowest allowed electrooptic effect is the quadratic one. The index change is then given by

$$\Delta n = -(\frac{n_{i.0}^3}{2})p_{eff}(E_o + E_{sc})^2 \tag{2.25}$$

where p_{eff} is the appropriate quadratic electrooptic coefficient and E_o is an externally applied field. In Chapter 4 use is made of one of the grating terms in the expansion of eq. (2.25) to modulate a diffraction grating with an externally applied field.

2.3. Photorefractive Wave Coupling

In section 2.2 solutions of the space charge field were found for the case of a uniform light intensity pattern. In a photorefractive material, light waves are coupled through self diffraction from the gratings which they create. This results in an exchange of both intensity and phase information between the two waves which in turn modifies the space charge field since the transport equations (sect. 2.3,2.4) depend on the intensity I. In this section the coupled mode equations will be used to self consistently solve for the interaction of light waves and the photorefractive grating which they create.

Consider two waves incident on a photorefractive sample as illustrated in Figure 2-3. The waves are taken to be of the form

$$\mathbf{E}_1(\mathbf{r},t) = A_1(\mathbf{r})e^{i(\mathbf{k}_1\cdot\mathbf{r}-\omega t)}\hat{\mathbf{e}}_1 + c.c. \tag{2.26a}$$

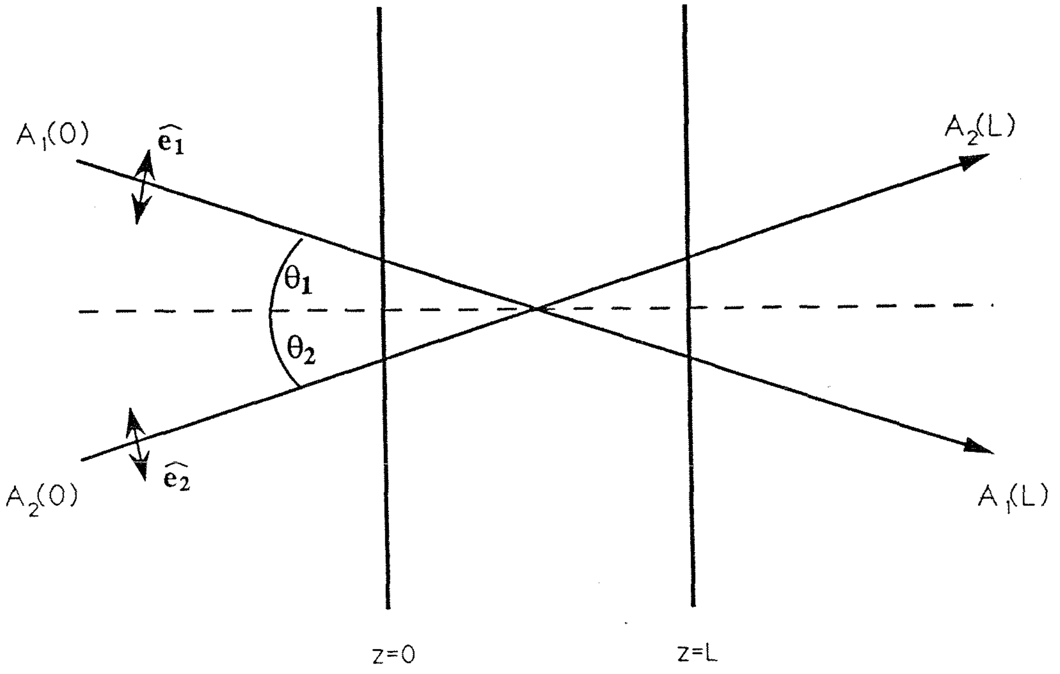

Fig. 2-3 Two wave mixing geometry in a photorefractive material. The two waves are incident on the sample with polarization $\hat{e}_1$ and $\hat{e}_2$ and with amplitudes A_1 and A_2.

$$\mathbf{E}_2(\mathbf{r},t) = A_2(\mathbf{r})e^{i(\mathbf{k}_2\cdot\mathbf{r}-\omega t)}\hat{\mathbf{e}}_2 + c.c. \tag{2.26b}$$

and are polarized along the unit vectors $\hat{\mathbf{e}}_1$ and $\hat{\mathbf{e}}_2$. The waves create a photorefractive index grating given by

$$\Delta n(\mathbf{r}) = \frac{1}{2}d_{eff}n_0^3\frac{A_1(\mathbf{r})A_2^*(\mathbf{r})}{A_1A_1^* + A_2A_2^*}E_{sc}e^{i(\mathbf{k}_1-\mathbf{k}_2\cdot\mathbf{r})}\hat{\mathbf{e}}_1\cdot\hat{\mathbf{e}}_2 + c.c \tag{2.27}$$

where E_{sc} is the ratio of the magnitude of the photorefractive space charge field to the intensity modualtion, m, and where

$$d_{eff} = r_{eff} + p_{eff}E_0 \tag{2.28}$$

is the effective electrooptic coefficient which is taken to include both the linear and the quadratic electrooptic effect with an applied field , E_0.

Substituting eqns.(2.26,27) into the scalar wave equation

$$\nabla E(\mathbf{r}) + k^2(\mathbf{r})E(\mathbf{r}) = 0 \tag{2.29}$$

where $k = \frac{\omega}{c}n$, and by using the slowly varying envelope approximation,

$$\frac{d^2A_i}{dz^2} \ll k\frac{dA_i}{dz} \tag{2.30}$$

results in the coupled wave equations

$$cos\theta_1\frac{dA_1}{dz} = -\gamma\frac{A_2A_2^*A_1}{A_1A_1^* + A_2A_2^*} - \frac{\alpha}{2} \tag{2.31}$$

$$cos\theta_2 \frac{dA_2}{dz} = -\gamma \frac{A_1 A_1^* A_2}{A_1 A_1^* + A_2 A_2^*} - \frac{\alpha}{2} \tag{2.32}$$

where

$$\gamma = \frac{i\omega}{4c} d_{eff} n_0^3 E_{sc} \frac{A_1 A_1^* + A_2 A_2^*}{A_1 A_2^*} \mathbf{\hat{e}_1} \cdot \mathbf{\hat{e}_2} \tag{2.33}$$

is the coupling coefficient, and α is the absorption coefficient. The equations can be expressed in terms of the intensities and phases of the waves using $A_i = I_i^{1/2} e^{i\psi_i}$

$$cos\theta_1 \frac{dI_1}{dz} = -\Gamma \frac{I_1 I_2}{I_1 + I_2} - \alpha I_1 \tag{2.34}$$

$$cos\theta_2 \frac{dI_2}{dz} = \Gamma \frac{I_1 I_2}{I_1 + I_2} - \alpha I_2 \tag{2.35}$$

$$cos\theta_1 \frac{d\psi_1}{dz} = -\gamma_i \frac{I_2}{I_1 + I_2} \tag{2.36}$$

$$cos\theta_2 \frac{d\psi_2}{dz} = -\gamma_i \frac{I_1}{I_1 + I_2} \tag{2.37}$$

where Γ=2Re[γ] and γ_i= Im[γ]. Solutions of the above equations for the symmetric geometry ($\theta_1 = \theta_2 = \theta$) are given by

$$I_1(\eta) = [I_1(0) + I_2(0)][1 + \frac{I_2(0)}{I_1(0)} e^{\Gamma\eta}] e^{-\alpha\eta} \tag{2.38}$$

$$I_2(\eta) = [I_1(0) + I_2(0)][1 + \frac{I_1(0)}{I_2(0)} e^{-\Gamma\eta}] e^{-\alpha\eta} \tag{2.39}$$

$$\psi_1(\eta) = \psi_1(0) - \gamma_i \eta + \frac{\gamma_i}{\Gamma} ln \left[\frac{1 + (I_1(0)/I_2(0))}{1 + (I_1(0)/I_2(0)) e^{-\Gamma\eta}} \right] \tag{2.40}$$

$$\psi_2(\eta) = \psi_2(0) - \gamma_i\eta - (\gamma_i/\Gamma)ln\left[\frac{1+(I_2(0)/I_1(0))}{1+(I_2(0)/I_1(0))e^{\Gamma\eta}}\right] \tag{2.41}$$

where $\eta = z/\cos\theta$.

The solutions indicate that when two waves interact in a photorefractive medium, one will gain intensity at the expense of another. The amount of gain is determined by the component of the space charge field, E_{sc}, which is $\pi/2$ out of phase with the intensity pattern. The coupling can be understood to arise from both waves scattering from the grating with the same amplitude, but one will scatter constructively and the other destructively into the other. Note that the direction of gain is determined by the sign of γ. This can be used to determine the sign of the photorefractive charge carrier if the sign of the electrooptic coefficient is known.

2.4 Photorefractive measurements

Wave coupling measurements provide information on the phase and the magnitude of the photorefractive nonlinearity. The two beam coupling constant, Γ, can be determined by measuring both the incident and transmited intensities for each wave. Γ is then determined from the identity

$$\Gamma = \frac{1}{l}ln[\frac{I_1(0)I_2(l)}{I_1(l)I_2(l)}] \tag{2.42}$$

where l is the thickness of the sample. For the case of low photorefractive coupling the grating can be approximated as a plane holographic grating. The diffraction efficiency from a plane thick hologram derived by Kogelnik from the coupled mode equations is given by[12]

$$\eta = e^{-\alpha l} sin^2(\frac{\pi l \Delta n}{\lambda cos(\theta/2)}) \tag{2.43}$$

where α is the absorption coefficient, Δn is the refractive index change, λ is the wavelength of the light, and θ is the angle between the incident and diffracted waves.

A parameter used to compare photorefractive materials is the photorefractive sensitivity, S, defined as the index change per absorbed unit of energy. It is a measure of how efficiently a material uses an absorbed photon to create a photorefractive grating. It is given by[26,27]

$$S = \frac{d\Delta n}{d(\alpha I t)} = \frac{\Delta n_0}{\alpha I \tau_e} \tag{2.44}$$

where Δn_0 is the amplitude of the refractive index change, I is the intensity, and τ_e is the photorefractive response time.

REFERENCES

1. A. Ashkin, G.D. Boyd, J.M. Dziedzic, R.G. Smith, A.A. Ballman, H.J. Levinstein, K. Nassau, "Optically-induced refractive index inhomegeneities in $LiNbO_3$ and $LiTaO_3$," Appl. Phys. Lett. **9**, 72 (1966).
2. F.S. Chen, "A laser-induced inhomogeneity of refractive indices in KTN," J. Appl. Phys. **38**, 3418 (1967).
3. W. Phillips, J.J. Amodei, D.L. Staebler, "Optical and holographic properties of transition metal doped lithium niobate," RCA Rev. **33**, 94 (1972).
4. M.G. Clark, F.J. DiSalvo, A.M. Glass, G.E. Peterson, "Electronic structure and optical index damage of iron-doped lithium niobate," J. Chem. Phys. **59**, 6209 (1973).
5. H. Kurz, E. Kratzig, W. Keune, H. Engelmann, U. Gonser, B. Dischler, A. Rauber, "Photorefractive centers in $LiNbO_3$ studied by optical-, Mossbauer-, and epr-methods," Appl. Phys. **12**, 355 (1977).
6. E. Kratzig and R. Orlowski, "Light induced transport in doped $LiNbO_3$ and $LiTaO_3$," Ferroelect. **27**, 241 (1980).
7. E. Kratzig and R. Orlowski, "$LiTaO_3$ as holographic storage material," Appl. Phys. **15**, 133 (1978).
8. J.B. Thaxter, "Electrical control of holographic storage in Strontium-Barium Niobate," Appl. Phys. Lett. **15**, 210 (1969).
9. J.J. Amodei, "Analysis of transport processes during holographic recording in insulators," RCA Rev. **32**, 185 (1971).

10. J.J. Amodei, "Electronic diffusion effects during hologram recording in crystals," Appl. Phys. Lett. **18**, 22 (1971).

11. A.M. Glass, D. von der Linde, D.H. Auston, T.J. Negran, "Excited state polarization, bulk photovoltaic effect and the photorefractive effect in electrically polarized media," J. Elect. Matls. **4**, 915 (1975).

12. H. Kogelnik, "Coupled wave theory for thick hologram gratings," B.S.T.J. **48**, 2909 (1969).

13. D.L. Staebler, J.J. Amodei, "Coupled-wave analysis of holographic storage in $LiNbO_3$," J. Appl. Phys. **43**, 1042 (1972).

14. Y. Ninomiya, "Recording characteristics of volume holograms," J. Opt. Soc. Am. **63**, 1124 (1973).

15. D. W. Vahey, " A nonlinear coupled-wave theory of holographic storage in ferroelectric materials," J. Appl. Phys. **46**, 3510 (1975).

16. N.V. Kukhtarev, V.B. Markov, S.G. Odulov, M.S. Soskin, and V.L. Vinetski, "Holographic storage in electrooptic crystals. I. Steady state," Ferroelect. **22**, 949 (1979).

17. G. C. Valley, " Simultaneous electron hole transport in photorefractive materials," J. Appl. Phys. **59**, 3363 (1986).

18. F.P. Strohkendl, J.M.C. Jonathan, R.W. Hellwarth, " Hole-electron competition in photorefractive gratings," Opt. Lett. **11**, 313 (1986).

19. M. Carrascosa, F. Agullo-Lopez, "Erasure of holographic gratings in photorefractive materials with two active species," **27**, 2851 (1988).

20. J.P. Huignard, A. Marrakchi, "Coherent signal beam amplification in two-wave mixing experiments with photorefractive $Bi_{12}SiO_{20}$ crystals," Opt. Comm. **38**, 249 (1981).

21. S.I. Stepanov, M.P. Petrov, "Efficient unstationary holographic recording in photorefractive crystals under an external alternating electric field," Opt. Comm. **53**, 292 (1985).

22. J. Feinberg, D. Heiman, A.R. Tanguay, R.W. Hellwarth, "Photorefractive effects and light-induced charge migration in barium titanate," J. Appl. Phys. **51**, 1297 (1980).

23. R. A. Mullen, "Photorefractive measurements of physical parameters," Photorefractive Materials and their Applications I., Springer-Verlag, Berlin (1987).

24. G.C. Valley, J. F. Lam, "Theory of photorefractive effects in electro-optic crystals," Photorefractive Materials and their Applications I., Springer-Verlag, Berlin (1987).

25. P. Refregier, L. Solymar, H. Rajbenbach, J.P. Huignard, "Large-signal effects in an optical BSO amplifier," Elect. Lett. **20**, 656 (1984).

26. A. M. Glass, "The photorefractive effect," Opt. Eng. **17**, 470 (1978).

27. G.C. Valley, M.B. Klein, "Optimal properties of photorefractive materials for optical data processing," Opt. Eng. **22**, 704(1983).

CHAPTER THREE

CRYSTAL GROWTH OF PHOTOREFRACTIVE KTN

3.1 Introduction

In order to investigate the photorefractive properties of a material it was deemed essential to also become involved in the growth of these materials. Many of the more promising photorefractive materials suffer from severe availability problems. In addition, a close interaction between crystal grower and materials researcher is expected to benefit both fields. Crystal growth is often described as an art rather than a science. The conditions necessary to produce good quality crystals vary for each material and growth system and can only be learned through experience. This chapter describes the crystal growth of photorefractive $KTa_{1-x}Nb_xO_3$. A high temperature crystal growth system was designed and constructed. The system as well as the top seeded solution growth method used to grow KTN will be described. The structural and ferroelectric properties of KTN will also be discussed.

3.2 Crystal growth system

The high temperature crystal growth system consists of two main assemblies: the furnace and the pulling apparatus. A schematic of the furnace is shown in Fig. 3-1. The furnace is formed by four concentric aluminum oxide ceramic cylinders. Several aluminum oxide discs, which are cemented together and fit into the ends of the cylinders, form the top and bottom of the furnace. The top assembly is removable to allow easy access into the furnace. Several holes are machined into this

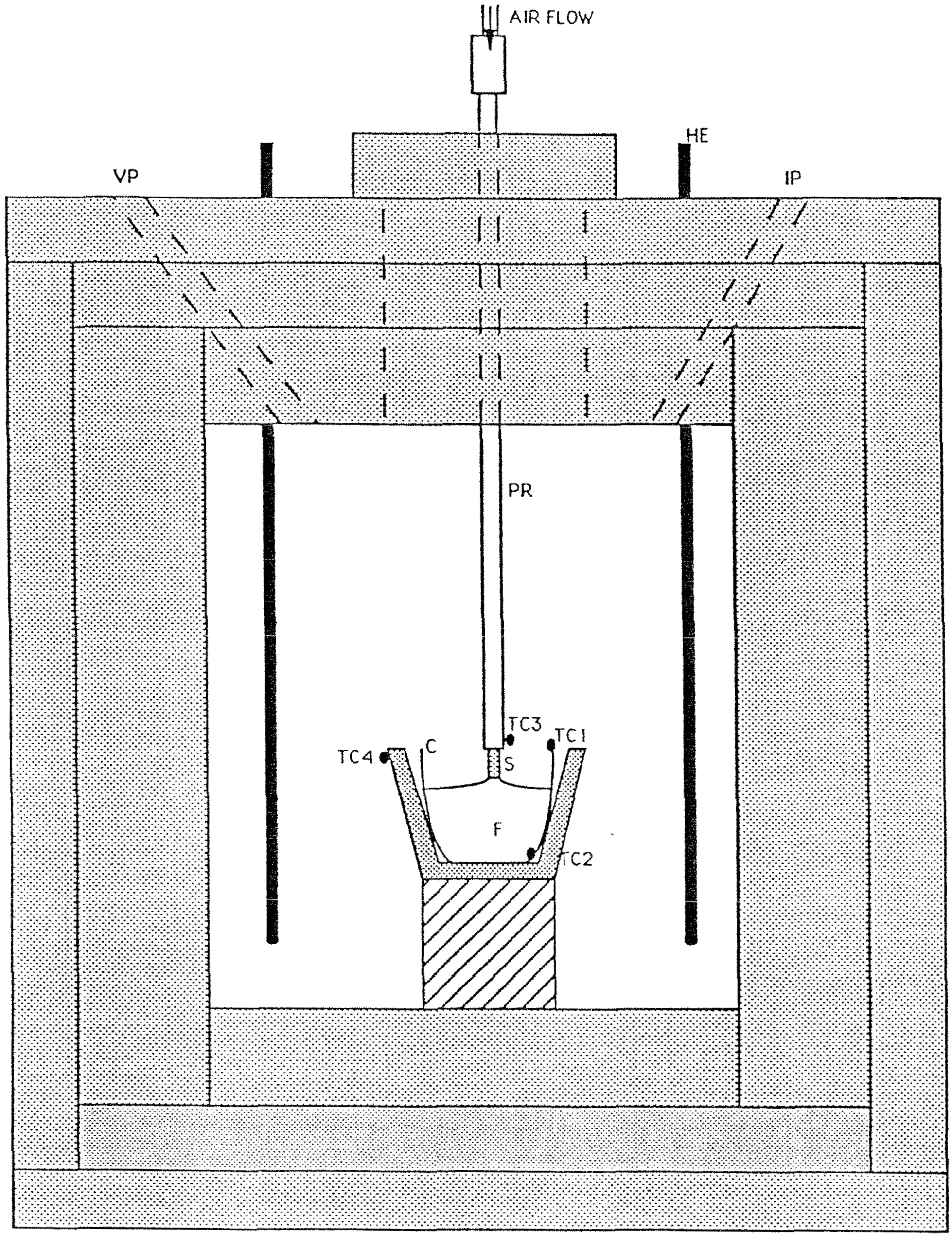

Fig. 3-1 High temperature crystal growth system used to grow photorefractive crystals: (PR) pulling rod, (HE) heating elements, (TC1-4) thermocouples, (VP) viewing port, (IP) illumination port.

assembly for the placement of the heating elements, access for the crystal pulling tube, and for two viewports. Four small 1/2" holes in the bottom assembly are used for the placement of thermocouples into the furnace. The inside of the furnace measures 9" in height with a 9" inner diameter and is open to the atmosphere during growth. A 100cc platinum crucible is located at the center of the furnace and is supported by a thin aluminum oxide crucible.

The furnace is heated by six molybdeum disilicide resistance heating elements arranged in series. A programmable temperature controller allows for the adjustment of the temperature to within 0.1C. It accepts input from a Pt/PtRh thermocouple placed within the furnace. The controller is connected to a silicon control relay switch (SCR) which adjusts the current to the heating elements. The line voltage to the SCR is stepped down to a nominal value of 30 volts by a variable transformer. Three other thermocouples within the furnace are monitored. These are located at the base and at the top lip of the crucible, and at the base of the seed crystal. The maximium temperature of the furnace is 1650C and is stable to 0.1C. Operating power is 1 kW at 1250C.

The purpose of the pulling apparatus is to support the crystal during growth and to provide the cooling force necessary to drive the growth process. It consists of a stainless steel pulling tube through which a stabilized air stream flows at approximately 5 l/min. At the end of the pulling tube is an aluminum oxide ceramic tube which is lowered into the furnace and to which a seed crystal, used to initiate growth, is attached by platinum wires. A concentric stainless steel inner tube allows cooling air to flow to the tip of the ceramic tube and cool the seed crystal. The air then flows out through a fixture which connects the ceramic and pulling tube. During growth the tube and attached crystal are rotated, at typically 20 rpm, with the direction of rotation reversed every 160 sec. The purpose of this is to present as uniform a temperature and flux composition as possible at the growth boundary. The pulling apparatus is mounted to a linear translation stage. The pulling rate can be controlled electronically between 0.225 mm/hr to 1mm/sec.

3.3 Top seeded solution growth method

This section describes the top seeded solution growth of KTN.[1,2] KTN is grown in a solution with an excess of K_2CO_3 (solvent). Solution growth is necessary since KTN as well as $KTaO_3$ and $KNbO_3$ melt incongruously.[3,4] That is, they decompose into different components before melting which prevents single crystal growth in a stoichiometric melt. One advantage of solution growth is that the solvent lowers the growth temperature below the melting point of the solid. The lower temperature makes possible the growth of a number of high melting point crystals and also leads to lower defect concentrations. However, the solvent also leads to significantly slower growth rates (roughly 1cm/day).

The phase diagram of the $KTaO_3$-$KNbO_3$ solid phase solution is given in Fig. 3-2.[5] In the top seeded solution growth method a seed crystal attached to the pulling tube is lowered into the flux of composition x_f. The temperature is lowered to slightly below the liquidus at temperature T_1. The solution is supersaturated and solid growth results on the seed. Note that the air cooling insures that the seed

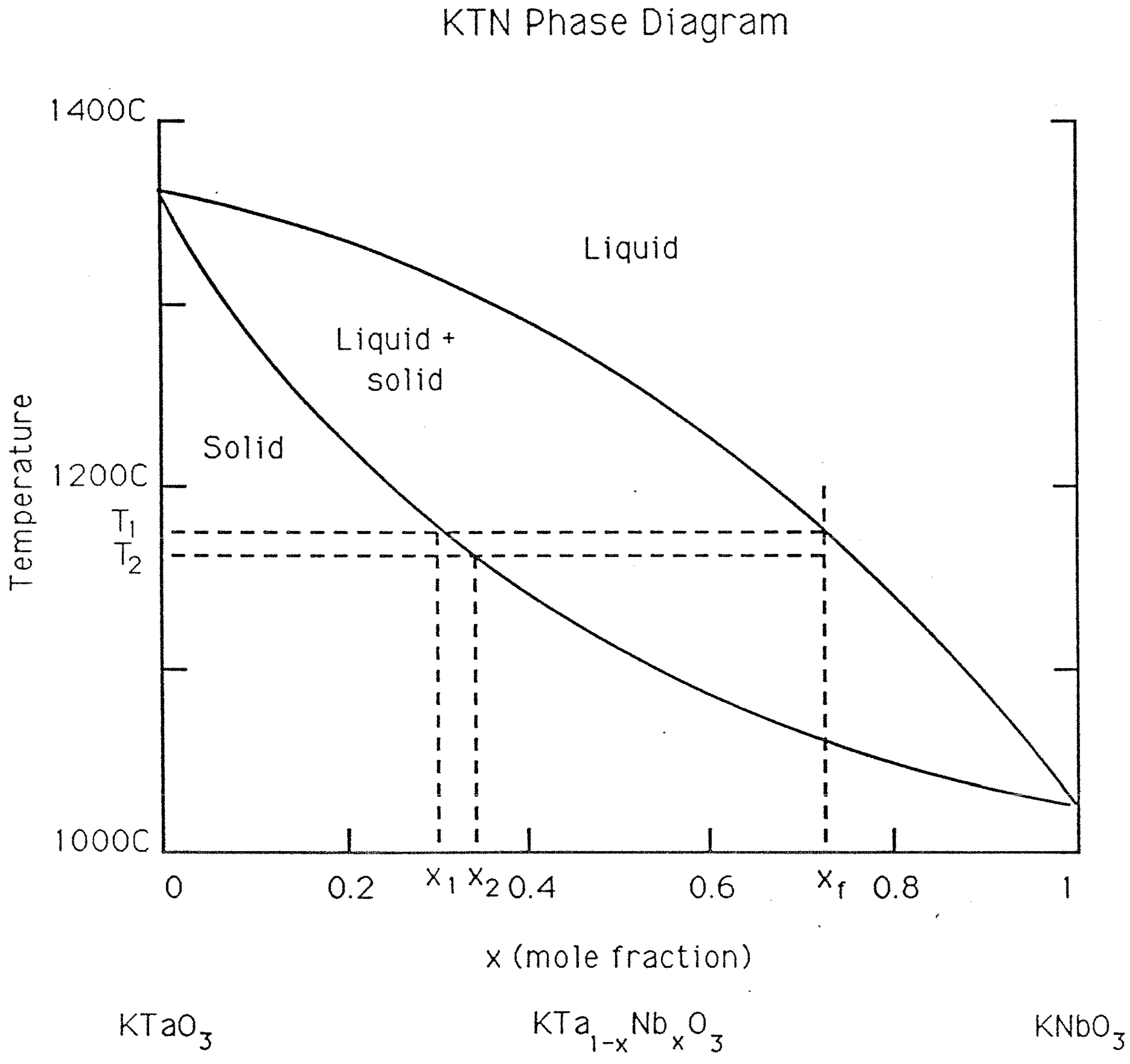

Fig. 3-2 Phase diagram for the $KTaO_3$-$KNbO_3$ (KTN) system. The flux is at concentration x_f. Growth is initiated at temperature, T_1, with crystal composition x_1 and is maintained by cooling to temperature T_2.

is the nucleation site. At this point equilibrium is soon reached between a solid of composition x_1 with a liquid solution of composition x_f. For growth to continue, the temperature is lowered continuously.

When growth occurs over the temperature range T_1 to T_2, the composition of the crystal varies between x_1 and x_2. This inherent concentration gradient can be reduced by growing crystals small in volume with respect to the melt but is always present when using the slow cooling method. The growth of good quality crystals is critically dependent on the furnace. The temperature within the furnace must be as uniform as possible to prevent nucleation sites other than the seed crystal to develop. In addition, any small temperature fluctuation will result in corresponding compositional variations or striations.

As an example of a typical growth process we summarize the steps for the growth of a KTN:Cu,V crystal. The main stages of the growth process are as follows:

(a) Preperation of the solution. First a solution of the crystal constituents is formed using K_2O as the solvent. The initial powder composition which placed into the crucible is given in table 3-1.

The powder was warmed up to 1300C and soaked at that temperature for approximately 20 hours.

(b) Seeding. A seed crystal was mounted on the pulling tube and lowered into the furnace. The seed was taken from a crystal with nearly the same composition

Material	% per mole
K_2CO_3	57
Ta_2O_5	22.8
Nb_2O_5	15.2
$2CuO$	2.5
V_2O_5	2.5

Table 3-1 Composition of the flux from which a KTN:Cu,V crystal was grown using the top seeded solution growth method.

as that being grown. It measured 0.35x0.25x0.75 mm^3 and was cut along the crystalographic [100] directions. The seed was lowered into the melt for several minutes, pulled out, and and observed through the viewports to determine whether growth had occurred at the seed. The process was repeated several times with the temperature being lowered after each step until growth was observed to occur at 1275C. Note that the air cooling of the seed insures that it is the only nucleation site. The temperature at the touching point is now at the liquidus of the solution and the seed and solution is at equilibrium. A rotation of the seed (20rpm) is initiated with the direction of rotation reversed every 160 seconds in order to maintain isotropy of the temperature and to stir the solution.

(c) Crystal Growth. After this equilibrium is reached a slow cooldown of the combined seed+solution system is started at 0.5 C/hr. This is the main growth stage and occurs over a 25-hour period with the temperature lowered from 1275C to 1262.5C. The crystal was then pulled out of the melt at a rate of 0.225 mm/hr for approximately 24 hours with the cooldown rate increased to 1.5C/hr.

(d) Anealing: The crystal is slowly cooled to room temperature at a rate of 15C/hr.

The crystal is shown in Fig. 3-3a. It is blue-green and weighed 25.89 gm. Its chemical composition was determined by electron microprobe analysis and was found to be $KTa_{0.87}Nb_{0.13}O_3$:Cu,V. (The Cu concentration was 0-0.0024% per mole, and the V concentration was 0-0.0006%). The optical quality was very good except for some external scratches.

3.4 Growth of photorefractive KTN crystals

A number of crystals were grown with varying Ta/Nb ratios and doped with a a variety of transition metals. The first crystals grown had a relatively low Nb concentration (x=0.1) with a T_c =100K. This was due to the availability of seed crystals with this composition. Successive KTN crystals were grown with slightly increasing Nb concentrations using seed crystals from the previous growths. By this method crystals were grown over the range x=0.10 to x= 0.35 with the corresponding phase transitions extending from T=100C to T=300C. All samples were doped with transition metals. Dopants used singly include Fe, Ti, Cr, and Cu. Double doping combinations include (Cu,V), (Fe,Ti), (Fe,Cr) and (Mn,Ti). Photographs of four KTN crystals: KTN:Cu,V, KTN:Fe, KTN:Ti and KTN:Fe,Cr, are shown in Figs.3-3(a)-(d).

Several types of defects occur in the grown crystals.[6] Inclusions occur for fast growth rates and always exist at the point where growth is first initiated at the tip of the seed crystal. The defect site usually propagates down the entire length of the crystal along the growth direction. Planar growth boundary defects occur along

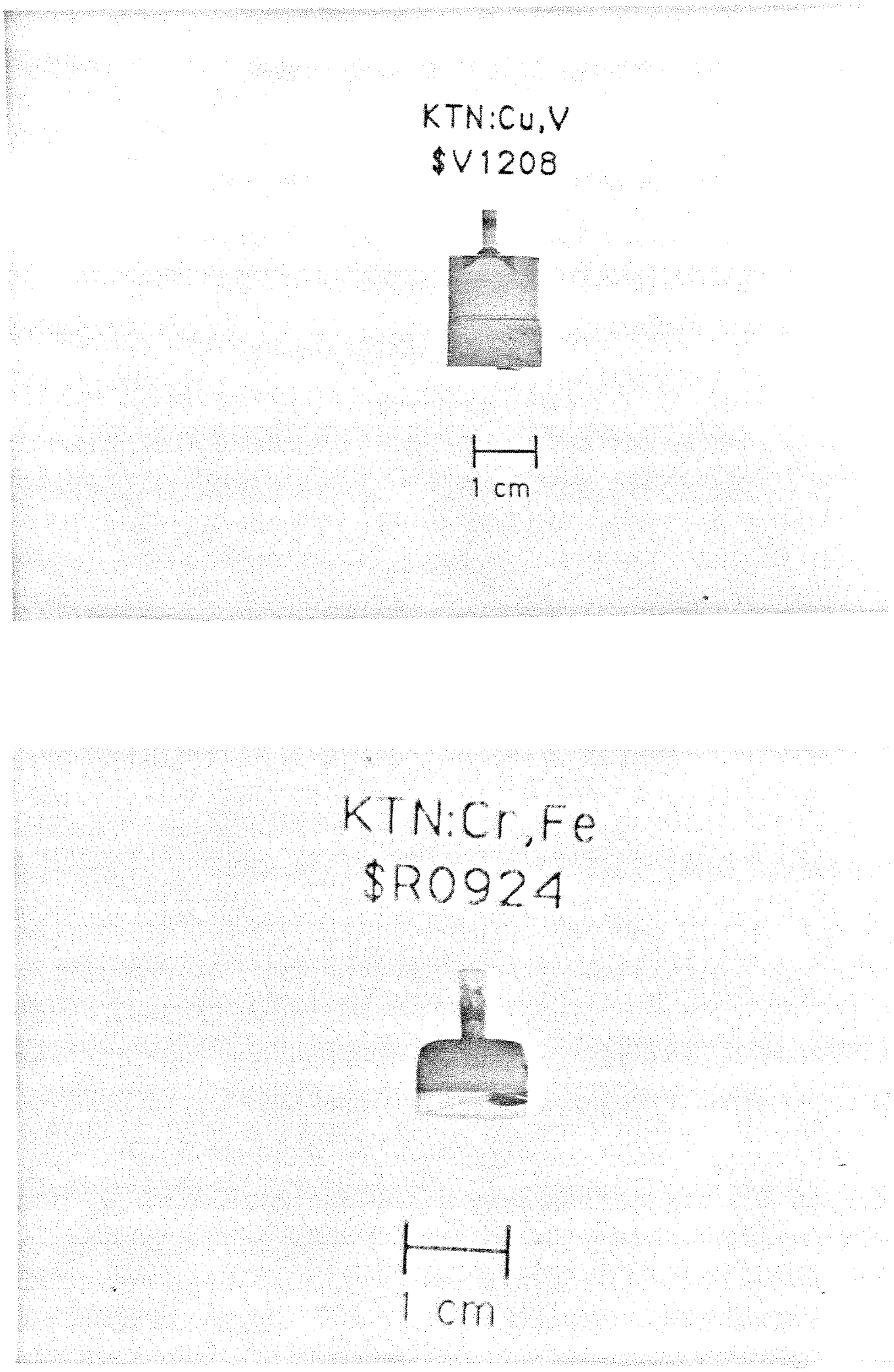

Fig. 3-3 (a),(b) Photographs of a KTN:Cu,V crystal and a KTN:Fe,Cr crystal.

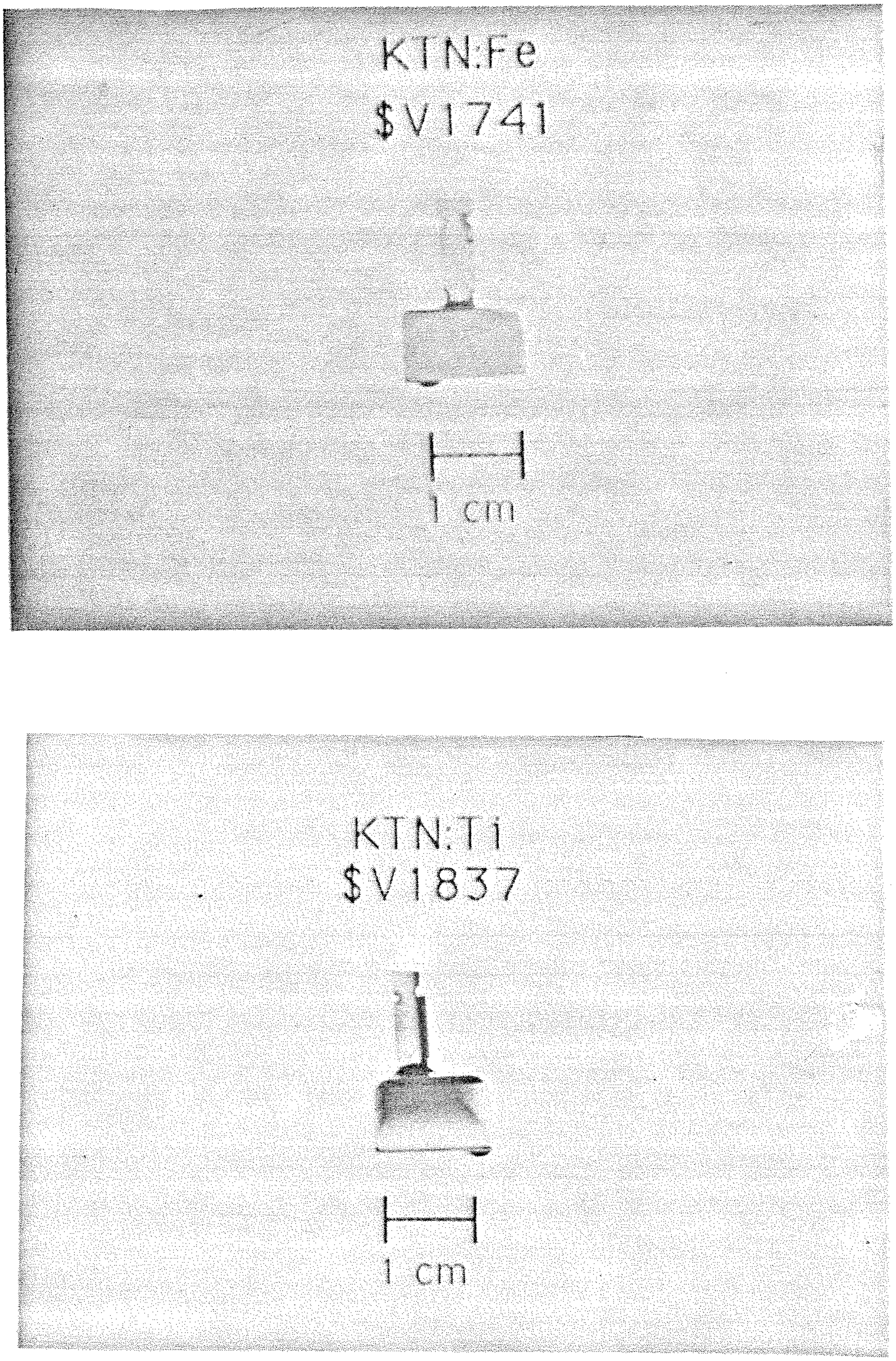

Fig. 3-3 (c),(d) Photographs of a KTN:Fe crystal and a KTN:Ti crystal.

the diagonals of a cross section of a crystal. They are the result of the boundary between regions of different growth directions. Both defects are visible from the strain they produce in a KTN sample placed between crossed polarizers. Samples are cut from a crystal using a wire saw so as to avoid these defects. The samples are then polished using a series of lapping and polishing steps. The sample is first mounted in a hand held jig and is then lapped flat on a glass surface using 5 micron aluminum oxide. This is followed by a rough polishing step with 3 micron diamond abrasive on a polishing cloth. The final polish is done using 0.3 micron aluminum oxide on cloth. After each step the sample and jig are ultrasonically cleaned to remove any abrasive. Cr and Au electrodes are then evaporated on two opposite sides the sample.

Six samples cut from different crystals were prepared for the photorefractive studies described in this thesis. The composition, dopants, Curie temperature, and chapter in which the samples are described are summarized in Table 3.2. The compositions were determined using electron microprobe analysis. The temperature dependence of the low frequency dielectric constant was determined from capacitance measurements. The Curie temperatures was taken to correspond to the high temperature peaks in the dielectric constant. In addition, the photorefractive properties of a series of KTN crystals doped with Fe and Cr with ferroelectric phase transitions near room temperature were also investigated. Their properties are reported elsewhere.[7]

Sample	T_c	Chapter
$KTa_{0.91}Nb_{0.09}O_3$:Cu,V	100K	4
$KTa_{0.87}Nb_{0.13}O_3$:Cu,V	120K	4
$KTa_{0.70}Nb_{0.30}O_3$:Cu,V	243K	5
$KTa_{0.70}Nb_{0.30}O_3$:Fe,Ti	244K	6
$KTa_{0.67}Nb_{0.33}O_3$:Ti	259K	6
$KTa_{0.68}Nb_{0.32}O_3$:Fe	265K	6

Table 3-2. The chemical composition, Curie temperature, and the chapter in which each sample is investigated.

3.5 Properties of KTN

$KTa_{1-x}Nb_xO_3$ (KTN) is a solid solution consisting of $KTaO_3$ and $KNbO_3$. The dimensions of the unit cell is relatively constant across the composition range of the solution. The lattice constant of a $KTa_{0.70}Nb_{0.30}O_3$:Cu,V sample in the cubic phase was determined from powder x-ray diffraction measurements to be a_o= 3.997 angstroms (Fig. 3-4). By comparison- that of $KTaO_3$ is a_o= 3.989 angstroms.[8] The small change in lattice constant with the addition of Nb makes possible the growth of KTN throughout the solution range. KTN has a perovskite structure given by the general formula ABO_3 (Fig. 3.5).[9] The K ion occupies the A site represented by the corners of the cubic cell. A Ta ion or a Nb ion occupies the B site at the center of the cell. The oxygen ions occupy face center sites and form an octahedral cage about the B cation.

KTN undergoes a paraelectric to ferroelectric phase transition with a Curie temperature which depends approximately linearly on Nb concentration (7 C per mole % of Nb).[10] The Curie temperture varies from that of $KTaO_3$, which approaches a ferroelectric phase transition at T=0K, to that of $KNbO_3$ at T=712K.

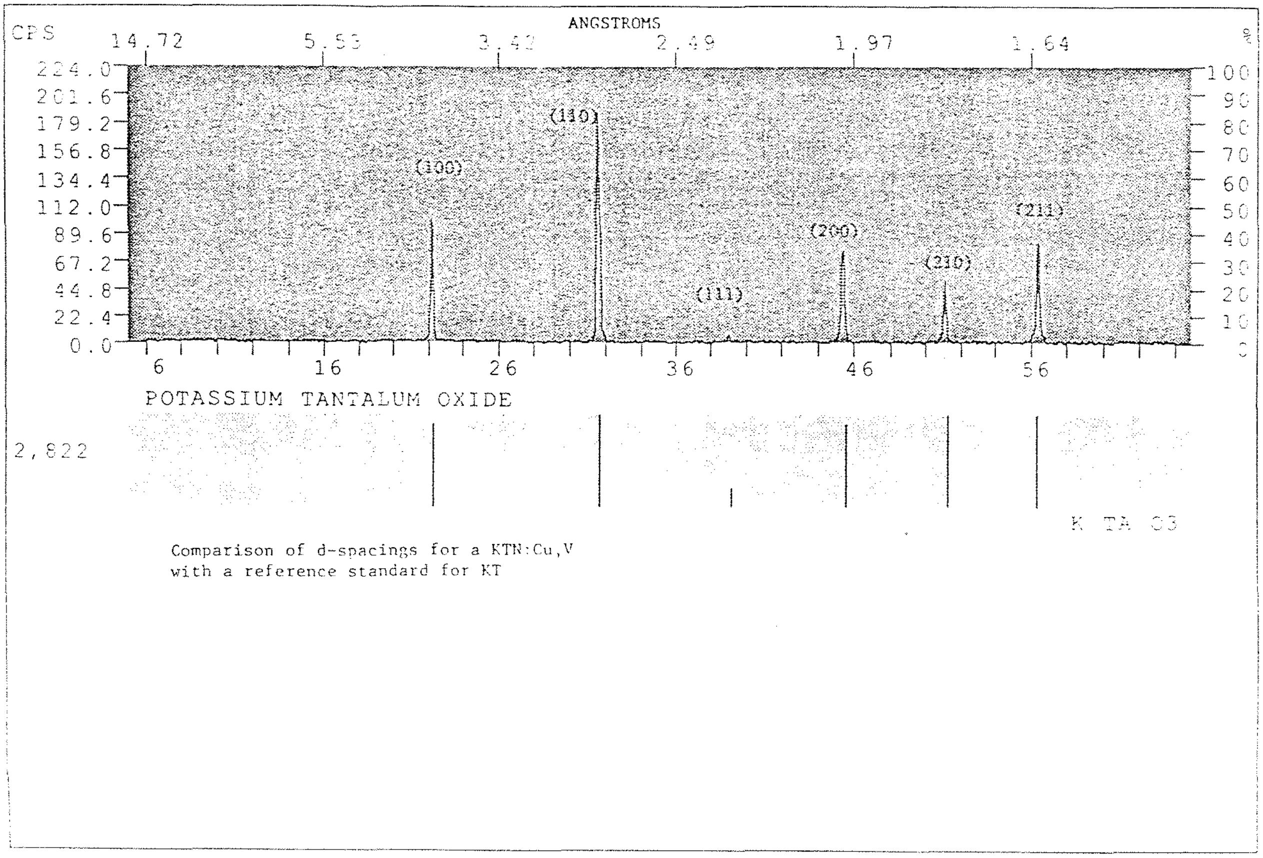

Comparison of d-spacings for a KTN:Cu,V
with a reference standard for KT

Fig. 3-4 Powder x-ray diffraction spectrum for a $KTa_{0.70}Nb_{0.30}O_3$:Cu,V sample. Also shown for comparison is that of a cubic $KTaO_3$ crystal.

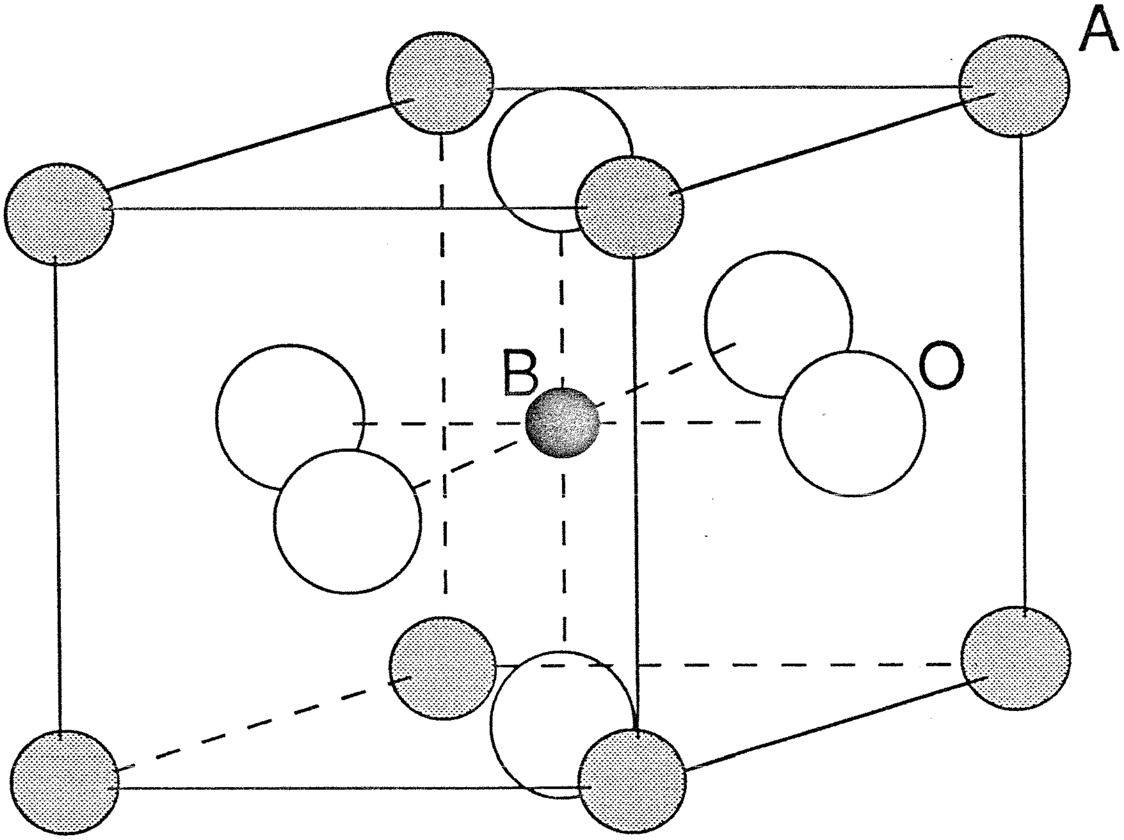

Fig. 3-5 Perovskite structure given by the general formula ABO_3.

For x>0.30 the transition is first order which results in a discontinuity in the spontaneous polarization as the temperature is lowered through the transition. It is second order for x<0.30 which produces a continuous change in the spontaneous polarization through the transition. In the paraelectric phase KTN is cubic with point group m3m. As the temperature is lowered it undergoes transitions from the tetragonal to the orthorhombic to the rhombohedral phases with the symmetry reduced to point groups 4mm, mm2, and 3m respectively. Each phase transition is a result of displacements of ions from the site occupied in the cubic phase.[9] The K ion remains essentially fixed. As the temperature is lowered from the cubic phase the (Ta,Nb) ions are displaced along [001] in the tetragonal phase, [011] in the orthorhombic phase, and [111] in the rhombohedral phase. The oxygen octahedra remains rigid and undergoes tilts along each of these directions.

References

1. A. Agranat, V. Leyva, K. Sayano, A. Yariv, "Photorefractive properties of $KTa_{1-x}Nb_x$ O_3 in the paraelectric phase," Nonlinear Optical Properties of Materials, SPIE Proceedings vol. 1148, 52 (1989).
2. V. Belruss, J. Kalnajs, A. Linz, R.C. Folweiler, "Top-seeded solution growth of oxide crystals from non-stoichiometric melts," Mat. Res. Bull. **6**, 899 (1971).
3. A. Reisman, F. Holtzberg, M. Berkenblit, M. Berry, "Reactions of the group VB pentoxides with alkalai oxides and carbonates. III. Thermal and x-ray phase diagrams of the system K_2O or K_2CO_3 with Ta_2O_5, " J. Am. Chem. Soc. **78**, 4514 (1956).
4. A. Reisman, F. Holtzberg, "Phase equilibria in the system K_2CO_3-Nb_2O_5 by the method of differential thermal analysis," J. Am. Chem. Soc. **77**, 2115 (1955).
5. A. Reisman, S. Triebwasser, F. Holtzberg, "Phase diagrams of the system $KNbO_3$-$KTaO_3$ by the methods of differential thermal and resistance analysis," J. Am. Chem. Soc. **77**, 4228 (1955).
6. D. Rytz, H.J. Scheel, "Crystal growth of $KTa_{1-x}Nb_xO_3$ $(0 < x < 0.04)$ solid solutions by a slow-cooling method," J. Crystal Growth **59**, 468 (1982).
7. K. Sayano, V. Leyva, A. Agranat, A. Yariv, "Photorefractive potassium tantalate niobate crystals with phase transitions near room temperature," unpublished.
8. F.S. Chen, J. Geusic, S. Kurtz, J. Skinner, and S. Wemple, "Light modulation

and beam deflection with potassium tantalate-niobate crystals," J. Appl. Phys. **37**,388 (1966).

9. M.E. Lines, A.M. Glass, "Principles and applications of ferroelectrics and related materials," Oxford University Press, Oxford (1979).

10. S. Treibwasser, "Study of ferroelectric transitions of solid-solution single crystals of $KNbO_3$-$KTaO_3$," Phys. Rev. **114**, 63 (1959).

CHAPTER FOUR

APPLICATIONS OF THE PHOTOREFRACTIVE EFFECT

4.1 Introduction

Perhaps the most promising use of photorefractive materials is as volume holographic storage media. In this section we describe two applications involving the storage of volume holographic gratings in KTN. The first is a voltage controlled photorefractive effect which allows for full amplitude modulation of a diffracted wave at speeds much faster than the space charge response time.[1] The effect utilizes the quadratic electrooptic effect and an externally applied field in paraelectric KTN. The second section describes a procedure used to fix a photorefractive grating in a KTN sample.[2] It involves the writing of a photorefractive grating in the cubic phase of KTN and cooling the sample under an applied field through succesive phase transitions into the rhombohedral phase.

4.2 Voltage controlled photorefractive effect

4.2.1 Photorefractive properties of paraelectric KTN

Most previous demonstrations of the photorefractive effect involved the use of materials with a linear electrooptic effect. The refractive index change is directly proportional to the magnitude of the photorefractive space charge field. Modulation of the diffracted wave is limited by the time needed to redistribute the electronic charge of the space charge distribution. Response times as fast as a 20 microseconds under 4 W/cm^2 illumination have been observed in semiconductors such as GaAs.[3] In materials which lack inversion symmetry, such as paraelectric KTN and PLZT ceramics, the linear electrooptic effect vanishes. For these materials the lowest allowed electrooptic effect is the quadratic one and an externally applied field is needed for light to diffract from the photorefractive gratings which they create.

In the paraelectric temperature range ($T>T_c$) KTN is cubic with the centrosymmetric space group m3m, and thus the electrooptic effect is quadratic and is given by[4]

$$\Delta n = \frac{1}{2} n_0^3 g P^2 \tag{4.1}$$

where Δn is the birefringence, n_0 is the refractive index, g is the appropriate quadratic electrooptic coefficient, and P is the static (low frequency) polarization, given in the linear region by

$$P = \epsilon_0(\epsilon - 1)E \tag{4.2}$$

where ϵ is the dielectric constant and E is the electric field. The photorefractive effect which arises in paraelectric KTN can be summarized as follows: A spatially modulated light distribution creates a photorefractive space charge field, E_{sc}, through the charge photoexcitation and transport mechanisms described in chapter 2. In the prescence of an external electric field, E_0, these space charge fields induce refractive index changes given by

$$\Delta n = \frac{1}{2} n_0^3 g \epsilon_0^2 (\epsilon - 1)^2 (E_0^2 + 2E_0 E_{sc} + E_{sc}^2) \tag{4.3}$$

The first term represents a uniform index change and will not diffract light. The last term has twice the spatial frequency of the light intensity grating, and in a thick hologram will not diffract the writing beams since the Bragg condition is not satisfied. The second term represents a diffraction grating with an index change given by

$$\delta(\Delta n) = n_0^3 g \epsilon_0^2 (\epsilon - 1)^2 E_0 E_{sc} \tag{4.4}$$

Therefore the diffraction gratings in paraelectric KTN are linearly proportional to and can be modulated by an externally applied electric field, E_o. This allows the use of KTN as a medium for amplitude modulated holographic interconnects or phase conjugation.

4.2.2 Experiment

A KTN crystal doped with Cu and V and grown using the top seeded solution growth method was used for the experiments. Its chemical composition was determined from electron microprobe analysis to be given by $KTa_{0.91}Nb_{0.09}O_3$. The sample measured 3.0x3.5x5.5mm^3 and was cut along the [100] crystallographic directions. It appeared uniform when viewed through crossed polarizers. Electrodes of Cr and Au were evaporated on the sides normal to the 5.5mm edges. The sample was then placed in a low temperature cryostat system in which the temperature could be controlled to within 0.1K.

The ferroelectric phase transition temperature was determined from capacitance measurements of the low frequency dielectric constant. The paraelectric-to-ferroelectric transition (cubic-to-tetragonal transition) corresponds roughly to the highest temperature peak observed at T_c=100K. The dielectric response, $\epsilon(\omega)$, was measured using capacitance measurements at several temperatures above T_c and at frequencies up to 100kHz (Fig. 4-1).

The linear response for the polarization given in Eq.(4.2) is only valid for small fields. In accordance with the Devonshire theory of ferroelectric phase transitions, the dependence in the paraelectric phase is approximated as

$$E = aP + bP^3 \tag{4.5}$$

A modified Sawyer-Tower circuit was used to measure the dependence of the static polarization P on the electric field, E.[5] It was determined that $a=4.08\text{x}10^8$cm/F and $b=4.15\text{X}10^{19}$ $\text{cm}^5/\text{V}^2\text{F}^3$.

Holographic diffraction measurements were made using the two wave mixing method. A schematic of the experimental setup is shown in Fig. 4-2. A photorefractive diffraction grating was written using two expanded beams from a 514nm Ar^+ laser. The beams were expanded to prevent the formation of an internal field due to the buildup of charge in dark regions. The exposure lasted 7.75 min under an applied field during writing of E_w=900V/cm. Each beam had an intensity of 32mW/cm^2 and was polarized in the plane of incidence. The angle between the two writing beams was 11degrees (2.7μm grating period). All measurements were made

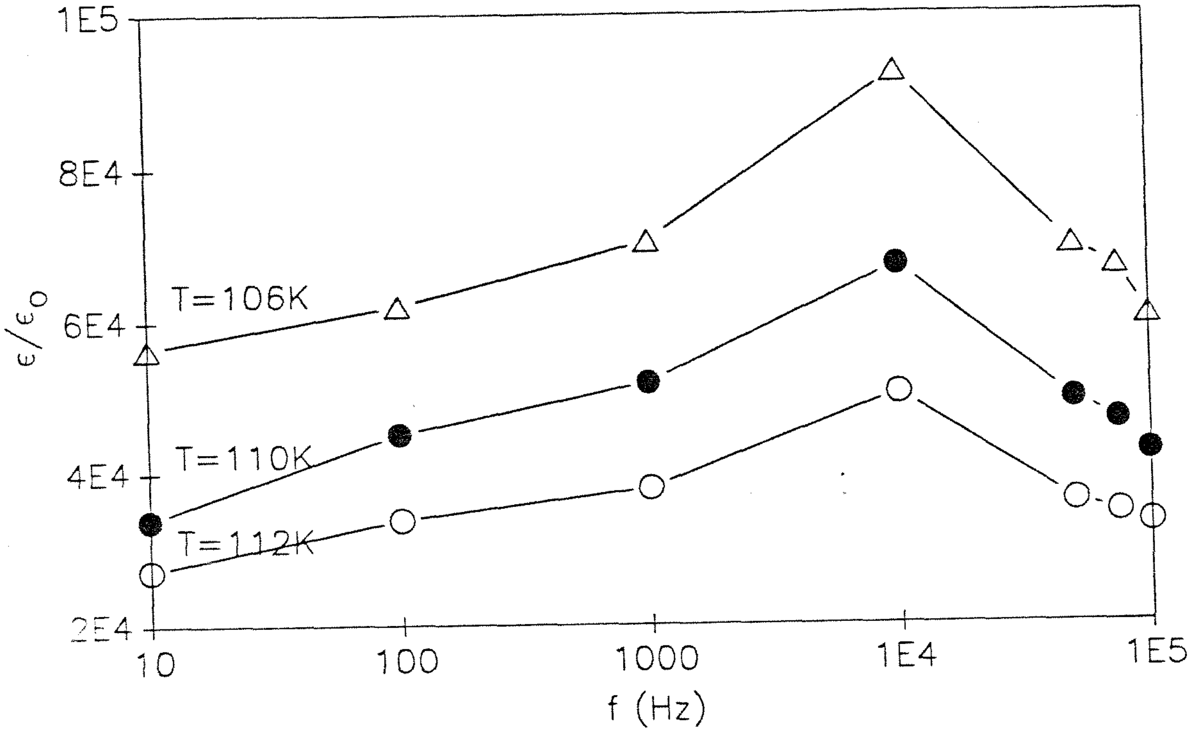

Fig. 4-1 The frequency dependence of the dielectric constant, $\epsilon(\omega)$, of a KTN sample at several temperatures in the paraelectric phase.

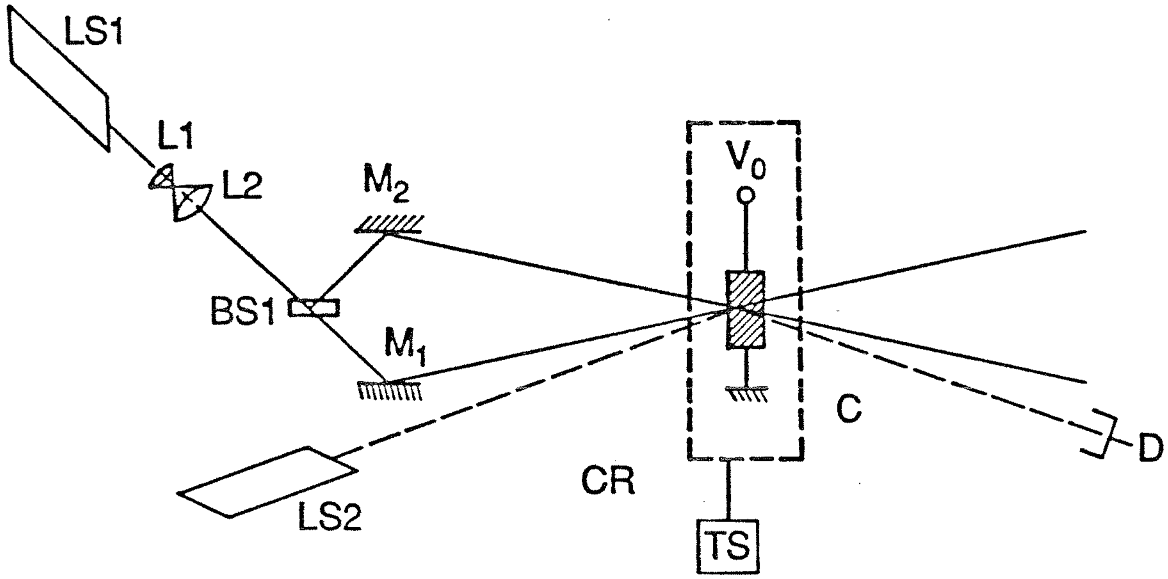

Fig. 4-2 Experimental set-up for the holographic diffraction measurements. A photorefractive index grating is written using two beams from a 514nm Ar laser. The strength of the grating is monitored by the diffraction of a weak HeNe beam alligned at the Bragg angle.

at T=112K. The magnitude of the index grating was monitored by the diffraction of a weak HeNe beam aligned at the Bragg angle. It was verified that the grating was not noticeably erased by the weak probe beam.

After the diffraction grating was written the writing beams were blocked and the diffracted intensity of the probe beam was measured as the applied voltage was varied. The dependence of the diffraction efficiency, η, on the applied voltage during readout is given in Fig. 4-3. The diffraction efficiency is observed to saturate at about 60% with a 1100 V applied field. A 50V/cm 20kHz ac field and a 400V/cm dc bias field were applied to the sample to demonstrate the modulation capability of the voltage controlled photorefractive effect. The modulating frequency in our experiments was limited to 20Khz by the bandwidth of our oscillator. The temporal behavior of the diffracted signal with the ac field is shown in Fig. 4-4.

4.2.3 Discussion

The diffraction efficiency in the geometry of Fig.4-3 is given approximately by that from a plane volume hologram[6]

$$\eta = e^{-\alpha l} sin^2(\frac{\pi \Delta n l}{\lambda cos(\theta/2)}) \tag{4.6}$$

where α is the absorption constant, l is the sample thickness, θ is the angle betweeen writing beams, and the refractive index change, Δn, given in Eq.(4.3) is proportional in magnitude to the externallly applied field. However, the dependence in Eq.(4.3) is not valid for large applied fields. To first order P varies as

$$P(x) = P_0 + \frac{dP}{dE} |_{E=E_0} E_{sc} \tag{4.7}$$

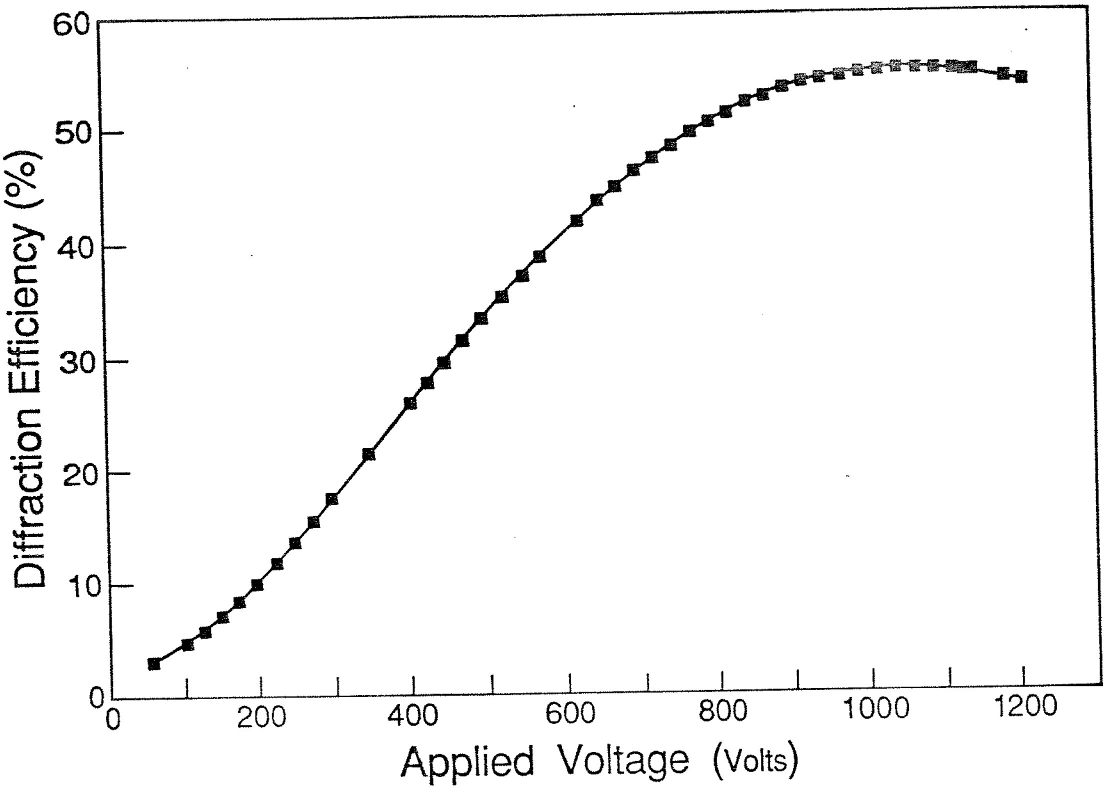

Fig. 4-3 The dependence of the diffraction efficiency of a photorefractive grating written in paraelectric KTN on an externally applied voltage.

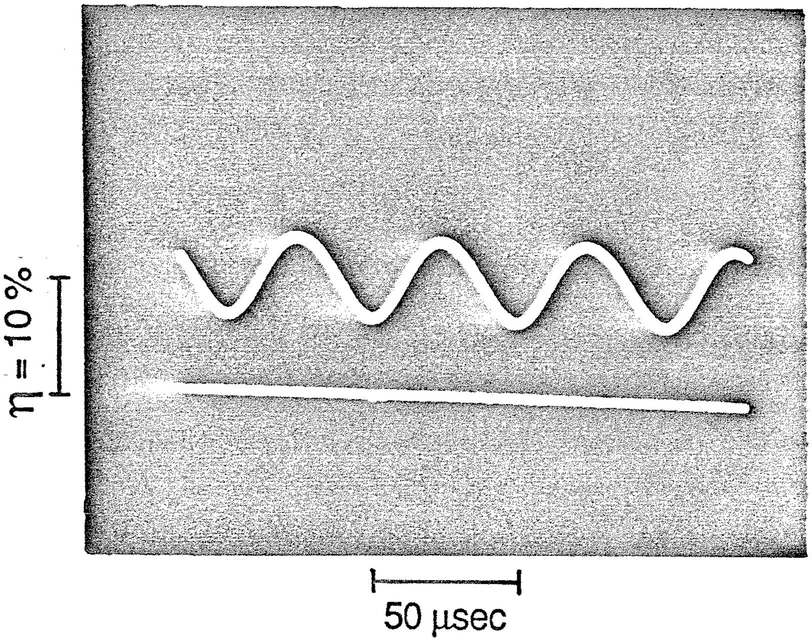

Fig. 4-4 The temporal dependence of the diffraction efficiency of a photorefractive grating in KTN under an applied 20KHz field.

where E_0 is the applied field and where $P_0=\epsilon_o(\epsilon-1)E_o$. Thus P^2 will contain a grating term of the same spatial frequency of the intensity pattern given by

$$\delta P^2(x) = 2P_0\frac{dP}{dE}\,|_{E=E_0}\,E_{sc} \tag{4.8}$$

The result is an induced refractive index grating given by

$$\delta(\Delta n) = n_0^3 g\epsilon_0(\epsilon-1)\frac{E_0E_{sc}}{(a+3b\epsilon_0^2(\epsilon-1)^2E_0^2)} \tag{4.9}$$

from which we expect $\delta(\Delta n)$ to vary nonlinearly with the applied field, E_o.

The time response of the conventional photorefractive grating utilizing the linear electrooptic effect, i.e., in ferroelectric crystals, is limited by the time needed to rearrange the electronic space charge, i.e., E_{sc}. The voltage controlled photorefractive effect which makes use of the quadratic electrooptic effect is limited by the dielectric response, $\epsilon(\omega)$, since E_{sc} can remain constant and Δn is controlled by E_o. The dielectric response contains both an ionic and electronic contribution. As the temperature approaches the ferroelectric phase transition the ionic component becomes damped and undergoes a critical slowing down. The response, $\epsilon(\omega)$, is seen in Fig. 4-1 to drop off at roughly 100khz. Note that this is many orders of magnitude faster than the photorefractive space charge response (roughly 1 sec^{-1}).

The results described above demonstrate the ability to modulate the amplitude of a photorefractive diffraction grating in paraelectric KTN by the use of an external field. Full amplitude modulation at frequencies limited by the dielectric response is possible. Such an effect may be useful in applications which require the external control of the strength of an optical interconnect. Examples of these arise in the areas of optical switching and optical neural networks.

4.3 Fixing of a photorefractive grating in KTN

Photorefractive materials have found wide use as volume holographic storage media. Several fixing procedures have been developed to create diffraction gratings which are not erased under readout illumination. Fixed gratings in $LiNbO_3$ were formed by heating the sample to a temperature which allowed a compensating ionic space charge grating to form.[7] After illumination at room temperature, the electronic space charge grating is erased by uniform illumination leaving only the fixed ionic grating. Micheron has demonstrated fixing procedures in SBN which create ferroelectric domains correlated with a photorefractive space charge field. One procedure makes use of an applied electric field of magnitude slightly less than the coercive field to locally switch domains.[8] The other creates locally switched ferroelectric domains by cooling the sample through the ferroelectric phase transition.[9] Fixing has also been demonstrated in $Bi_{12}TiO_{20}$ (BTO) using a combination of thermal cycling and the application of an ac electric field.[10] In this section we describe a procedure used to fix photorefractive gratings in $KTa_{1-x}Nb_xO_3$ (KTN) which involves cooling the sample through the ferroelectric phase transition.[2]

4.3.1 Experimental measurements and procedure

The KTN crystal was grown using the top seeded solution growth method from a melt doped with Cu and V. A thorough characterization of the photorefractive properties of KTN:Cu,V will appear in Chapter 5. Cu has been identified as the photorefractive active species, with charge transport due to electron photoexcitation from the Cu^{1+} ion and subsequent retrapping by a Cu^{2+} ion. A sample measuring 0.44x0.46x0.69cm^3 was cut and polished along the [001] crystallographic direction. The sample was then reduced, converting Cu^{2+} ions to Cu^{1+} ions, using a thermal heat treatment[11]. This involved sealing the sample in a quartz ampule filled with 0.3 atm of nominally pure Ar gas, which was then heated to 800C and kept at that temperature for 12 hours before being cooled to room temperature. Cr and Au electrodes were evaporated on faces perpendicular to the 0.69cm edges. The chemical composition was determined from electron microprobe analysis to be $KTa_{0.87}Nb_{0.13}O_3$. Cu was found to be present at a concentration of $3.0(10^{19})/cm^3$. The V concentration was below the detection limit of $10^{18}/cm^3$. The sample was then mounted in a low temperature cryogenic system which allowed the temperature to be stabilized to within 0.1K.

The temperature dependence of the low frequency dielectric constant of the $KTa_{0.87}$ $Nb_{0.13}O_3$:Cu,V sample, determined from capacitance measurements, is given in Fig. 4-5. The peaks correspond roughly to the phase transition temperatures of KTN. The high temperature paraelectric phase is cubic. As it is cooled it undergoes ferroelectric transitions from the tetragonal to the orthorhombic to the rhombohedral phase. In these ferroelectric phases the spontaneous polarization lies respectively along the [001], [011], and [111] directions. Also shown in Fig. 4-5 is the temperature dependence of the spontaneous polarization along the [001] direction. It was determined by measuring the pyroelectric current on heating the sample after it was cooled to the low temperature phase under a 1000V bias. The spontaneous polarization decreases rapidly on approaching the tetragonal phase.

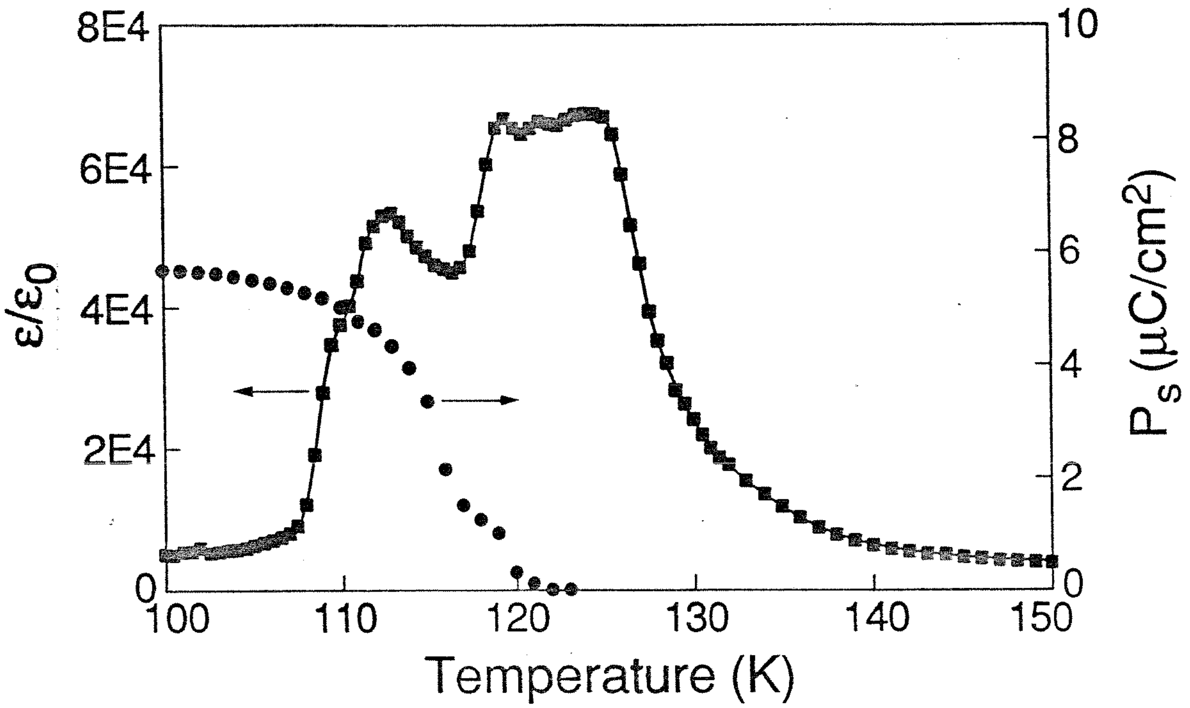

Fig. 4-5 The dependence of the static dielectric constant and the spontaneous polarization of a KTN:Cu,V sample on temperature.

A similiar temperature dependence of the spontaneous polarization was measured in a $K_{1-x}Li_xTaO_3$ sample.[12] The cubic to tetragonal transition is found to be of second order which reduces the danger of damaging the sample on cooling through the phase transitions.

The temperature dependence of the photocurrent under a 1000V bias was measured. The sample was illuminated uniformly with an expanded 20mw/cm^2 514nm beam. The light was polarized along the direction of the applied field. The measurements were made on cooling the sample from the cubic phase. The photocurrent is seen to be roughly constant in the cubic phase and to steadily drop on cooling through the ferroelectric region (Fig. 4-6).

Photorefractive diffraction gratings were written using two equal intensity 150 mw/ cm^2 beams from a 514nm Ar laser. The beams were expanded to uniformly illuminate the sample to which an electric field was applied in the plane of incidence. The beams crossed at a 16 degree angle and were ordinary polarized to prevent strong beam fanning and coupling. An expanded beam norminally incident from the reverse side was used as an "erase" beam. In order to monitor the diffraction efficiency of the grating an extraordinary polarized 15μw 632.8nm HeNe beam was aligned at the bragg angle. The HeNe beam was chopped and a lock-in amplifier was used to detect the diffracted signal.

Photorefractive measurements were made at T=135K in the paraelectric cubic phase under a 1000V bias voltage. At this temperature photorefractive diffraction gratings could be written and erased in the usual manner. The gratings had an

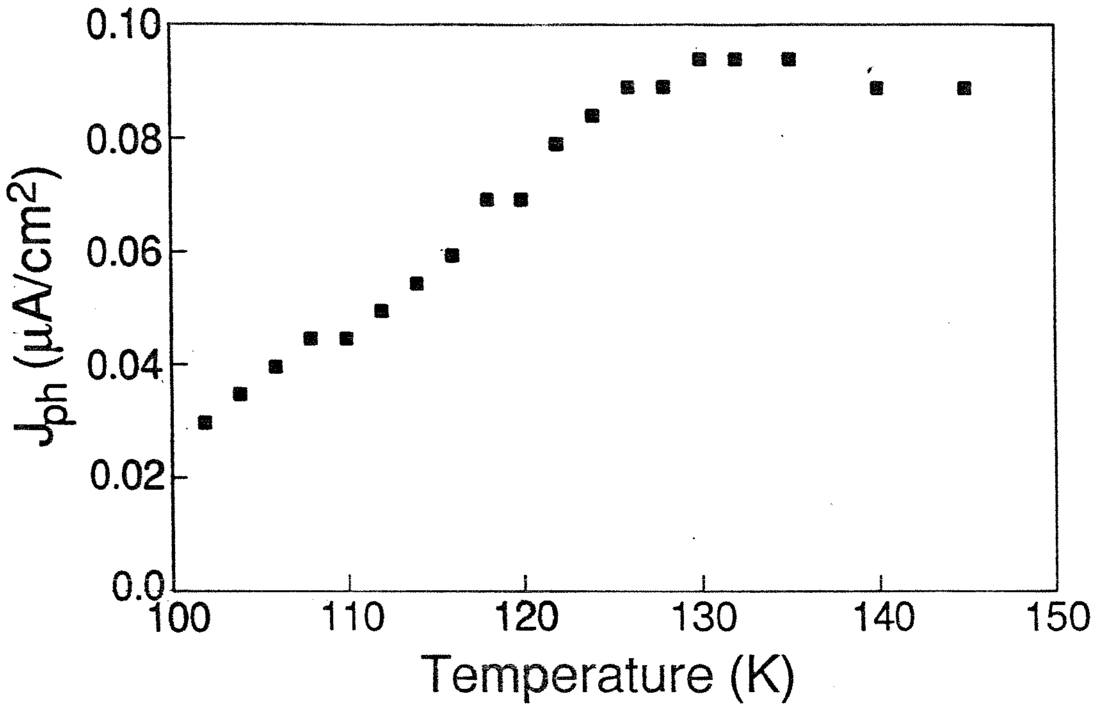

Fig. 4-6 The temperature dependence of the photocurrent of a KTN:Cu,V sample under a 1000V bias and under 20mw/cm^2 514nm illumination.

erase time of 3 sec under 250 mW/cm^2 illumination. A grating with a diffraction efficiency, η, of 10% was written after which the writing beams were turned off. The dark storage time of these gratings has been determined to be of the order of several days. The sample was then cooled from the cubic phase through the tetragonal and orthorhombic phases to T=108K in the rhombohedral phase. During the cooling the HeNe probe beam was used to monitor the strength of the grating (Fig. 4-7). The diffraction efficiency increased on approaching the ferroelectric transition and peaked at a value of 38% before falling to η=10% at T=108K. The bias voltage was then removed and the sample was illuminated with the normally incident 250 mw/cm^2 erase beam. The diffracted intensity initially rose and within a few seconds decreased to its original value of η=10 % (Fig. 4-8). The diffraction efficiency of the fixed grating was observed to remain at this value for half an hour. The bias voltage was then reapplied and the sample was slowly reheated under illumination with the erase beam. The grating remained fixed until T=123K at which the grating disappeared abruptly.

The fixing procedure was repeated under varying conditions. The fixed gratings have been observed to undergo no change in diffraction efficiency after several hours of illumination. To create a fixed grating, it was found necessary to cool the sample from the cubic phase through the orthorhombic and tetragonal phases to the low temperature rhombohedral phase. If the sample is cooled to temperatures slightly above the tetragonal to rhombohedral transition the photorefractive grating is erased under illumination. However, once a grating is fixed it remains so on

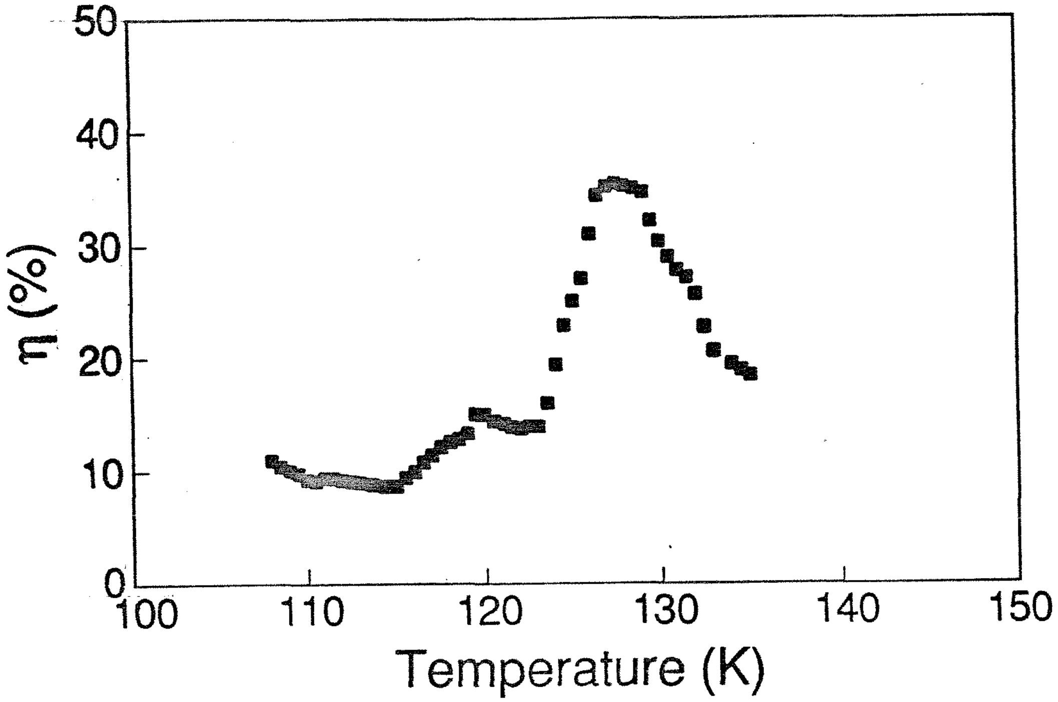

Fig. 4-7 The temperature dependence of the diffraction efficiency of a photorefractive grating written in the paraelectric phase and cooled through the tetragonal and orthorhombic phases into the rhombohedral phase under a bias field.

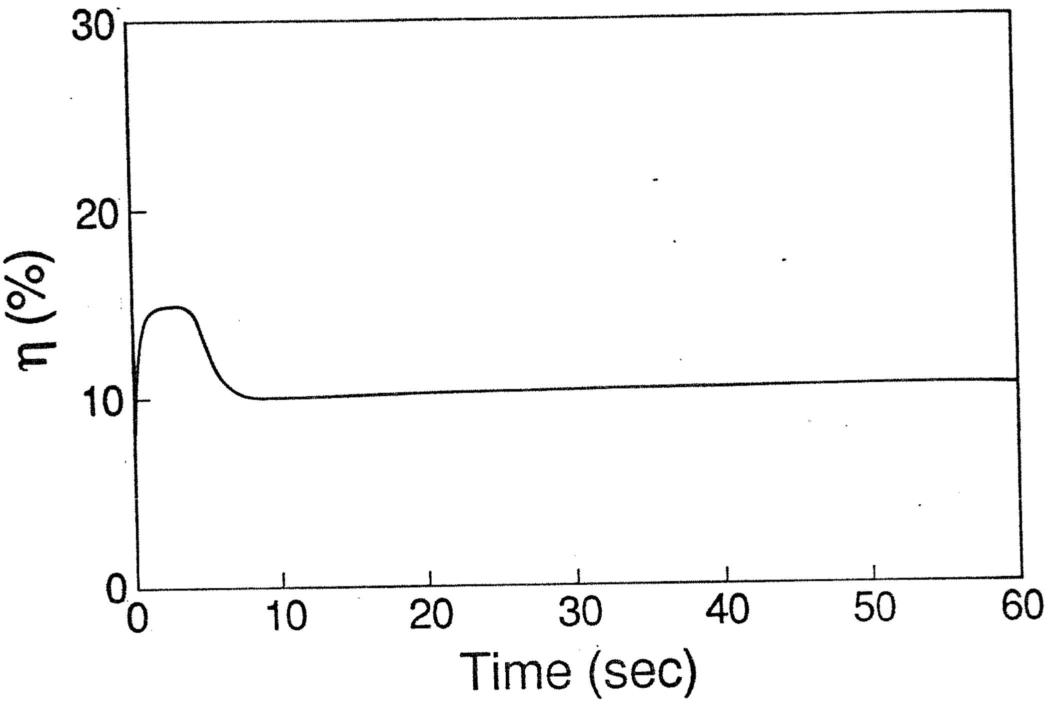

Fig. 4-8 The diffraction efficiency of a fixed grating in KTN after being cooled into the rhombohedral phase and then illuminated.

heating into the orthorhombic and tetragonal phases but disappears on heating into the paraelectric phase. Also the quality of the grating as determined by the amount of scattered light improved with increasing temperature. It has been observed that even after a single grating is fixed it is still possible to write and erase other unfixed gratings. Other evidence for this is the existence of dynamic beam fanning in the sample in the prescence of a fixed grating. After a grating has been fixed it can be restored to its unfixed state, one in which it is erasable under illumination, simply by reheating the sample back to the cubic phase.

4.3.2 Discussion

The fixing process just described is not similiar to those which rely on an ionic compensation of the photorefractive space charge field.[7] From Fig. (4-7) and Fig. (4-8) it is observed that the diffraction grating and hence the space charge grating, is not compensated by another. Nor is the fixing procedure similiar to those which locally switch ferroelectric domains.[8,9] In these procedures the electronic spacecharge field is erased after domain formation. In addition, the applied field parallel to the grating vector during cooling insures that the sample has a large spontaneous polarization along the [001] direction.

The above results are consistent with the existence of two types of photorefractive species. In the cubic phase both species are absorbing and contribute to the photorefractive effect. As the temperature is lowered into the rhombohedral phase the species responsible for the fixed grating becomes photorefractively inactive. That is it neither photoexcites or traps free carriers. Evidence for this is the steady drop of the photocurrent on cooling into the ferroelectric region. On reheating the fixed grating to the cubic phase this species once again becomes photoexcitable and the grating becomes eraseable. The second species, possibly present at lower concentrations, remains photoexcitable at all temperatures. It is responsible for the observed dynamic photorefractive effect in the rhombohedral phase in the presence of a fixed grating.

Such a process would involve the interaction of the photorefractive species with the ferroelectric phase transition. The ferroelectric properties of perovskites are strongly effected by the symmetry and dynamics of impurities.[13–15] In KTN it is believed that in the cubic phase the Nb ions hop between eight equivalent sites along the [111] directions of a cube.[15] The tetragonal and orthorhombic phases, respectively, result when the Nb ions are constrained to hop between sites in the direction of the corners of a half cube and in the directions of two adjacent corners of a cube. The rhombohedral phase is due to the constraint of the Nb ions to a single off center site in the directions of the corners of a cube. For the case of a photoexcitable impurity center, Levanyuk has shown that interaction with the ferroelecric soft mode or phase transition , can cause the ion to be displaced from its symmetric position.[16] This off-center displacement can then raise the energy required for photoexcitation to a value such that the state no longer is absorbing. In KTN:Cu,V Cu has been determined to be the predominant photorefractive species in the cubic phase.[11] On cooling into the rhombohedral phase the Cu ions, as do the Nb ions, may freeze out at an off center site. Such a distortion may result in the Cu ions becoming photorefractively inactive or fixed. On reheating into the cubic phase the distortion vanishes and the center may once again become photorefractively active.

In summary, we have demonstrated a procedure for fixing photorefractive gratings in KTN. It involves the writing of a photorefractive grating in the cubic phase and cooling a sample the through the tetragonal and orthorhombic phases to the rhombohedral phase under an applied bias. Diffraction efficiencies of 10% in a 0.43cm thick sample were reported for a fixed grating. The fixed grating can be restored to the erasable state by reheating the sample to the cubic phase. The mechanism responsible for this effect is believed to be due to the displacement of an impurity center on cooling to the rhombohedral phase causing it to become photorefractively inactive.

References

1. A. Agranat, V. Leyva, A. Yariv, "Voltage-controlled photorefractive effect in paraelectric $KTa_{1-x}Nb_xO_3$:Cu,V," Opt. Lett. **14**, 1017 (1989).
2. V. Leyva, A. Agranat, A. Yariv, "Fixing of a photorefractive grating in $KTa_{1-x}Nb_x)_3$ by cooling through the ferroelectric phase transition," Opt. Lett. **16**, 554 (1991).
3. M. B. Klein, "Beam coupling in undoped GaAs at 1.06μm using the photorefractive effect," Opt. Lett. **9**, 350 (1984).
4. J.E. Geusic, S. K. Kurtz, L. Van Uitert, S.H. Wemple, "Electro-optic properties of some ABO_3 perovskites in the paraelectric phase," Appl. Phys. Lett. **4**, 141 (1964).
5. J.K. Sinha, J. Sci. Instrum. **42**, 696 (1965).
6. H. Kogelnik, "Coupled wave theory for thick hologram gratings," B.S.T.J. **48**, 2909 (1969).
7. J. Amodei, D. Staebler, "Holographic pattern fixing in electro-optic crystals," Appl. Phys. Lett. **18**, 540(1971).
8. F. Micheron, G. Bismuth, "Field and time thresholds for the electrical fixation of holograms recorded in $Sr_{0.75}Ba_{0.25}Nb_2O_6$ crystals," Appl. Phys. Lett.**22**,71 (1973).
9. F. Micheron, J. Trotier, Ferroelect., "Photoinduced phase transitions in $(Sr,Ba)Nb_2O_6$ crystals and applications," **8**, 441 (1974).
10. S. McCahon, D. Rytz, G. Valley, M. Klein, B. Wechsler, "Hologram fixing in

$Bi_{12}TiO_{20}$ using heating and an ac electric field," Appl. Opt.**28**, 1967 (1989).

11. V. Leyva, A. Agranat, A Yariv, "Determination of the physical parameters controlling the photorefractive effect in $KTa_{1-x}Nb_xO_3$:Cu,V," JOSA B. **8**, 701 (1991).
12. V.S. Vikhnin, E.G. Nadolinskaya, A.V. Shil'nikov, N.K. Yushin, " Feasibility of formation of an incommensurate phase induced by a noncentral lithium impurity in a potassium tantalate crystal," Sov. Phys. Solid State **30**, 349 (1988).
13. B. I. Halperin, C.M. Varma, "Defects and the central peak near stuctural phase transitions," Phys. Rev. B **14**, 4030 (1976).
14. Y. Yacoby, S. Just, "Differential raman scattering from impurity soft modes in mixed crystals of $K_{1-x}Na_xTaO_3$ and $K_{1-x}Li_xTaO_3$," Solid State Comm. **15**, 715 (1974).
15. L.L. Chase, J. Sokoloff, "Disorder-induced dynamic fluctuations in KTN," Solid State Commun. **55**, 451 (1985).
16. A.P. Levanyuk, V.V. Osipov, "Theory of an optically induced change in the refractive index," Sov. Phys. Solid State **17**, 2340 (1976).

CHAPTER FIVE

INVESTIGATION OF THE PHYSICAL PARAMETERS GOVERNING THE PHOTOREFRACTIVE EFFECT IN KTN:Cu,V

5.1 Introduction

A large effort has gone toward the development of photorefractive materials and the characterization of their properties. Properties can be modified during the growth stage by the type and amount of dopant added to the flux.[1,2] After growth, properties are modified by changes to the valency of the dopant ions through thermal oxidation or reduction treatments.[3,4] The difficulty in measuring material parameters which enter into the Kukhtarev model[5,6] of the photorefractive effect has prevented a careful comparison of holographic diffraction measurements with those expected from theory. In many samples the photorefractive active species remains unidentified. Even samples cut from the same boule can have widely different properties.

In this chapter the photorefractive effect in a KTN:Cu,V sample which underwent a series of thermal oxidation and reduction treatments is described.[7,8] The photorefractive species is identified and all the relevant physical parameters which enter into the Kukhtarev model are determined using electron microprobe, absorption, and photoconductivity measurements. Results allow a comparison of the dependence of photorefractive diffraction and time response measurements on trap concentration with those expected from theory. The thermal oxidation/reduction process is modelled which allows the determination of the temperature and partial pressure of oxygen needed to produce a given photorefractive property. Finally, approaches to increase the photorefractive sensitivity by controlling the dopant density and valence state are discussed.

5.2 Experimental results and discussion

5.2.1 Sample preparation and thermal treatments

A 15x16x17 mm^3 KTN:Cu,V crystal was grown using the top seeded solution growth method. The flux contained an excess of K to which 3 molar % of Cu and 3 molar % of V were added. V will be shown not to be the photorefractive active species. However, it has been found that a few percent of V added to the flux possibly acts as a solvent and results in significantly better quality crystals.[9] A 0.52x0.41x0.31 cm^3 sample was cut and polished along the principal [001] crystallographic axis. Viewed through crossed polarizers the sample appeared homogenous and free of striations. Its chemical composition was determined by electron microprobe analysis to be $KTa_{0.70}Nb_{0.30}O_3$:Cu,V. Cu was found to be present at 600 parts per million (ppm) by weight with a 150 ppm detection limit. V was present at 40 ppm with a 15 ppm detection limit. The density of Cu is thus $1.80(10^{19})/cm^3$, while that of V is $1.50(10^{18})/cm^3$.

The ferroelectric phase transition temperature of the KTN:Cu,V sample was determined from capacitance measurements of the dielectric constant to occur at T=-30°C. An undoped KTN sample, to be used as a standard for the absorption measurements, was found to have a ferroelectric phase transition at T=-32°C. As the transition temperature depends roughly linearly on Nb concentration,[10] the chemical composition of these two samples is nearly identical.

The KTN:Cu,V sample underwent a series of heat treatments in various oxygen atmospheres. After each treatment, absorption, photoconductivity, and photorefractive measurements were made on the sample. For the first treatment the sample was sealed in a quartz ampule containing 0.33 atm of nominally pure argon gas. The sample was then heated to 800°C and kept there for 15 hours before cooling to room temperature. The other treatments consisted of sealing the sample in an ampule which contained .33 atmosphere of pure oxygen. The ampule was then heated to a set temperature and kept there for 15 hours before returning to room temperature. The temperatures used were 400°C, 450°C, 500°C, 600°C, and 700°C. The heating and cooling rates for all the treatments, except the 700°C one, were 75°C/hour. The rates for the 700°C treatment were 180°C/hr.

5.2.2 Absorption measurements

Absorption mechanisms which occur in KTN include fundamental transitions and transitions involving impurities and dopants. Several of these are illustrated in Fig. 5-1. The fundamental absorption or band edge is due to electronic transitions from the valence to the conduction band. The band gap in $KTa_{1-x}Nb_xO_3$ for x=0.35 is 3.6eV and is broadened with an exponential Urbach dependence.[11] Absorptions involving transition metal dopants are of two types, charge transfer and crystal field transitions.[12,13] Charge transfer transitions result in free carriers which contribute to the photorefractive effect. An electron can be photoexcited from a

ABSORPTION MECHANISMS IN PHOTOREFRACTIVE KTN

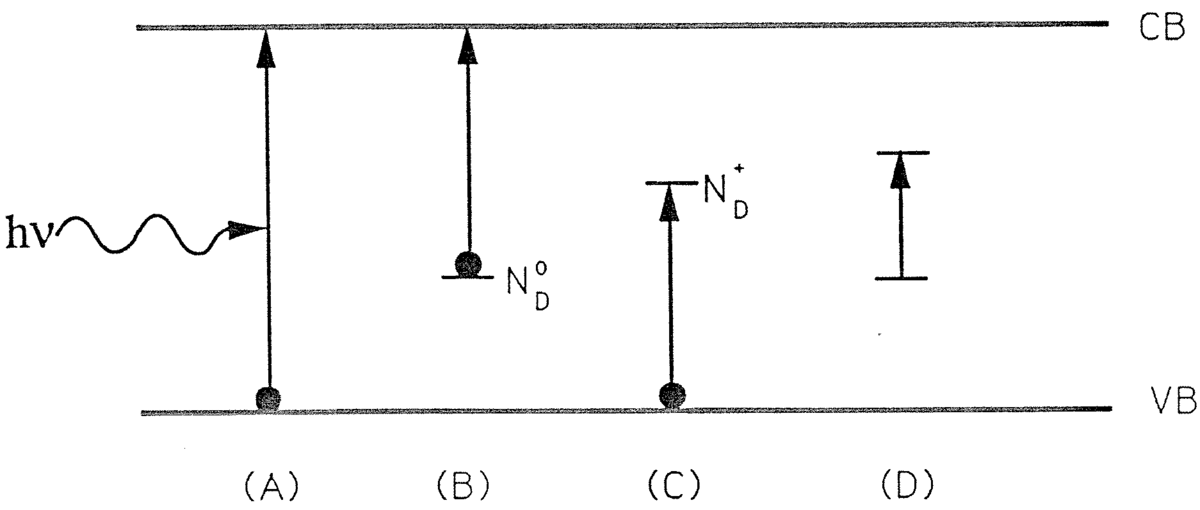

(A) Intrinsic absorption

(B) Charge transfer - electron photoexcitation

(C) Charge transfer - hole photoexcitation

(D) Crystal field transitions

Fig. 5-1 Absorption mechanisms which occur in transition metal doped KTN. (A) Intrinsic (band) absorption, (B) electron photoexcitation, (C) hole photoexcitation, (D) Crystal field transitions.

filled donor into the conduction band. Similiarly, an electron can be photoexcited from the valence band into an empty donor site creating a free hole carrier in the valence band. Crystal field transitions are localized electronic transitions which do not contribute to the photorefractive effect. They are responsible for the color of many minerals and their characteristic absorption can be used to identify the presence, site occupancy, and valence state of transition metal ions. They are due to electronic transitions between d orbital energy levels of a transition metal ion. The electronic energy levels are split due to an electrostatic interaction with the surrounding oxygen ions or ligands.

After each of the oxidation and reduction treatments, unpolarized absorption spectra were taken using a double beam spectrophotometer. The absorption coefficient, α, was determined from the relation

$$T = (1 - R)^2 exp(-\alpha l)/(1 - R^2 exp(-2\alpha l)) \tag{5.1}$$

where l is the thickness of the sample, T is the measured transmission, and R is the reflection coefficient. R was determined using the dispersion relationship for the index of refraction of Chen.[14]

The difference in the absorption spectra of the KTN:Cu,V sample after each of the reduction and oxidation treatments and that of the undoped KTN sample are shown in Fig. 5-2. Two absorption bands are clearly visible. As the KTN:Cu,V and the undoped KTN sample are nearly of the same composition, features visible in the difference spectra should be a result of the dopants and not of the fundamental absorption. Cu is present in larger concentrations than V and is a much more

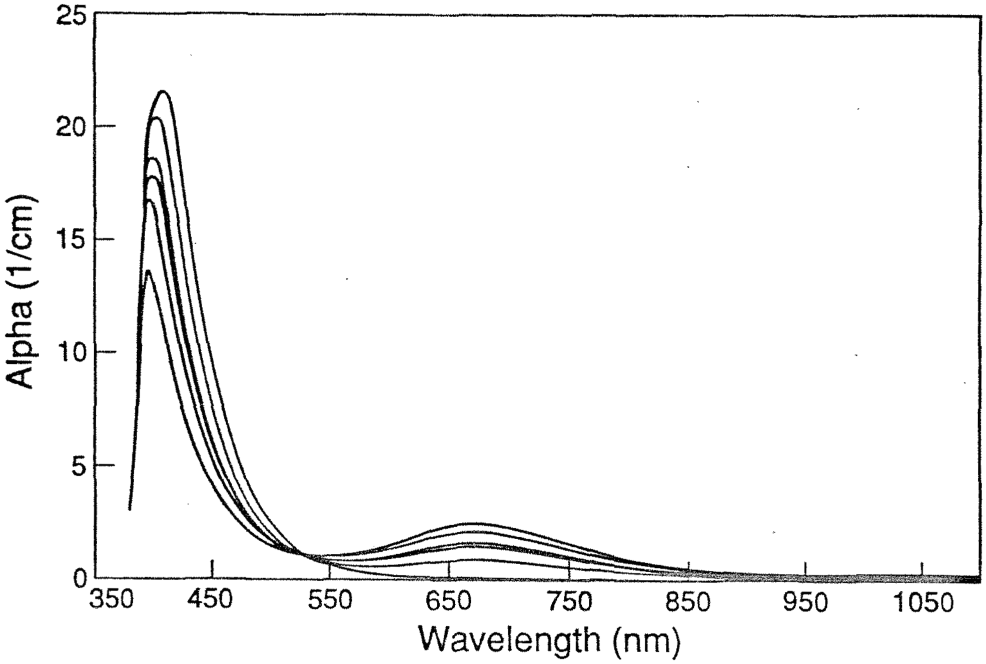

Fig. 5-2 Difference in the absorption spectra between the undoped KTN sample and the KTN:Cu,V sample after a series of reduction and oxidation treatments. Features should be a result of the dopants. Spectra with highest peak at 410nm corresponds to the reduction treatment. Other spectra with decreasing magnitude at 410nm correspond to oxidation treatments at 400C, 450C, 500C, 600C, and 700C.

intense absorber. Cu is stable in two valence states, Cu^{1+} and Cu^{2+}. Cu^{1+} has a filled 3d electronic shell, hence crystal field transitions do not occur in this valence state. An electron charge transfer transition, exciting an electron from Cu^{1+} into the conduction band is possible. The band centered at 410nm which decreases in magnitude with increasing oxidation treatment is identified as the electron charge transfer band given by

$$Cu^{1+} + h\nu \longrightarrow Cu^{2+} + e^{-} \tag{5.2}$$

which is responsible for the photorefractive effect in our sample. The Cu^{1+} ion corresponds to the photorefractive filled donor site and the Cu^{2+} to the electron trap site. The band centered at 680nm is characteristic of crystal field transitions of Cu^{2+} in an octahedrally coordinated site.[13] Cu^{2+} can also be involved in a transition which creates a free hole in the valence band as illustrated by (c) in Fig. 5-1. In $LiNbO_3$:Cu hole conductivity is observed at photon energies above 3.6eV.[15] No evidence for this transition is found. The other dopant, V, is stable over a wide range of valence states. No absorption features characteristic to V are found.[16] As it is isoelectronic with Ta and Nb we expect it to enter the lattice as V^{5+}.

According to Beers law the absorbance is proportional to the concentration of absorbing ions. The intensities of the two bands can thus be used to determine the relative concentration of the Cu^{1+} and Cu^{2+} ions after each reduction and oxidation treatment.[15,17] The absolute concentration of each valence ion can be determined since the total concentration of Cu ions is known from the microprobe analysis. Using the ratio of the peak magnitudes of the bands in Fig. 5-2, the oxidation treatments converted 10%, 18%, 21%, 27%, and 36% of the Cu into the Cu^{2+} valence state. In Fig. 5-2 it is seen that after the reduction treatment the 680nm band has disappeared. This implies almost complete conversion of the Cu to the Cu^{1+} valence state. An upper limit of roughly 1%, determined by the the minimum band at 680nm that could be discerned, is determined for the Cu^{2+}/Cu ratio after this treatment.

An important parameter of photorefactive materials is the photoexcitation cross section, $s_e(\lambda)$. Along with the electronic recombination coefficient, it is the only parameter that enters into the Kukhtarev band transport model that is characteristic of the dopant. All other parameters are that of the host crystal or are related to the concentration of the dopants. Its spectral dependence determines the suitability of a dopant as a photorefractive donor in the red and infra-red regions. For the excitation from the Cu^{1+} ion it is given by

$$s_e(\lambda) = \alpha_{ct}/[Cu^{1+}] \tag{2}$$

where α_{ct} is the absorption coefficient of the transition which results in an electron excited into the conduction band and $[Cu^{1+}]$ is the concentration of the absorbing ions. $s_e(\lambda)$ can be determined from the difference absorption spectra after the reduction treatment. For this spectrum most all of the Cu is in the Cu^{1+} state whose only allowed absorption is one which results in a free electron. Figure 5-3 shows the spectral dependence of $s_e(\lambda)$. It is observed to peak at a value of $9.08(10^{-20})$ cm^2 at 410nm(3.0eV) with a full width at half maximum (FWHM) of 0.38 eV. Due to the sharp drop of $s_e(\lambda)$ in the red, Cu is not expected to and does

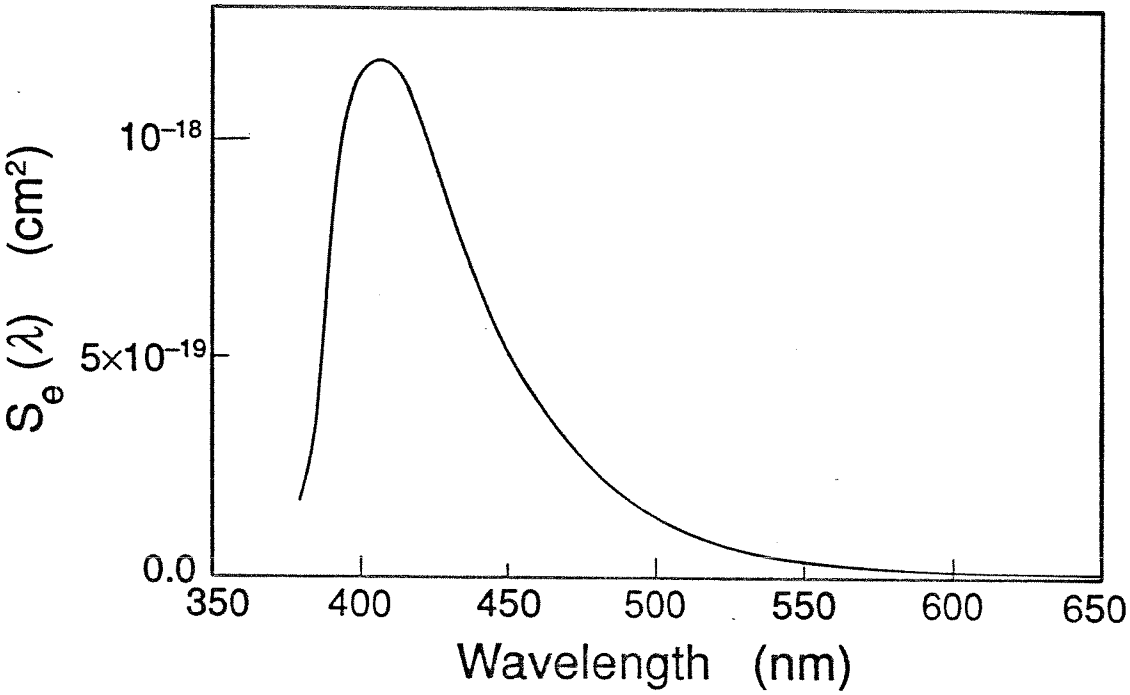

Fig. 5-3 Spectral dependence of the electron photoexcitation cross section which results in an electron photoexcited from the Cu^{1+} ion into the conduction band. Peak at 3.0 ev corresponds to optical excitation energy of this level.

not show high photorefractive response in this spectral region.

The excitation cross section for crystal field transitions at 680nm is found to be $s_{cf} = 1.5(10^{-19})$ cm^2. This non photorefractive absorption is proportional to the concentration of Cu^{2+} ions. Both s_e and s_{cf} can be used as a standard to determine the concentration of Cu in each valence state for other Cu doped KTN samples.

5.2.3 Photoconductivity measurements

Photoconductivity measurements were made after each of the thermal oxidation and reduction treatments to provide information on the transport parameters involved in the photorefractive effect. Under illumination the photocurrent, J, is given by

$$J = e\mu(n_d + \tau_R \alpha_{ct} I/h\nu)E \tag{5.4}$$

where e is the electronic charge, μ is the mobility, n_d is the free electron density in the dark, τ_R is the electron recombination time, α_{ct} is the coefficient for absorption which results in a free carrier, I is the intensity, $h\nu$ is the energy of an incident photon, and E is the applied electric field. There is no photovoltaic effect in the paraelectric region.

After each of the reduction and oxidation treatments, the photocurrent was measured as a function of incident intensity and applied voltage . 514nm illumination was used at intensities of 42mW/cm^2 to 525mW/cm^2 in 105mW/cm^2 increments. Voltages from 200V to 1000V in 200V increments were applied along the 0.52 cm sides of the sample.

The sample was found to be highly insulating in the dark which precluded measurements of the dark conductivity. The photocurrent was found to be linear in intensity and applied voltage. The mobility lifetime product, $\mu\tau_R$, was determined from the photocurrent using the relation $\alpha_{ct} = s_e(514nm)[Cu^{1+}]$, where $s_e(514nm)$ was determined from Figure 5-3. The drift length of a free carrier before it is retrapped is given by $l_d=\mu\tau_R E$. Figure 5-4 shows the dependence of $\mu\tau_R$, and hence the transport distance, on Cu^{2+} concentration. It is seen to vary inversly with, $[Cu^{2+}]$, the concentration of electron traps. Fewer electron traps leads to a corresponding increase in the lifetime and transport distance of a free carrier. The inverse dependence on $[Cu^{2+}]$ allows a determination of $[Cu^{2+}]/[Cu]=.0027$ for the reduction treatment which we were unable to determine from the absorption measurements. The free electron lifetime, τ_R, is related to the electron recombination coefficient, γ_R, and the trap concentration by

$$\tau_R = 1/\gamma_R[Cu^{2+}] \tag{5.5}$$

from which we determine μ/γ_R=6.20(10^8) 1/V-cm. From the experimentally determined inverse dependence of $\mu\tau_R$ on $[Cu^{2+}]$ and using relation (5.5), the mobility was relatively constant over the wide range of oxidation treatments. So any changes in the photorefractive properties by these treatments is due to changes in the valence states of the Cu ions and not to changes in the mobility.

5.2.4 Photorefractive measurements

Photorefractive diffraction efficiency and erase time measurements were made after each of the heat treatments. The sample was placed in a vacuum chamber

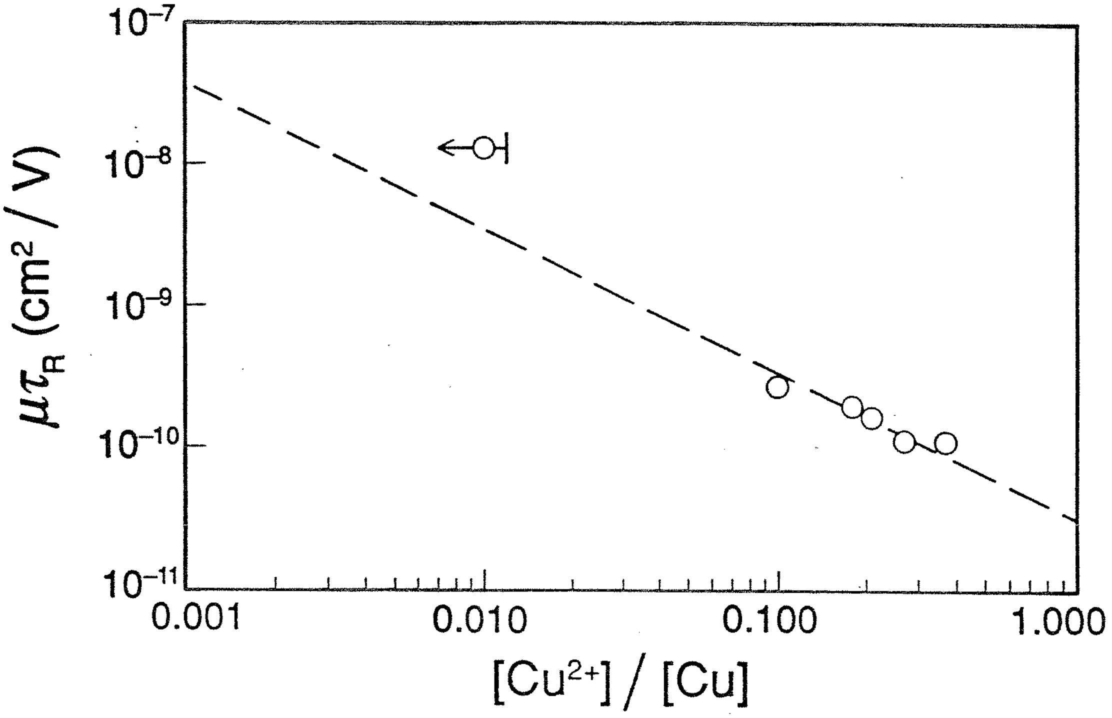

Fig. 5-4 Values of the mobility electron lifetime product, $\mu\tau_R$, versus trap concentration ratio. Trap concentration was varied through a series of reduction and oxidation treatments.

on a thermoelectrically cooled mount. Measurements were made in the paraelectric region at T= -27°C. The dielectric constant was found from capacitance measurements to be $\epsilon = 12000\epsilon_o$. An 800V field was applied along the 0.52cm sides. Two 514nm beams intersecting at a 12° angle were used to write a holographic diffraction grating with a 2.3 micron period. Each beam had an intensity of 42mw/cm^2 and was expanded to uniformly illuminate the sample. The light polarization was in the plane of incidence. Beam fanning was in a direction consistent with electron conductivity. A photorefractive diffraction grating was written by exposing the 0.31 cm thick sample to the two beams for up to several minutes. One of the beams was then blocked. The diffracted intensity from the grating was then measured as a function of time.

The absorption and photoconductivity measurements indicate that electrons are photoexcited from the Cu^{1+} level into the conduction band and are retrapped at the Cu^{2+} level. There is no evidence of hole conductivity or the existence of another species. Consequently the Kukhtarev band transport model with a single carrier and single species will be used to model the results. For small intensity index modulation, m, and neglecting the dark conductivity the photorefractive space charge field, E_{sc}, is given in Eq.(2.11) The photorefractive response time, τ_e, under an applied field and neglecting the dark conductivity is given in eq. (2.13) In these expressions ,N_D, the density of donors corresponds to the total Cu concentration. and N_D^+ corresponds to the density of ionized donors, Cu^{2+}. The electron microprobe, absorption, and photoconductivity measurements, have determined values for all of the parameters involved in expressions (2.11) and (2.13). These include the density of filled and ionized donors after each of the heat treatments, the electron photoexcitation cross section, and the ratio of the electron mobility to recombination rate. This allows us to compare our experimental results with those expected from the Kukhtarev model.

In the centrosymmetric paraelectric phase of KTN an external electric field, E_o, is needed to produce an index grating which diffracts the incident beams. The index grating, $\delta(\Delta n)$, is given by[18,19]

$$\delta(\Delta n) = n_o^3 g(\epsilon - \epsilon_o)^2 E_{sc} E_o \tag{5.6}$$

where n_o is the index of refraction and g the quadratic electro-optic coefficient. For the geometry used in KTN, $g=g_{11}=1.36(10^7)\text{cm}^4/\text{C}^2$ and $n_o=2.34$ at 514nm.[20] For small coupling the scattering from the grating can be approximated by Kogelnik's expression for the diffraction efficiency from a thick plane holographic grating given by[21]

$$\eta = e^{-\alpha l} sin^2\left(\frac{\pi\delta(\Delta n)l}{\lambda cos(\theta/2)}\right) \tag{5.7}$$

where α is the total absorption, l is the thickness of the sample, λ is the wavelength of the illuminating radiation , and θ is the angle between the writing beams.

The experimental results for the diffraction efficiency versus trap density, are given in Figure 5-5. The diffraction efficiency is defined as the ratio of the incident to diffracted intensity. For the reduction treatment, $[\text{Cu}^{2+}]/[\text{Cu}]=.0027$, the diffraction efficiency is 0.81%. All of the other oxidation treatments resulted in a fairly constant diffraction efficiency of about 13%.

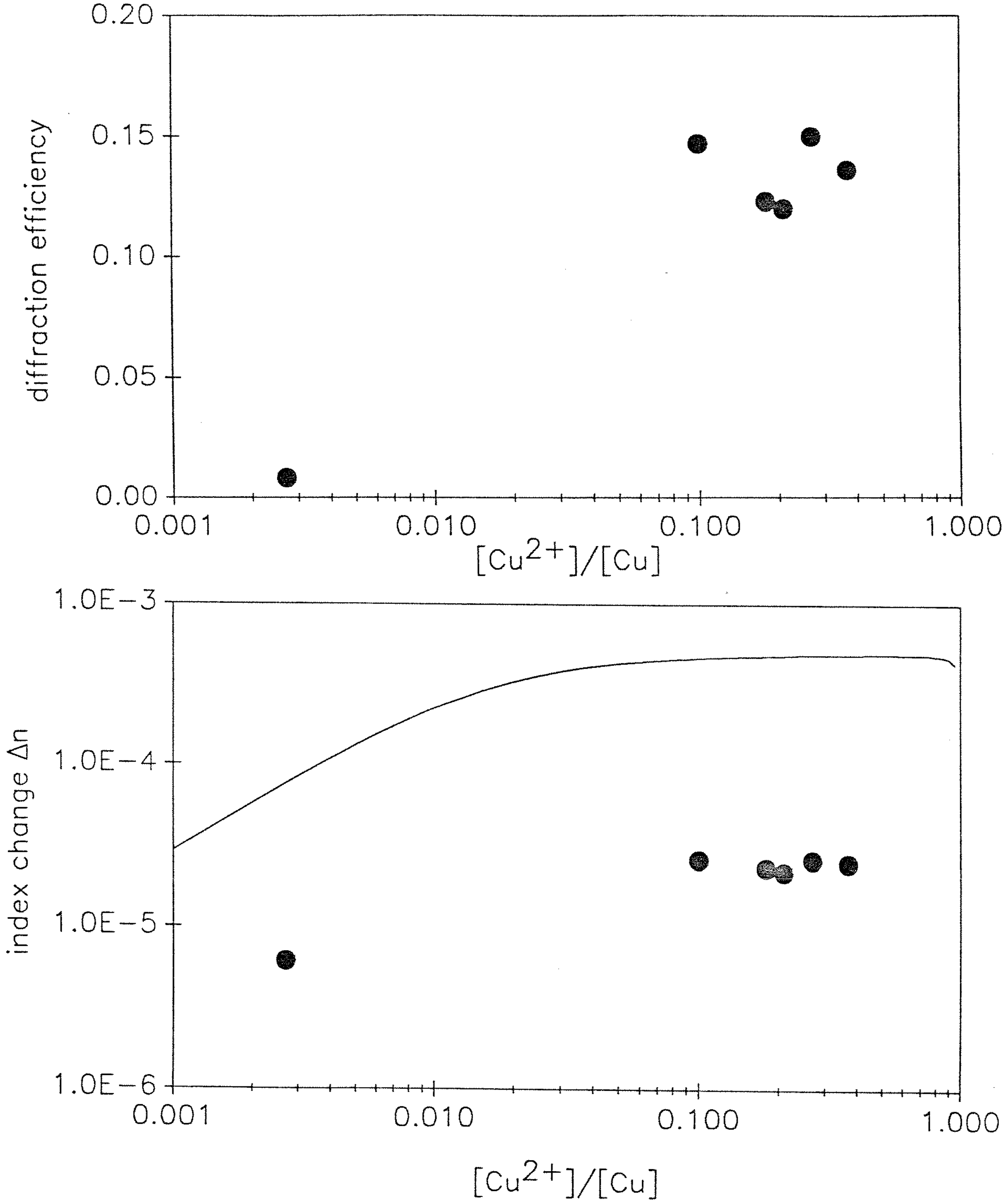

Fig. 5-5, Fig. 5-6 Experimentally measured diffraction efficiencies and refractive index change versus trap concentration ratio and the refractive index change expected from the Kukhtarev model in paraelectric KTN:Cu,V.

The photorefractive index change for each of the measurements was determined using relation (5.6). Fig. 5-6 shows the experimentally determined dependence of the index change on trap density versus that expected from theory. The measured values are over an order of magnitude smaller than theory although both show the same qualitative dependence. Both model and experiment show an index change nearly independent of the trap density in the space charge limiting region, $E_q >> E_o$, E_D. This occurs roughly for $[Cu^{2+}]/[Cu] > 0.10$.

The lower measured index changes may be a result of several factors. A discrepancy may occur due to the use of large intensity modulation, m. For large values of m, nonlinear terms in the expression for the space charge field lead to a smaller index changes. It was also assumed that the voltage was uniform across the sample. The sample was illuminated uniformly to insure this, but regions of large voltage drops may occur at or near the electrodes. Photorefractive beam fanning would also lead to a reduction in the measured diffraction efficiencies. The results are also consistent with those of a much more lightly doped crystal. This suggests that not all of the Cu ions may participate in the photorefractive effect. It was assumed that all of the Cu ions enter into the crystal lattice with similiar electronic properties. But impurities often occur in clusters and form complex defect states which differ from the single electronic band level assumed by the Kukhtarev model. This is especially expected to occur in heavily doped samples such as this one.

The dependence of the experimentally measured erase times on trap density and that expected from the band transport model Fig. (5-7). The erase time, τ_e, was

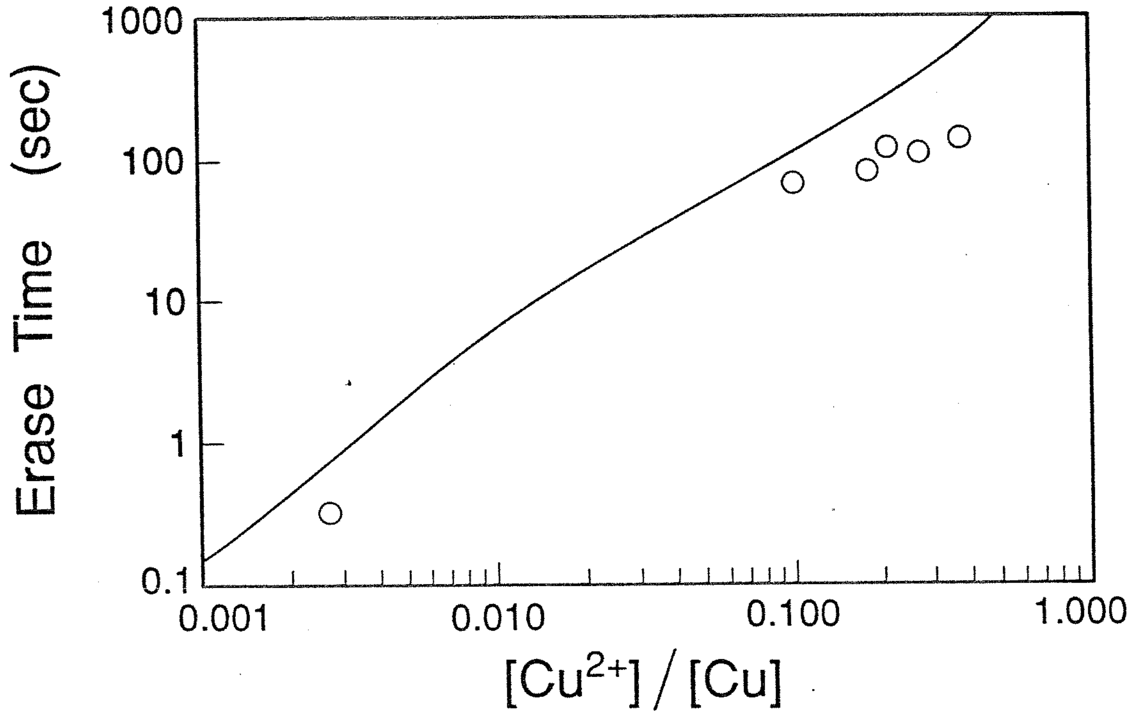

Fig. 5-7 Experimentally measured erase times of a photorefractive grating during readout and that expected from the Kukhtarev model versus trap concentration ratio. Erase rates are for a 42mW/cm^2 514nm readout beam.

found by fitting an exponential decay to $\delta(\Delta n)$. The decay of $\delta(\Delta n)$ during readout was determined from the diffracted intensity by using (5.7). The oxidation and reduction treatments modified the response times over two orders of magnitude. The erase times under 42mW/cm^2 illumination varied from 0.60 seconds to 138 seconds. Reasonable agreement is found with equation (2.13), although the measured times are slightly lower.

5.2.5 Reduction and oxidation of Cu

The reduction and oxidation treatments significantly altered the Cu valence state concentrations and photorefractive properties of the sample. The thermal treatments reduce or oxidize the valence state of the Cu through the creation or elimination of oxygen vacancies.[3,4,22] When heated in an oxygen deficient atmosphere, oxygen vacancies are induced in the sample. The two electrons paired with the oxygen site can remain free or be trapped either at the vacancy site or by a multivalent metal ion. The oxidation process is given by

$$Cu^{1+} + 1/2V_O + 1/4O_2 - - > Cu^{2+} \tag{5.8}$$

where V_O represents an oxygen vacancy and O_2 an oxygen gas molecule.In the KTN crystal the K ions are assigned a +1 valence charge, the Ta/Nb ions a +5 valence charge, and the O ions a -2 valence charge. Electron paramagnetic resonance (epr) measurements[23] indicate that Cu substitutionally occupies the Ta/Nb site. Oxygen vacancies are relatively shallow and will be assumed to be unfilled or ionized at room temperature. Charge neutrality relative to the neutral lattice is thus given by

$$4[Cu^{1+}] + 3[Cu^{2+}] + n = 2[V_O] + p \tag{5.9}$$

where n is the free electron concentration and p is the free hole concentration. A mass action equation[24] can be used to determine the concentration of the the solid and gas components of the chemical reaction (5.8) in equilibrium,

$$[Cu^{1+}][V_O]^{1/2}P_{O_2}^{1/4}/[Cu^{2+}] = Kexp(\Delta H/kT) \tag{12}$$

where ΔH is the change in enthalpy of the reaction, K is a constant, and P_{O_2} is the partial pressure of oxygen at the processing temperature. The values of $[Cu^{1+}]$, $[Cu^{2+}]$, and P_{O_2} are known for each of the heat treatments. By neglecting the free electron and hole concentrations, (5.9) can be used to determine $[V_O]$ after each thermal treatment. Figure 5-8 plots the value of the left side of the mass action equation (5.12) versus inverse processing temperature. A value of $K=2.83(10^{18})$ $atm^{1/4}cm^{-3/2}$ and $\Delta H = 0.295eV$ is determined from Figure 5-8. These values determine the required temperature and partial pressure of oxygen needed to produce a given Cu valence state concentrations. Figure 5-9 shows the Cu^{2+} fraction versus partial pressure of oxygen at a processing temperature of 700C for various doping levels. As expecxted a lower oxygen partial pressure reduces the crystal(increased Cu^{1+} concentration). For a given oxygen partial pressure, lower doping levels are seen to result in a higher fraction of filled donors, Cu^{1+}.

The change in enthalpy of the reaction, Δ H, is given by half the energy to fill the vacancy site with an oxygen ion and two free electrons minus the energy needed to thermally ionize an electron from Cu^{1+} to the conduction band. For an ionic solid, no energy is required to place a neutral oxygen ion in the vacancy site. The valence band in KTN is composed of oxygen 2p orbitals, thus the energy needed

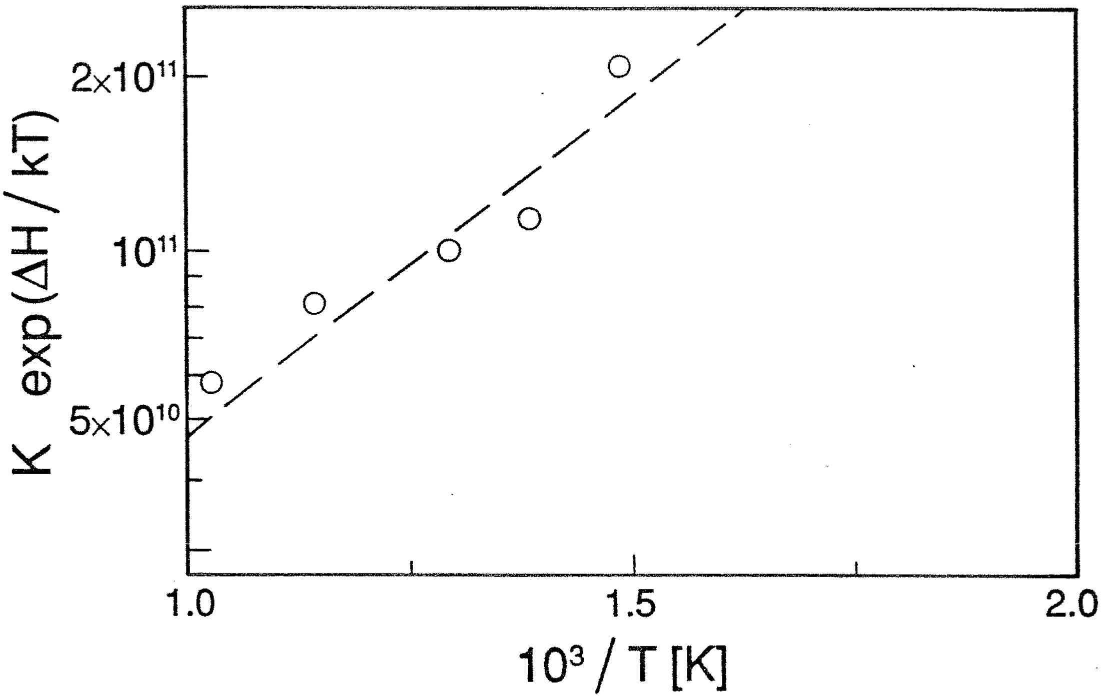

Fig. 5-8 Plot of the left hand side of the mass action equation (12) for the oxidation/reduction process versus inverse temperature. The dotted line corresponds to K=2.83 (10^{18}) atm$^{1/4}$cm$^{-3/2}$ and ΔH= -0.295eV.

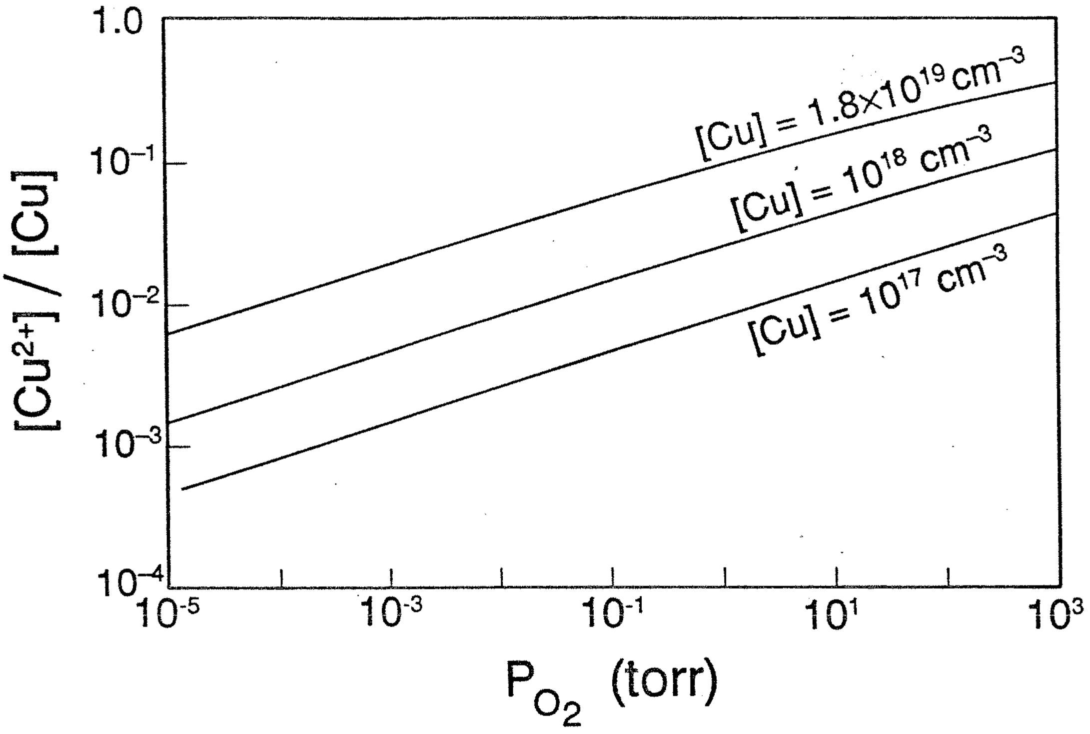

Fig. 5-9 Fraction of the Cu converted to the Cu^{2+} valence state versus partial pressure of oxygen at a processing temperature of 700°C. Three doping levels are shown, $[Cu]=1.8(10^{19})cm^{-3}$, $10^{18}cm^{-3}$, and $10^{17}cm^{-3}$.

to place two free electrons from the conduction band into the neutral oxygen site is twice the band gap energy. The band gap energy was found from the absorption measurements to be E_{gap}=3.25eV. The thermal energy needed to ionize the Cu^{1+} donor level is thus determined to be $E_{Cu^{+1}}$=2.95eV below the conduction band. Note that this is slightly less than the peak in the optical excitation energy of 3.00 eV (Fig. 5-2). As pointed out by Mott[25] the thermal energy is always the smaller of the two due to ionic lattice movements after absorption.

5.3 Optimizing the photorefractive effect

The reduction and oxidation treatments described in this chapter significantly altered the magnitude of the photorefractive index change and the response time of the sample. A parameter which compares the photorefractive properties of samples is the photorefractive sensitivity, S,[6] defined as the index change per absorbed energy per unit volume. With an exponential decay of the index grating with time constant of τ_e, it is given in paraelectric KTN:Cu,V by

$$S = \frac{d(\Delta n)}{d(\alpha I \tau_e)} = \frac{n_o 3g(\epsilon - \epsilon_o)^2 E_{sc} E_o}{s_e [Cu^{1+}] I \tau_e} \tag{5.11}$$

Note that E_{sc} depends on E_o, ϵ, and on the concentration of Cu^{1+} and Cu^{2+}. Figure 5-10 plots the experimentally determined sensitivity of the sample after each of the heat treatments versus the $[Cu^{2+}]/[Cu]$ trap concentration ratio. The index change, Δn, was determined from the diffraction efficiency measurements using eqn. (5.7). Also plotted is the sensitivity expected from theory for three different doping levels under similiar experimental conditions. The experimental points correspond to the

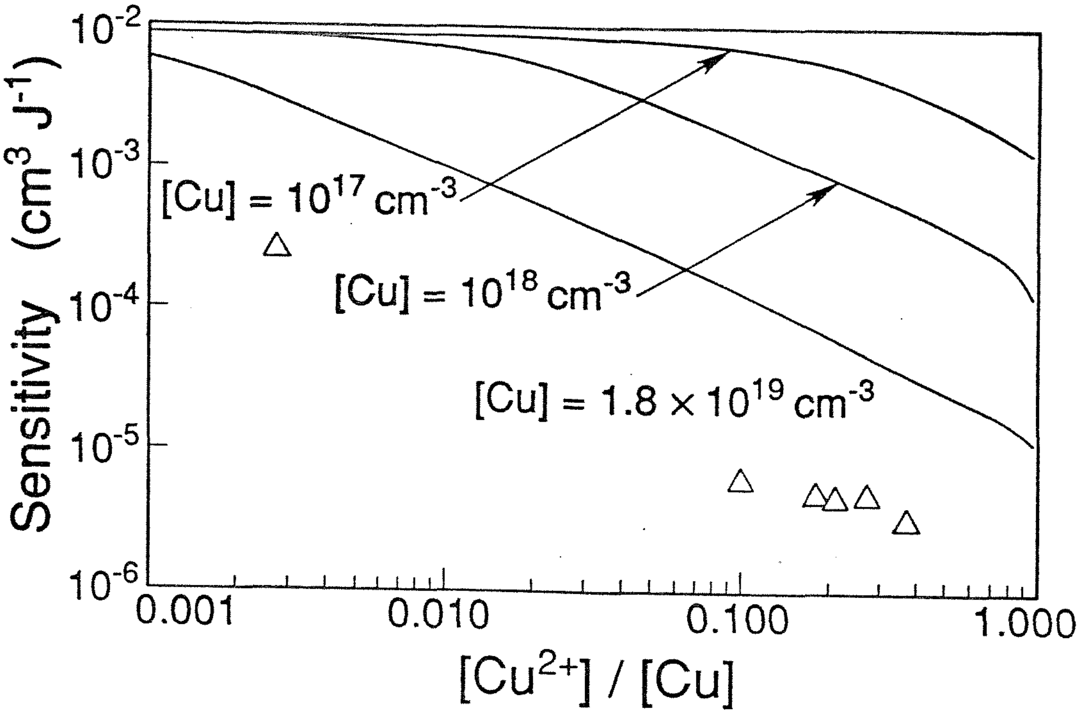

Fig. 5-10 Experimentally measured photorefractive sensitivity versus trap concentration ratioof the KTN:Cu,V sample. Also plotted is the sensitivity expected from theory for three different doping levels.

[Cu]=$1.8(10^{19})\mathrm{cm}^{-3}$ curve. Measured values are roughly an order of magnitude lower than those expected from theory.

A significant improvement in S is found for reduced samples, i.e. those with a low trap concentration. Figure 5-9 indicates that for a given processing temperature and oxygen partial pressure, lower doped samples are more highly reduced. This may explain the high sensitivities reported in nominally undoped samples as compared to heavily doped ones.

Approximating τ_e by the dielectric relaxation time simplifies (5.11) to

$$S = \frac{4\pi e n_o^3 g \epsilon E_{sc} E_o \mu}{h\nu\gamma[Cu^{2+}]} \tag{5.12}$$

where use has been made of $\epsilon >> \epsilon_o$. S is proportional to the mobility, μ. The mobility is a property of the host material (KTN), and in our sample was found to be unaffected by the heat treatments.

The sensitivity of a sample can be increased by the use of thermal treatments, the application of an external field, or by the control of the temperature. Two limiting cases are considered. In the space charge limiting case, $E_{sc} \sim E_q = e[Cu^{2+}][Cu^{1+}]/\epsilon K[Cu]$, S is linearly dependent on the applied field and on the ratio [Cu^{1+}]/[Cu]. This ratio can be increased by thermal reduction treatments. S is independent of the strongly temperature dependent dielectric constant. So no improvement is expected in cooling the sample closer to the phase transition. In the second case where $E_q >> (E_o, E_D)$, the field varies as $E_{sc} \sim (E_o^2 + E_D^2)^{1/2}$. S is now inversely proportional to the trap concentration,Cu^{2+}, which can be reduced through thermal treatments. In this limiting case, S, is more strongly dependent on applied field. Also S is proportional to ϵ and can be increased by cooling to a temperature near the ferroelectric phase transition. Generally the sensitivity is improved when the photoexcited carrier is transported large distances before it is trapped. So large applied fields and low trap concentrations achieved through reduction heat treatments are needed.

5.4 Summary

In summary, we have presented an investigation of the material parameters which are involved in the photorefractive effect in KTN:Cu,V. Following a series of oxidation and reduction treatments, all of the relevant material parameters which enter into the Kukhtarev model of the photorefractive effect are determined from electron microprobe analysis, absorption measurements, and photoconductivity measurements. These include the determination of the filled and ionized electron donor concentrations, the electron photoexcitation cross section and the ratio of the electron mobility to recombination rate. This allows us to compare photorefractive measurements with those expected from theory. Good agreement is found for the photorefractive erase time measurements but the magnitude of the index change is smaller than expected. We model the oxidation/reduction process which allows us to determine the temperature and partial pressure of oxygen needed to result in a given filled and ionized donor concentration. The energy level of the Cu^{1+} is found to agree closely with the optical excitation energy. Approaches to increase the photorefractive sensitivity are discussed.

REFERENCES

1. W. Phillips, J.J. Amodei, D.L. Staebler, "Optical and holographic properties of transition metal doped lithium niobate," RCA Rev. **33**, 94 (1972).
2. G. Rakuljic, A. Yariv, R. Neurgaonkar, "Photorefractive properties of undoped, cerium-doped, and iron-doped single-crystal $Sr_{0.6}Ba_{0.4}Nb_2O_6$," Opt. Eng. **25**, 1212 (1986).
3. W. Phillips and D.L. Staebler, "Control of the Fe^{2+} concentration in iron-doped lithium niobate," J. Elect. Matl. **3**, 601 (1974).
4. S. Ducharme and J. Feinberg, "Altering the photrefractive properties of $BaTiO_3$ by reduction and oxidation at 650C," J. Opt.Soc. Am. B **3**, 283 (1986).
5. N.V. Kukhtarev, V.B. Markov, S.G. Odulov, M.S. Soskin, and V.L. Vinetski, "Holographic storage in electrooptic crystals. I. Steady state," Ferroelect. **22**, 949 (1979).
6. G.C. Valley, M.B. Klein, "Optimal properties of photorefractive materials for optical data processing," Opt. Eng. **22**, 704(1983).
7. V. Leyva, A. Agranat, A. Yariv, "Dependence of the photorefractive properties of $KTa_{1-x}Nb_xO_3$:Cu,V on Cu valence state concentration," J. Appl. Phys. **67** , 7162 (1990).
8. V. Leyva, A. Agranat, A. Yariv, "Determination of the physical parameters controlling the photorefractive effect in $KTa_{1-x}Nb_xO_3$:Cu,V," JOSA B. **8**, 701 (1991).
9. P.Bohac, H. Kaufmann, "KTN optical waveguides grown by liquid-phase epi-

taxy," Elect. Lett. **22**, 861 (1986).

10. S. Triebwasser, "Study of ferroelectric transitions of solid-solution single crystals of $KNbO_3$-$KTaO_3$," Phys. Rev. **114**, 63 (1959).
11. Y. Brada, M. Roth, "Optical absorption of $KTa_{1-x}Nb_xO_3$ single crystals," +Phys. Rev. B **39**, 10402 (1989).
12. A.S. Marfunin," Physics of Minerals and Inorganic Materials," Springer-Verlag, Berlin, (1979).
13. G. Rossman, "Optical spectroscopy," Rev in Mineralogy **18**, 207 (1988).
14. F.S. Chen, J. Geusic, S. Kurtz, J. Skinner, and S. Wemple, "Light modulation and beam deflection with potassium tantalate-niobate crystals," J. Appl. Phys. **37**, 388 (1966).
15. E. Kratzig and R. Orlowski, "Light induced transport in doped $LiNbO_3$ and $LiTaO_3$," Ferroelect. **27**, 241 (1980).
16. K. Schmetzer, "Absorptionsspektroskopie und Farbe von V^{3+} -haltigen naturlichen oxiden und silikaten-ein beitrag zur kristallchemie des vanadiums," N. Jb Miner. Abh. **144**, 73 (1982).
17. E. Kratzig and R. Orlowski, "$LiTaO_3$ as holographic storage material," Appl. Phys. **15**, 133 (1978).
18. A. Agranat, V. Leyva, and A. Yariv, "Voltage-controlled photorefractive effect in paraelectric $KTa_{1-x}Nb_xO_3$:Cu,V," Opt. Lett. **14**, 1017 (1989).
19. R. Orlowski, L.A.Boatner, and E. Kratzig, "Photorefractive effects in the cubic phase of potassium tantalate-niobate," Opt. Comm. **35**, 45 (1980).

20. F.S. Chen, J. Geusic, S. Kurtz, J. Skinner, and S. Wemple, "Light modulation and beam deflection with potassium tantalate-niobate crystals," J. Appl. Phys. **37**, 388 (1966).

21. H. Kogelnik, "Coupled wave theory for thick hologram gratings," B.S.T.J. **48**, 2909 (1969).

22. B.A. Wechsler, M.B. Klein, "Thermodynamic point defect model of barium titanate and application to the photorefractive effect," J. Opt. Soc. Am. B **5**, 1711 (1988).

23. L.A. Boatner, A. Kayal, U.T. Hochli, "Electronic properties of pure and Cu-doped $KTaO_3$," Helv. Phys. Acta **50**, 167 (1977).

24. F. Rosenberger, "Fundamentals of crystal growth I.," Springer-Verlag, Berlin (1979).

25. N.F. Mott, R.W. Gurney, "Electronic processes in ionic crystals," Dover Publications, New York (1964).

CHAPTER SIX

INVESTIGATION OF THE PHOTOREFRACTIVE PROPERTIES OF Fe AND Ti DOPED KTN

6.1 Introduction

A number of approaches have been used to modify the photorefractive properties of a material. Dopants introduced into the flux during the growth stage determines the concentration and identity of the photorefractive center which enters into the crystal.[1,2] After growth, thermal treatments are used to reduce or oxidize the valence state of the photorefractive species.[3] In this chapter the use of a particular double dopant combination, Fe and Ti, is shown to lead to improved photorefractive response as compared to single doped samples. Samples were prepared from three KTN crystals, one doped with Fe, one doped with Ti , and another doped with both Fe and Ti. Absorption and photoconductivity measurements indicate that the combination of Fe and Ti leads to an increased Fe^{2+} concentration as well as an increased total Fe concentration which enters into the crystal. The dependence of the photorefractive properties of each sample on temperature, electric field, and grating period are characterized. Results are interpreted using the Kukhtarev model of the photorefractive effect. Approaches to optimize these properties are discussed.

6.2 Experimental results and discussion

6.2.1 Sample preparation and composition

Three KTN crystals with different dopant combinations were grown using the top seeded solution growth method. The first crystal was doped with 0.5 molar% of Fe in the flux, the second with 0.5 molar% of Ti, and the third with 0.25 molar% of Fe and 0.25 molar% of Ti. Samples were cut from each crystal and polished along the [001] crystallographic axes. Metal electrodes of Cr and Au were evaporated on each sample. The KTN:Fe sample measured 5x5.7x3.7mm^3, the KTN:Ti sample measured 6.4x6.7x2.9 mm^3, and the KTN:Fe,Ti sample measured 3.8x3.8x5.5mm^3. The chemical composition of each sample was determined using electron microprobe analysis. Results are summarized in Table 6-1. The Fe and Ti concentrations were below the detection limit of roughly 100 parts per million (ppm) by weight. The temperature dependence of the low frequency (10hz) dielectric constant of each sample was determined from capacitance measurements and is shown in Fig. 6-1. The slight variation in the Ta/Nb concentration ratio of the samples results in strong variations in the temperature and compositional dependent ferroelectric properties.

6.2.2 Absorption measurements

Absorption features which involve the transition metal dopants are of two types, charge transfer and crystal field transitions.[4] The first results in the generation of a free charge carrier which can participate in the photorefractive effect, and the second results in localized electronic transitions which produce absorption features characteristic of the valence state of the ion. Fe enters into the crystal primarily in the 2+ and 3+ valence states. An electron can be photoexcited from a Fe^{2+} ion

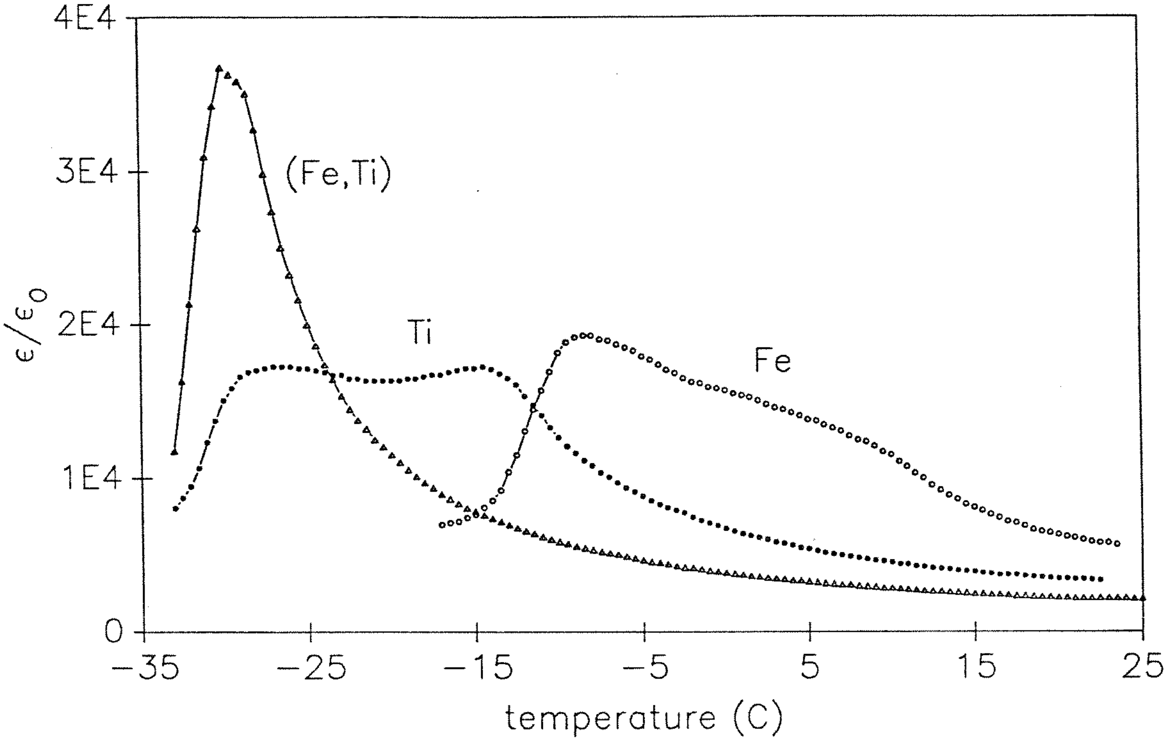

Fig. 6-1 The temperature dependence of the low frequency dielectric constant of the KTN:Fe, KTN:Ti, and KTN:Fe,Ti sample.

into the conduction band by the charge transfer transition

$$Fe^{2+} + h\nu \rightarrow Fe^{3+} + e^- \tag{6.1}$$

where $h\nu$ is the energy of the incident photon. Similiarly a free hole, p, can be generated in the valence band by the transition

$$Fe^{3+} + h\nu \rightarrow Fe^{2+} + p \tag{6.2}$$

Both valence states of the ion also undergo crystal field transitions which do not produce a free carrier which can participate in the photorefractive effect. Crystal field transitions of the Fe^{2+} ion generally result in a broad absorption band centered at 1000nm. Crystal field transitions of the Fe^{3+} ion are electronicaly spin forbidden and thus show weak absorbance.

Ti is stable in the 3+ and 4+ valence states and is a much weaker absorber than Fe. Similiar to those transitions described in eqns. (6.1) and (6.2) free electrons can be generated by photoexcitation from the Ti^{3+} ion and free holes by photoexcitation from the Ti^{4+} ion. The Ti^{4+} ion has no electrons in its outer d orbital and hence does not undergo crystal field transitions. The single outer d shell electron of the Ti^{3+} ion can undergo crystal field transitions. Use is made of this transition to produce a laser medium in saphire.

The absorption spectrum of each sample was measured using a double beam spectrophotometer. The absorption coefficient, α, was determined from the measured transmission using expression (5.1). The absorption spectra are displayed in Fig. 6-2. The KTN:Ti sample has low absorption which indicates that the the

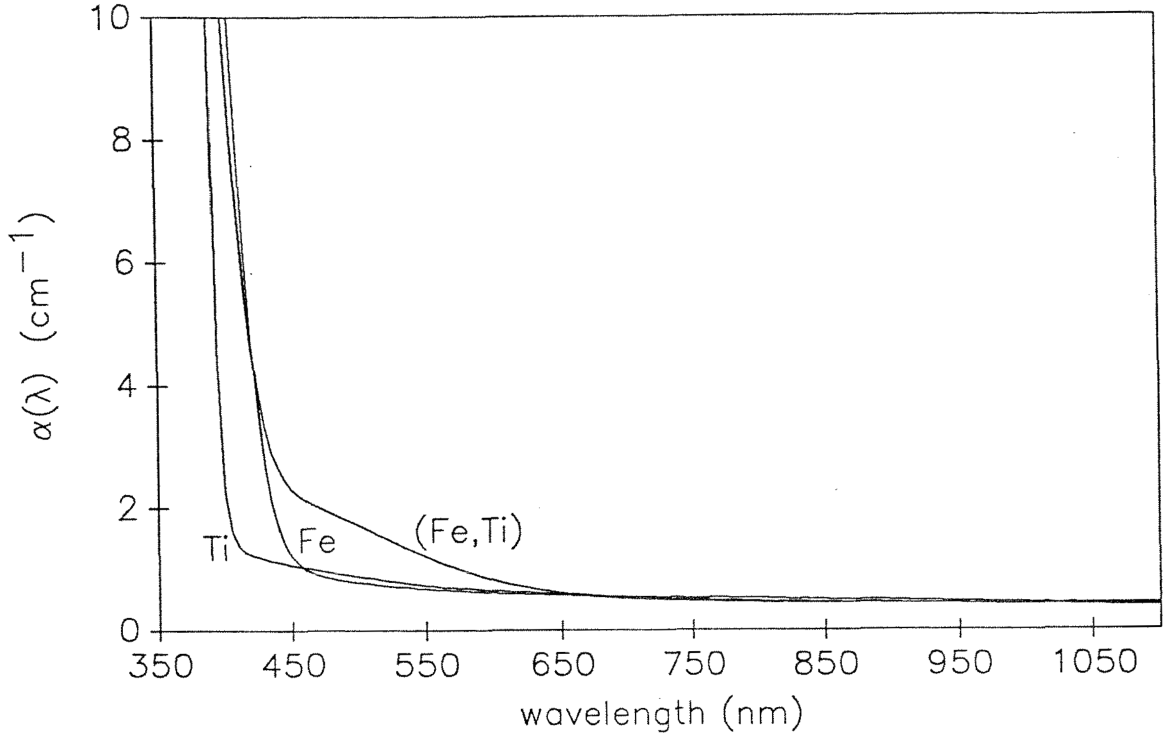

Fig. 6-2 Absorption spectra of the KTN:Fe, KTN:Ti, and the KTN:Fe,Ti sample.

absorption due to the Ti in the KTN:Fe,Ti sample can be neglected relative to the absorption due to the Fe.

The difference in the absorption between the KTN:Fe,Ti and the KTN:Fe sample is shown in Fig. 6-3. Features in the difference spectra should be a result of the dopant ions and have a magnitude proportional to the difference in concentration of the absorbing ions of the samples. Two features are visible in the difference spectra. The band centered at 460nm(2.70 eV) is identified as that of eq. (6.1) which produces a free electron by photoexcitation from a Fe^{2+} ion. It is the band responsible for the photorefractive effect in the Fe doped samples observed under 514nm illumination. The width of the transition is 0.66eV. Note that the Fe charge transfer transition is broader and peaked at lower energy than that determined for Cu (peak=3.0eV, width=0.38 eV) in Chapter 5. For similiar concentrations in a crystal, Fe is thus expected to have improved photorefractive response than that of Cu in the red spectral region. No peak is obseved in the weak KTN:Ti absorption spectra in Fig. 6-1. Ti is thus expected to have the weakest spectral response at longer wavelengths. The other feature visible in the difference spectra is the edge of an absorption band visible at 400nm. This is identified as that given by eq. (6.2) which generates a free hole by photoexcitation from the Fe^{3+} ion. Hole conducivity in $LiNbO_3$:Fe has also been observed to occur at higher energies than that for electron conductivity.[5]

The magnitude of both bands is proportional to the difference in the concentration of the absorbing ions in each sample. The band at 460nm is thus propotional to

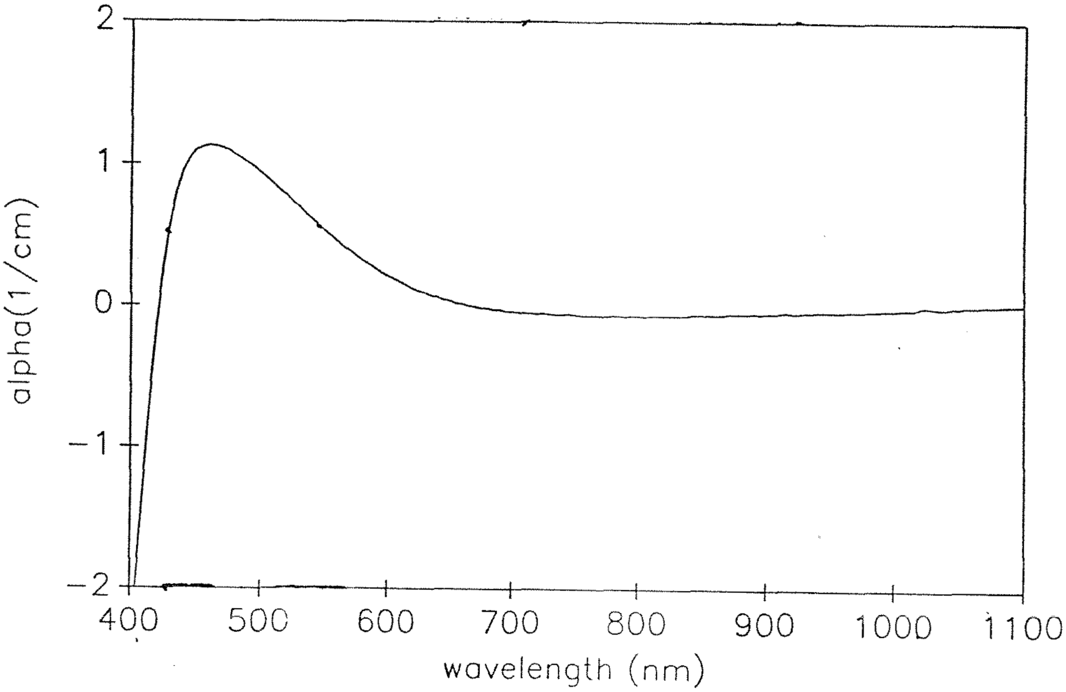

Fig. 6-3 Difference in the absorption spectra between the KTN:Fe,Ti and the KTN:Fe samples. Features should be a result of the dopant ions with a magnitude proportional to the difference in the absorbing ions in each crystal.

the concentration difference $([Fe^{2+}]_{KTN:Fe,Ti} - [Fe^{2+}]_{KTN:Fe})$. While the edge of the absorption band visible at 400nm is proportional to the concentration difference $([Fe^{3+}]_{KTN:Fe,Ti} - [Fe^{3+}]_{KTN:Fe})$. The magnitude of the bands in the difference spectra when compared to the absorption spectra in Fig. 6-1 determines the relative concentration of Fe^{2+} and the relative concentration of Fe^{3+} in each crystal (Table 6-1). The KTN:Fe,Ti sample is detemined to have a factor of 2.9 increased Fe^{2+} (filled donor) concentration than the KTN:Fe sample. Similiarly the KTN:Fe sample is determined to have a factor of 1.3 increased Fe^{3+} (electron trap) concentration than the KTN:Fe,Ti sample. The addition of Ti is thus seen to increase the total Fe concentration which enters into the crystal and to bias the Fe to enter in the Fe^{2+} valence state. The effect is even more pronounced when one considers that the flux used to grow the KTN:Fe,Ti crystal had half as much Fe as the flux used to grow the KTN:Fe crystal. The effect of increased Fe^{2+} concentration can also be achieved through thermal reduction treatments. But these can not always be used if a material undergos a phase transition above room temperature.

Similiar effects were observed in waveguides formed in $LiNbO_3$ through Ti indiffusion.[6] Fe impurities were present which produced an unwanted photorefractive effect for waveguide applications. Measurements of the photorefractive response time, indicate that the indiffusion of Ti results converted some of the Fe into the Fe^{2+} valence state. Not all of the increased Fe may participate equally in the photorefractive effect. Fe dopants usually substitutionally occupy the Ta,Nb site but epr measurements of Hannon indicate that the addition of Ti to Fe doped $KTaO_3$

forces some of the Fe to enter in the K site.[7,8] The increased Fe concentration in KTN in the prescence of Ti is a result of a charge compensation of the lattice whereby a Fe^{2+} ion occupies a K^{1+} site and a Ti^{4+} ion occupies a $(Ta,Nb)^{5+}$ site.

6.2.3 Photoconductivity measurements

The photocurrent,J_{ph}, of each sample was measured under 85mW/cm^2 illumination from a 514nm Ar laser. Neglecting the dark conductivity the photocurrent is given by

$$J = e\mu_e\tau_R\alpha_{ct}(I/h\nu)E \tag{6.3}$$

where e is the electronic charge, μ_e is the electron mobility, τ_R is the free electron lifetime (recombination time), α_{ct} is the coefficient for absorption which results in a free carrier, I is the intensity, hν is the energy of an incident photon, and E is the applied electric field. There is no photovoltaic effect in the paraelectric region. Results for J_{ph} are given in Table 6-1 normalized to I=85mW/cm^2 and E=1000V/cm. The KTN:Fe,Ti has over a factor of 30 increased photocurrent as compared to the KTN:Fe and KTN:Ti samples.

The mobility lifetime product, $\mu\tau_R$, for each sample was determined from the photocurrent using Eq. 6.3 and are listed in Table 6-1. The average distance a free electron drifts before it is retrapped is given by $l_d = \mu\tau_R E$. The mobility lifetime product and hence the average drift length do not vary much between samples. The mobility is a property of KTN and in lightly doped samples should not depend on the doping. The recombination time, τ_R, varies roughly inversely with the electron trap concentration. The results are consistent with the absorption measurements which indicate that the two Fe doped samples have roughly the same Fe^{3+} (electron trap) concentration. So the increased photocurrent in the double doped KTN:Fe,Ti sample is the result of increased generation of free carriers due to an increased absorption.

Sample	$[Fe^{2+}]$ $(AU)_1$	$[Fe^{3+}]$ $(AU)_2$	J_{ph} (amp/cm^2)	$\mu\tau_R (cm^2/Vs)$
$KTa_{0.70}Nb_{0.30}O_3$:Fe,Ti	2.9	1	$2.0x10^{-8}$	$4.99x10^{-10}$
$KTa_{0.68}Nb_{0.32}O_3$:Fe	1	1.3	$3.26x10^{-9}$	$2.72x10^{-10}$
$KTa_{0.67}Nb_{0.33}O_3$:Ti	-	-	$2.70x10^{-9}$	$1.72x10^{-10}$

Table 6-1: Chemical composition, photocurrent, and mobility lifetime product of three KTN crystals determined from electron microprobe, absorption, and photocurrent measurements. The photocurrent is under $85mW/cm^2$ 514nm illumination with a 1000V/cm applied field.

6.2.4 Photorefractive diffraction measurements

Holographic diffraction measurements were made on each sample using the geometry shown in Fig. (4-2). The samples were placed on a thermoelectrically cooled mount. All measurements were made in the paraelectric cubic phase which required the application of an external field. Photorefractive diffraction gratings were written using two expanded beams from a 514nm Ar laser. The beams had intensities of 20 mw/cm^2 and $110mw/cm^2$ and were ordinary polarized in order to limit photorefractive wave coupling. The ratio of the beam intensities satisfies the small intensity modulation approximation used in the band transport model but also results in smaller refractive index changes. The diffracted intensity of an extraordinarily polarized weak probe beam from a HeNe laser aligned at the Bragg angle was used to monitor the strength of the grating.

The diffraction efficiency is defined as the ratio of the incident to the diffracted intensity of the HeNe probe beam. Its value was determined from the maximum diffracted intensity during the writing stage. For weak coupling the diffraction efficiency, η, is given by that from a thick plane holographic grating[9]

$$\eta = e^{-\alpha l} sin^2 (\frac{\pi \delta(\Delta n) l}{\lambda cos(\theta/2)}) \tag{6.4}$$

where α is the total absorption, l is the thickness of the sample, λ is the wavelength of the illuminating radiation , and θ is the angle between the writing beams. The refractive index change, $\delta(\Delta n)$, is given in the paraelectric phase by[10]

$$\delta(\Delta n) = n_o^3 g(\epsilon - \epsilon_o)^2 E_{sc} E_o \tag{6.5}$$

where n_o is the index of refraction, g is the quadratic electro-optic coefficient, E_{sc} is the photorefractive space charge field, and E_o is the applied field. The erase time was determined by monitoring the decay of the index grating under 110mW/cm^2 illumination after one of the writing beams was blocked.

For the writing wavelength of 514nm, the absorption measurements indicate that hole conductivity can be neglected in each sample. Also, in the KTN:Fe,Ti sample the photorefractive effect is expected to be dominated by the strongly absorbing Fe. As such the single species, single carrier band transport model of the photorefractive effect will be used to describe the results.[11,12] In the Fe and (Fe,Ti) doped samples N_D corresponds to the total Fe concentration and N_D^+ to [Fe^{3+}]. Similiarly,in the KTN:Ti sample N_D corresponds to [Ti] and N_D^+ to Ti^{4+}.

The dependence of the holographic diffraction efficiency and erase time on temperature, grating period, and electric field for each sample was determined. Measurements were made at several temperatures above the ferroelectric phase transition of each sample. Electric fields of 455V/cm, 910V/cm, 1365V/cm, and 1820V/cm were used to write and readout gratings. The angle between the writing beams was adjusted to form gratings with periods of 6.1μm ,5.1μm , 2.9μm , 1.6μm , and 1.1μm.

The dependence of the holographic refractive index change and erase time on grating period was determined. Fig. 6-4 shows the dependence of the refractive index change on grating period for the KTN:Fe,Ti sample for two applied fields. Fig. 6-5 shows the same dependence for the KTN:Fe sample and Fig.6-6 for the KTN:Ti sample. Both the KTN:Fe,Ti and the KTN:Fe sample exhibit peaks near $\Lambda = 5\mu m$. With no applied field the photorefractive space charge field peaks at a grating period equal to the Debye length, Λ_d given by

$$\Lambda_d = 2\pi\left(\frac{\epsilon_o \epsilon k_B T}{e^2 N_D^+ (1 - N_D^+/N_D)}\right)^{\frac{1}{2}} \tag{6.6}$$

KTN exhibits large Debye lengths due to large values for the dielectric constant near the phase transition temperature. In materials with much smaller dielectric constants the Debye length is difficult to determine from photorefractive measurements due to the difficulty in making measurements at small grating periods. For small grating periods the photorefractive space charge field, E_{sc}, approaches the limiting space charge field, E_q, given by

$$E_q = \frac{e}{\epsilon_o \epsilon K} N_D^+ (1 - N_D^+/N_D) \tag{6.7}$$

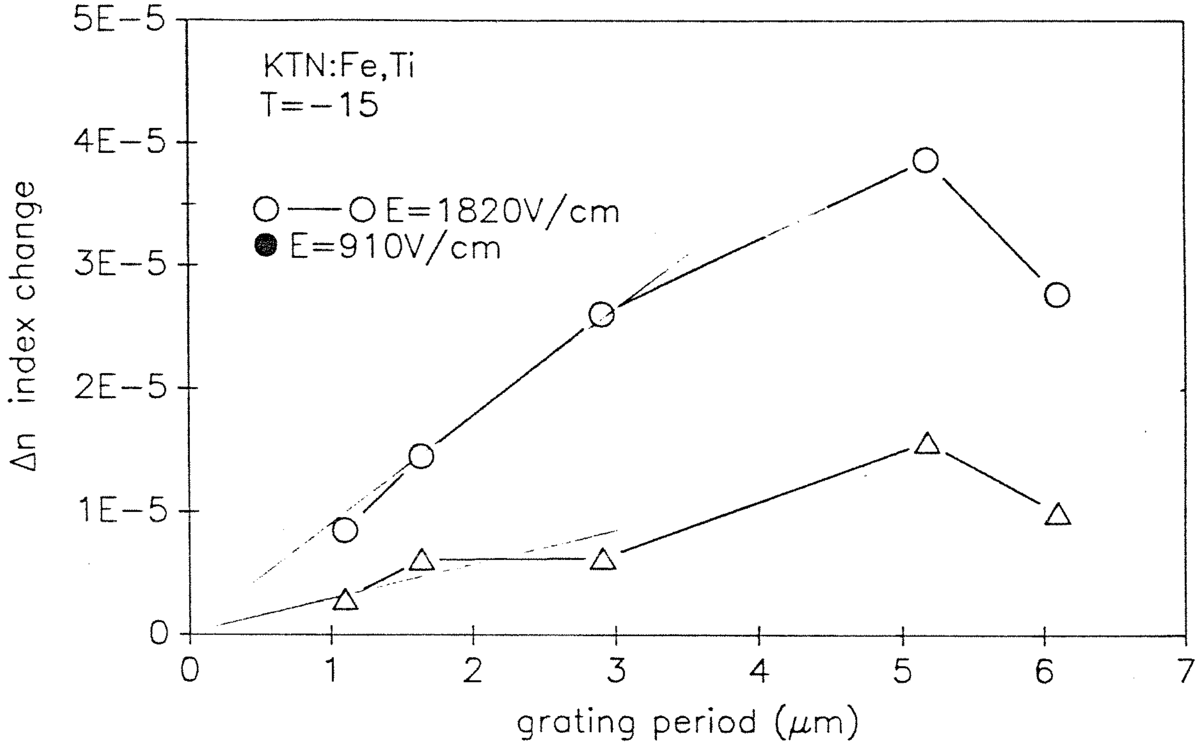

Fig. 6-4 Dependence of the photorefractive index change on grating period for the KTN:Fe,Ti sample.

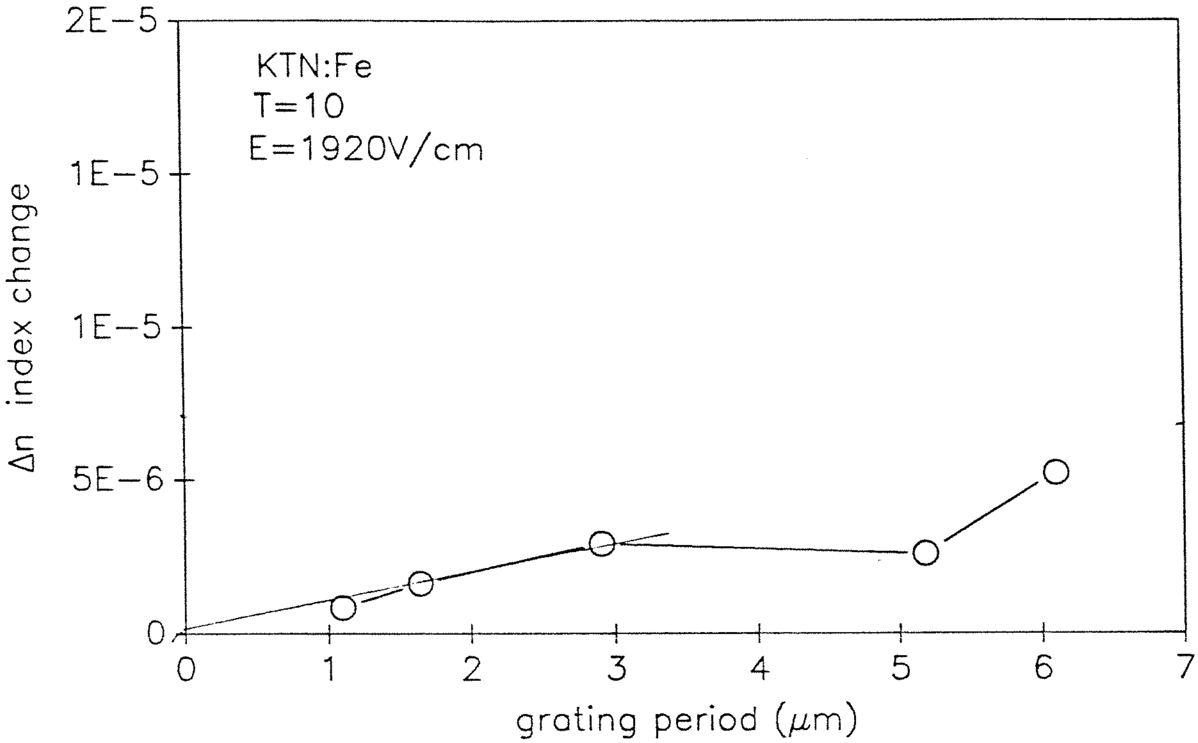

Fig. 6-5 Dependence of the photorefractive index change on grating period for the KTN:Fe sample.

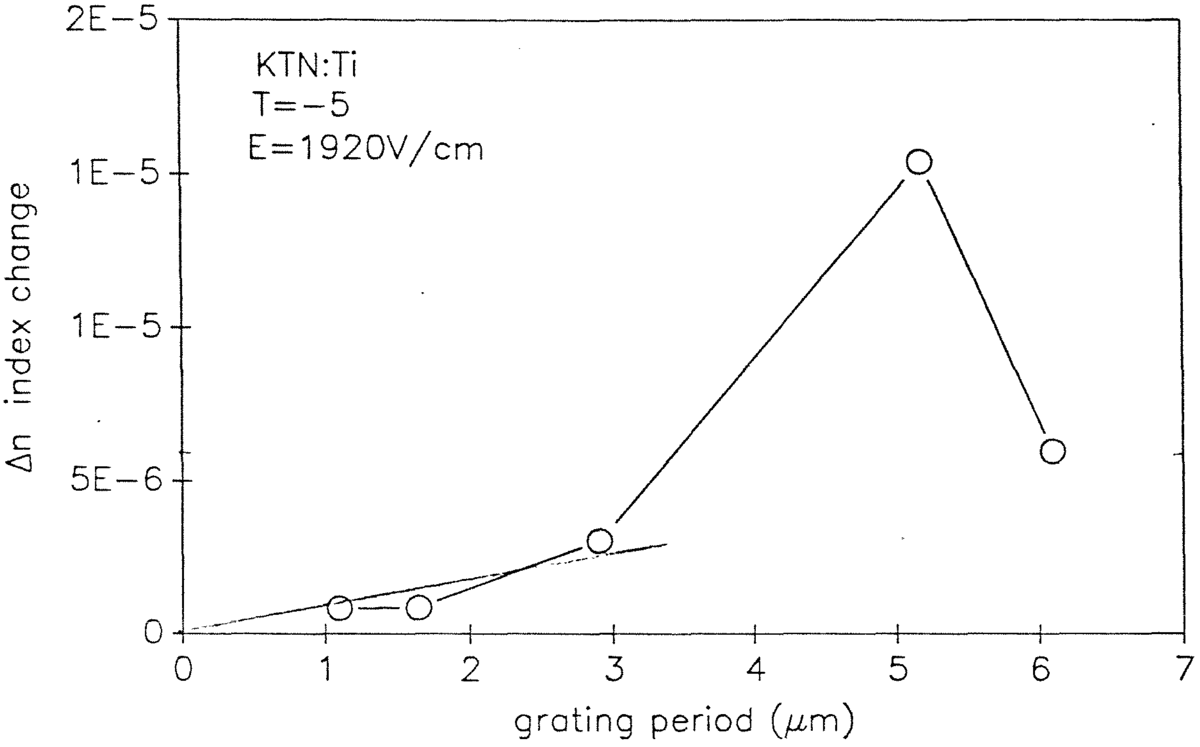

Fig. 6-6 Dependence of the photorefractive index change on grating period for the KTN:Ti sample.

which is linearly proportional to the grating period. From a linear fit of the refractive index change to grating period at small grating periods, values for $N_D^+(1-N_D^+/N_D)$ are determined to be 1.5x10^{16} cm^{-3} for KTN:Fe,Ti, 1.3x10^{15} cm^{-3} for KTN:Fe, 1.3x10^{15} cm^{-3} for KTN:Ti. The effect of double doping with (Fe,Ti) is to increase the effective dopant concentration, $N_D^+(1-N_D^+/N_D)$, by an order of magnitude as compared to single doped samples. For equal values of the dielectric constant the maximum space charge field, E_q, is also increased by an order of magnitude.

The dependence of the erase time for each crystal on grating period is given in Fig. 6-7. In the KTN:Ti sample the erase time varies between 140sec for $\Lambda = 6$ microns to 20sec for $\Lambda = 1$ micron. For large grating periods the photorefractive erase time approaches the response of a uniform charge distribution given by the dielectric relaxation time. For small grating periods compared to the Debye length, the erase time approaches the inverse of the sum of the photoproduction and recombination rates, τ_{Ie}, given in eq.(2.19). In materials with large photoconductivities, such as BSO and GaAs, the dielectric relaxation time is the smaller of the two and the response time decreases with increasing grating period. In KTN the reverse is true and the response time increses with grating period. It can be understood as the need for the charge carrier to undergo an increasing number of photoexcitation and retrapping steps before it can undergo transport by a distance equal to a grating period.

The photorefractive index change of holographic gratings written at different temperatures in each sample under a 1820V/cm applied field with a 5.1μm grating

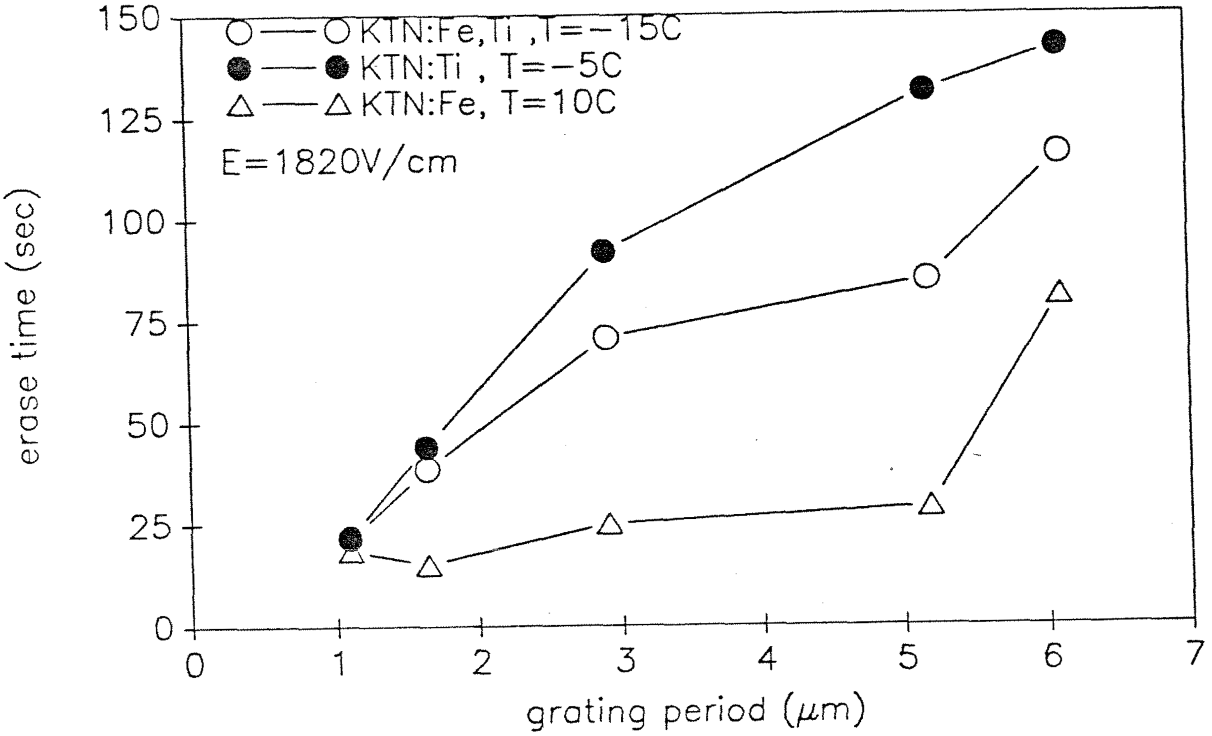

Fig. 6-7 The dependence of the erase time of each of the three samples on grating period under an applied field of 1820 V/cm.

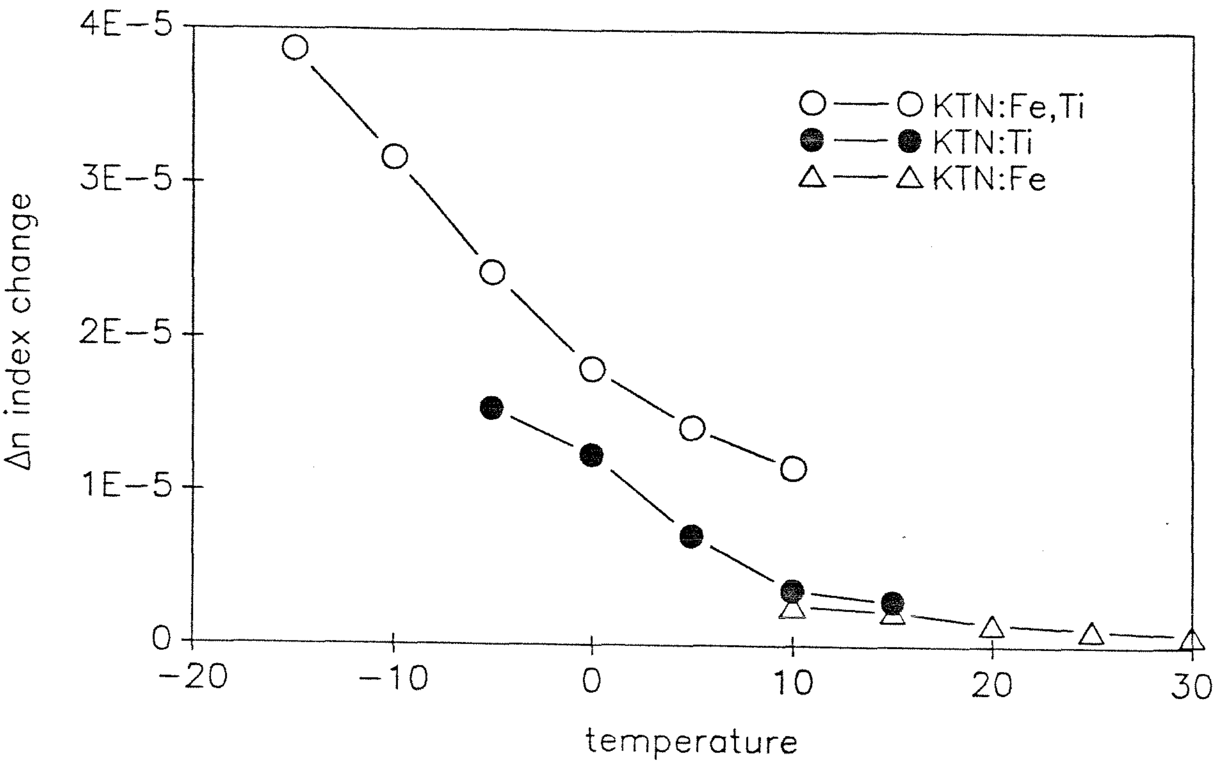

Fig. 6-8 Temperature dependence of the refractive index gratings written in each sample a 1820 V/cm applied field and with a 5.1μm grating period.

period is given in Fig 6-8. The magnitude of the index change is observed to increase with the dielectric constant as the temperature approaches the ferroelectric phase transition. The largest index change occurs in the KTN:Fe,Ti sample. In the expression for the space charge field(2.11) both E_D and E_q and thus E_{sc} decrease as the phase transition temperature is approached from above. The increase in the index change is thus a result of the increase in the quadratic electrooptic effect with increasing dielectric constant in eq.(5.6) and not due to an increase in the photorefractive space charge field.

The dependence of the erase time of the gratings on temperature under 110mW/ cm^2 illumination is given in Fig. 6-9. In (2.13), the expression for the response time can be approximated by the product of the dielectric relaxation time and weakly temperature dependent term. The erase time is thus essentially proportional to the dielectric constant. The increased refractive index changes as the phase transition temperature is approached is seen to occur only at the expense of slower response. The photorefractive sensitivity for each grating is plotted in Fig. 6-10. The KTN:Fe,Ti has the highest sensitivities by about a factor of three. Unlike the other two samples its sensitivity decreases on approaching the phase transition temperature. The increased index change does not make up for the slower response in the expression for the photorefractive sensitivity of eq.(2.44).

The dependence of the refractive index change on the externally applied electric field for the KTN:Fe,Ti sample is given in Fig. 6-11. Note that the same value for the electric field was used for the writing and readout stages. The index change

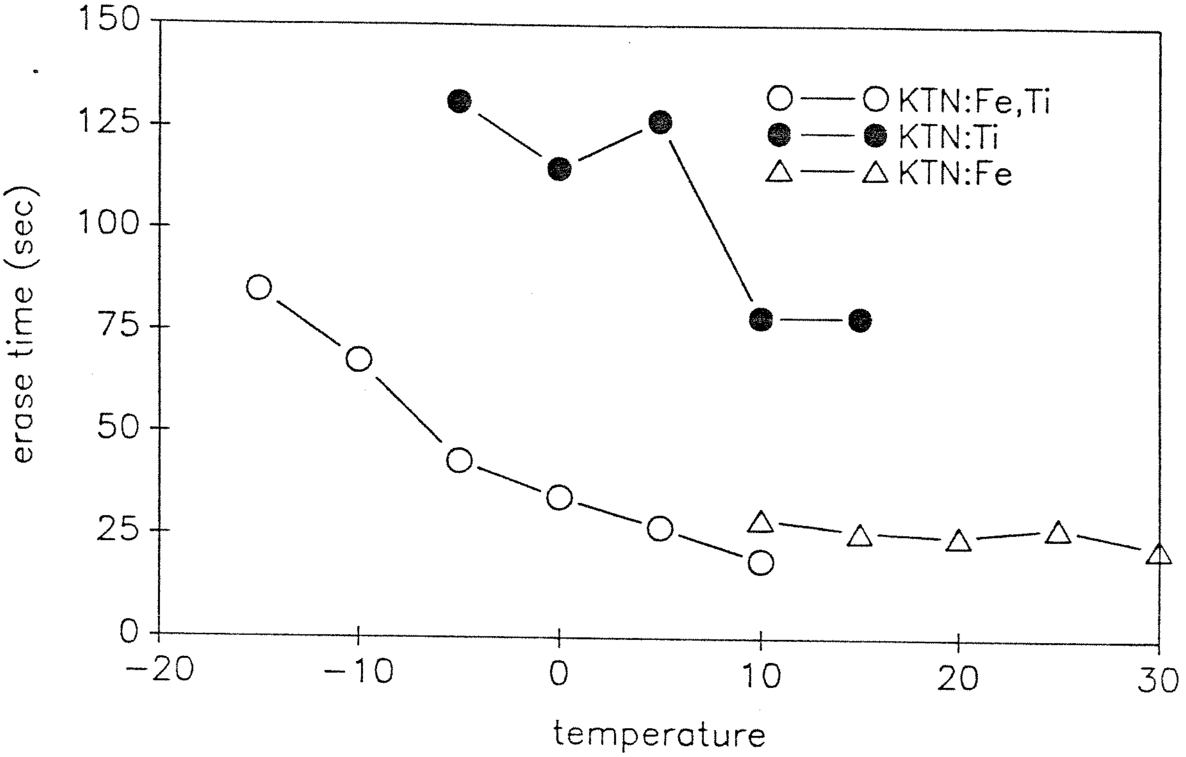

Fig. 6-9 Temperature dependence of the erase time of refractive index gratings in each sample under 110mW/cm^2 514nm illumination.

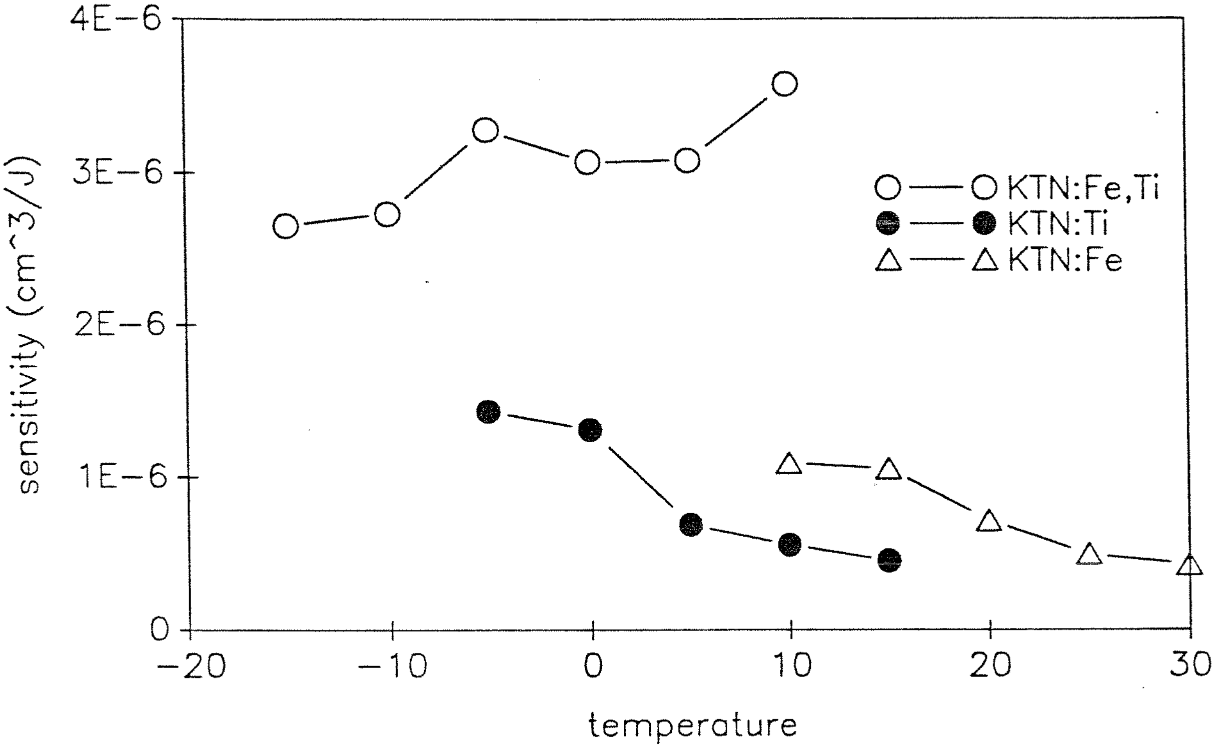

Fig. 6-10 The photorefractive sensitivity of each sample under an applied field of 1820 V/cm and with a 5.1μm grating period.

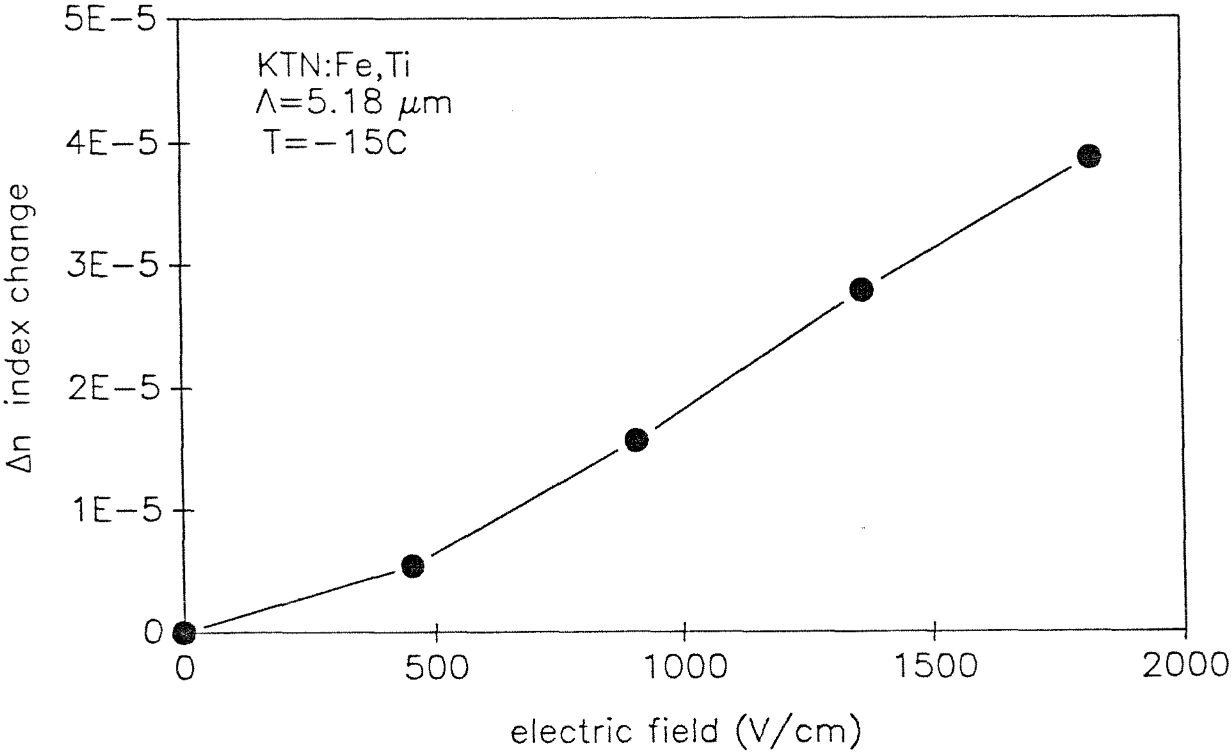

Fig. 6-11 Dependence of the refractive index change on electric field for the KTN:Fe,Ti sample.

given in eq.(4.4) is the product of the applied field, E_o, and E_{sc}, which increases with E_o. The index change is thus superlinearly dependent on the applied field. For large applied fields, however, the polarization as well as the index change saturates. The dependence of the response time for the gratings written in the KTN:Fe,Ti sample on applied field is given in Fig. 6-12. Increasing applied fields aid in the seperation of the photoexcited charge and results in slightly faster erase times.

6.3 Summary

The photorefractive properties of an Fe doped, a Ti doped, and a Fe and Ti double doped KTN samples are investigated. Absorption measurements indicate that the double dopant combination of Fe and Ti leads to an increased total Fe^{2+} concentration and total Fe concenetration which enters into the crystal as compared to single doped samples. Photocurrent measurements are used to determine the mobility lifetime product of the photoexcited carriers in each sample. The dependence of the photorefractive properties of the three samples on electric field, temperature, and grating period are characterized and interpreted using the Kukhtarev band transport model. The use of the double dopant combination of Fe and Ti leads to significantly improved photorefractive properties as compared to single doped samples. The double doping combination is determined to lead to an order of magnitude increase in the effective dopant density and a similiar increase in the photorefractive limiting space charge field, E_q.

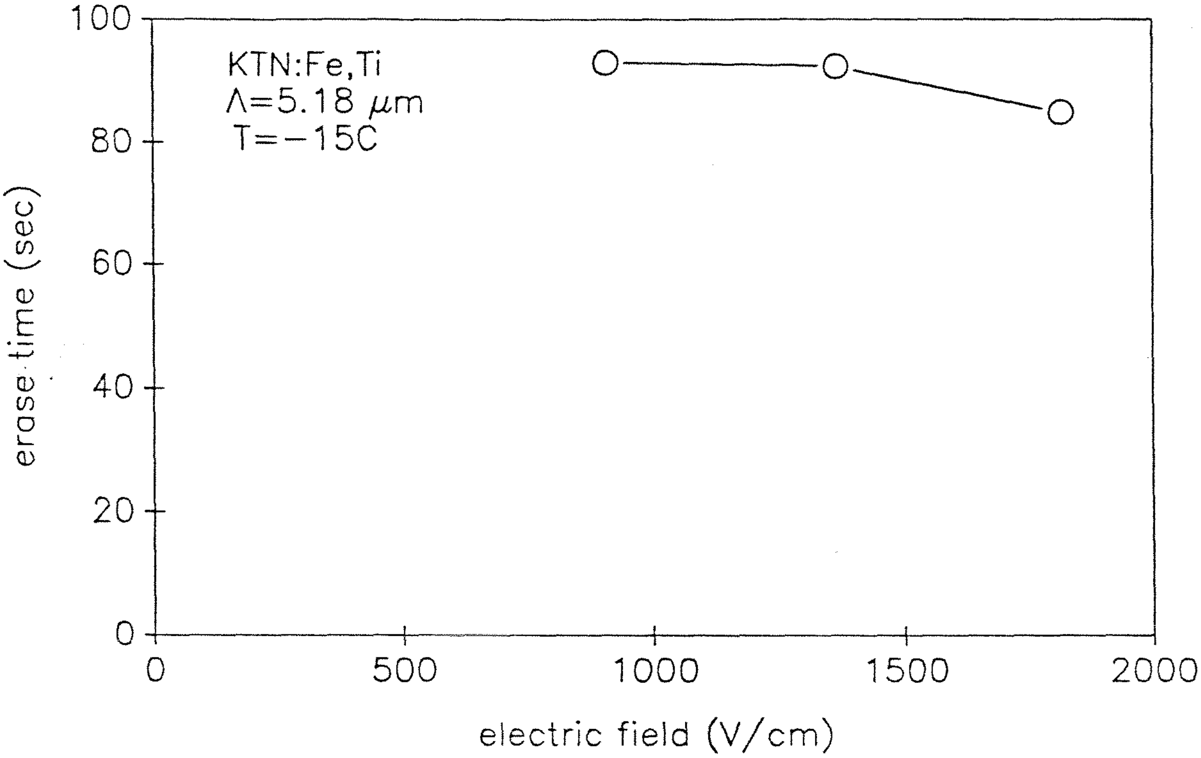

Fig. 6-10 Dependence of the erase time on electric field for the KTN:Fe,Ti sample.

References

1. G.E. Peterson, A.M. Glass, T.J. Negran, "Control of the susceptibility of lithium niobate to laser-induced refractive index changes," Appl. Phys. Lett. **19**, 130 (1971).
2. W. Phillips, J.J. Amodei, D.L. Staebler, "Optical and holographic properties of transition metal doped lithium niobate," RCA Rev. **33**, 94 (1972).
3. W. Phillips and D.L. Staebler, "Control of the Fe^{2+} concentration in iron-doped lithium niobate," J. Elect. Matl. **3**, 601 (1974).
4. G. Rossman, "Optical spectroscopy," Rev in Mineralogy **18**, 207 (1988).
5. E. Kratzig and R. Orlowski, "Light induced transport in doped $LiNbO_3$ and $LiTaO_3$," Ferroelect. **27**, 241 (1980).
6. P. Gericke, P. Hertel, E. Kratzig, J.P. Nisius, R. Sommerfeldt, "Light-induced refractive index changes in $LiNbO_3$:Ti waveguides," Appl. Phys. B **44**, 155 (1987).
7. G. Wessel, H. Goldick, "Electron spin resonance of iron-doped $KTaO_3$," J. Appl. Phys. **39**, 4855 (1968).
8. D.M. Hannon, "Electron paramagnetic resonance of Fe^{3+} and Ni^{3+} in $KTaO_3$," Phys. Rev. **164**, 164 (1967).
9. H. Kogelnik, "Coupled wave theory for thick hologram gratings," B.S.T.J. **48**, 2909 (1969).
10. A. Agranat, V. Leyva, and A. Yariv, "Voltage-controlled photorefractive effect in paraelectric $KTa_{1-x}Nb_xO_3$:Cu,V," Opt. Lett. **14**, 1017 (1989).

11. N.V. Kukhtarev, V.B. Markov, S.G. Odulov, M.S. Soskin, and V.L. Vinetski, "Holographic storage in electrooptic crystals. I. Steady state," Ferroelect. **22**, 949 (1979).

12. G.C. Valley, M.B. Klein, "Optimal properties of photorefractive materials for optical data processing," Opt. Eng. **22**, 704(1983).

CHAPTER SEVEN

SUMMARY AND FUTURE DIRECTIONS

7.1 Summary

The photorefractive effect was first observed in the late 1960s. Subsequent work led to an understanding of the mechanisms which lead to the light induced changes in the refractive index. A number of applications and devices have been demonstrated which make use of the photorefractive effect. These include holographic data storage, optical phase conjugation, optical processing, and coherent beam amplifiers. As of yet none of these has progressed past the laboratory demonstration stage primarily due to material limitations. Depending on the application, desired properties include large changes in the refractive index, fast response, especially in the infrared spectral regions, and the ability to fix gratings with high diffraction efficiencies.

The work described in this thesis was aimed at developing approaches to overcome the material limitations. Due to the limited availability of photorefractive crystals, a high temperature crystal growth system was designed and constructed and used to provide samples for the investigations. A number of transition metal doped KTN crystals were succesfully grown. The photorefractive index change and erase time of a KTN:Cu,V sample were modified by a series of thermal treatments which oxidized and reduced the Cu ions. The process by which oxygen vacancies lead to a reduction of valence state of the Cu ions was modelled. All parameters which govern the photorefractive effect were determined for the sample after each of the thermal treatments. Photorefractive measurements were then compared with those expected from the Kukhtarev model. Measured values for the photorefractive index change are significantly smaller than those expected from theory and suggest that not all of the Cu ions participate in the photorefractive effect. The use of the double dopant combination of Fe and Ti was found to lead to significantly enhanced photorefractive properties as compared to single doped samples. It is a result of an increased Fe^{2+} concentration which occurs when the sample is also doped with Ti. This occurs due to a charge compensation in the lattice by a Ti^{4+} ion with a Fe^{2+} ion.

Two applications which take advantage of the ferroelectric properties of KTN were developed. The first makes use of the quadratic electrooptic effect in the cubic phase to modulate the magnitude of a diffracted wave using an externally applied field at speeds limited by the dielectric response of the sample. The second application is a procedure used to fix a photorefractive grating by cooling the sample from the cubic phase through successive phase transitions into the rhombohedral phase.

7.2 Future directions

This work has identified several transition metal dopants dopants which lead to a large photorefractive effect in KTN. In addition, approaches were developed which modify the photorefractive properties of a sample through the control of the valence state of the photorefractive species. In order to make more viable use of these crystals a considerable effort is still required in the optimization of the crystal growth process. Work is needed to improve the optical quality and to increase the size of these crystals. Samples are also needed with ferroelectric phase transitions closer to room temperature. This is achieved by increasing the Nb concentration of the crystals.

Much work remains in the development of photorefractive materials for optical storage and optical processing applications. The only materials in which fixing procedures have been demonstrated are the ferroelectric oxides. These materials also suffer from poor response in the longer wavelength spectral regions where compact light sources exist. The infrared response can be improved through the choice of transition metal dopant introduced during growth. Also, a better understanding of the fixing process and of the identity of the ionic defect responsible for the fixing process is needed.